BULLETIN OF THE EARTHQUAKE
RESEARCH INSTITUTE
UNIVERSITY OF TOKYO
Vol. 59 (1984) pp. 127-196

Focal Mechanisms and Spatial Distribution of Subcrustal Earthquakes Occurring in Clusters beneath the Kanto District

Tadashi MAKI

Earthquake Research Institute
University of Tokyo

(Received April 25, 1984)

Abstract

Subcrustal earthquakes beneath the Kanto District and vicinity show some intense clusters of hypocenters at some regions and depths, especially in the western part of Ibaraki and Chiba Prefectures. Relative locations and spatial alignments of the hypocenter clusters are derived from the precisely relocated hypocenters by correcting the Pn station biases. For 487 out of 1029 subcrustal earthquakes, which occurred with magnitudes of 4.0 or more in and around the Kanto District during the period from 1963 to 1980, 704 fault-plane solutions, satisfying 10 or more first-motion data have been determined. Variable focal mechanisms of subcrustal earthquakes are caused by the convergence of three lithospheric plates, the intersection of the Northeast Honshu and Izu-Bonin slabs at depths and such additional processes as the back-arc spreading and bending of the lithospheric plate near the trench. Focal mechanisms of earthquakes in the intense clusters have a consistency with the spatial trend in the hypocenter distribution. Two clusters separated by the 140°E line and at different depths beneath the southwestern part of Ibaraki Prefecture show the northwest lineament with the reverse faults of the NW-SE or N-S compression and the western side sinking along the vertical plane. The latter type of earthquake occurrence is also observed for earthquakes beneath the middle part of Chiba Prefecture.

1. Introduction

Features of the hypocenter distribution in the Kanto District became noticeable since the recent observation of small and micro earthquakes by the high-sensitivity seismograph network of the Earthquake Research In-

Read on Oct. 25, 1983, at the monthly meeting (Danwakai) of the Earthquake Research Institute.

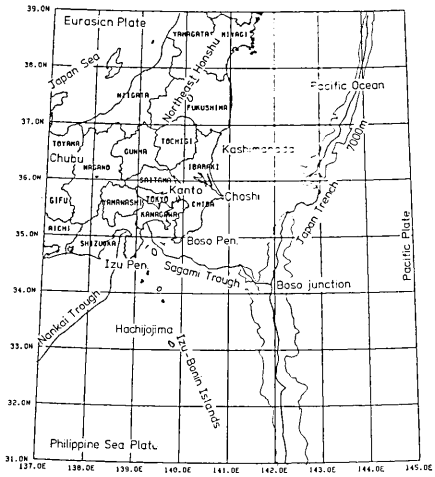

Fig. 1. Location map of the Kanto District and vicinity, with relation to the occurrence of subcrustal earthquakes. The trench axes and troughs are shown by thick lines, and the depth contours of 7000 m are shown by thin lines.

stitute (ERI) (TSUMURA, 1973). The spatial distribution of hypocenters in the Kanto District is characterized by (1) some intense clusters of subcrustal hypocenters, (2) a minor seismic zone inclined from the west besides the gross seismic zone associated with the descending Pacific Plate inclined from the east, and (3) a double-layered seismic zone at the intermediate-depths. For some intense clusters of subcrustal hypocenters beneath the southwestern part of Ibaraki Prefecture and the middle part of Chiba Prefecture (Fig. 1), the systematic trends of hypocenter distribution were derived by relating to focal mechanisms of the relatively large earthquakes (MAKI and TSUMURA, 1978, 1980). The most intensely active region beneath the western end of Ibaraki Prefecture (on the western side of the 140°E line) at depths around 50 km were interpreted by the relative motion between the Pacific and continental plates (MAKI *et al.*, 1980; MAKI and TSUMURA, 1980; MAKI, 1981b). On the other hand the deeper active regions at depths from 60 to 80 km beneath the southwestern part of Ibaraki Prefecture and the northern and middle part of Chiba Prefecture (on the eastern side of the 140°E line) were interpreted by the vertical slip with the western side sinking along the N-S plane within the slab of the Pacific Plate. These deeper earthquakes are produced by the collision of the northeastern end of the Philippine Sea Plate derived with the inclined Pacific Plate as revealed by the minor seismic zone inclined from the west.

Hypocenter data in the Kanto District and vicinity have been provided

by the Japan Meteorological Agency (JMA) and ERI, but these hypocenter data are insufficient with respect to the accuracy of focal coordinates for the JMA data or the area and period covered by the observation for the ERI data. Hypocenter locations are affected by the azimuth and distance coverages of stations around epicenters and observational errors in travel times, and the accuracies of hypocenter location can be improved by correcting the station biases (MAKI, 1982a). In the previous studies based on the ERI hypocenter data of small and micro earthquakes (MAKI *et al.*, 1980; MAKI and TSUMURA, 1978, 1980), only a part of the Kanto District was treated, and features of the intersection of the Northeast Honshu and Izu-Bonin slabs were not taken into consideration. Recently earthquakes which occurred during the period from 1963 to 1980 in and around the Kanto District are precisely relocated by correcting the JMA travel-time data with the Pn station biases (MAKI, 1981a). Relative locations and alignments of clustering hypocenters in and around the Kanto District should be studied by using the precise location of subcrustal earthquakes.

Recently fault-plane solutions have been obtained by a new numerical method (MAKI, 1982b) for a number of earthquakes in and around the Kanto District during the period from 1963 to 1979 or 1980, including the relatively large earthquakes ($n=454$, $M \geqq 5.0$) by MAKI (1983b), smaller shallow earthquakes ($h<40$ km, $5>M \geqq 4$, $n=226$) by MAKI (1983a, b), and smaller intermediate-depth earthquakes ($200>h>80$ km, $5>M \geqq 4$, $n=144$) by MAKI (1984). These fault-plane solutions show the spatial variation of focal mechanisms and suggest the complicated structure of earthquake-generating stress for larger and smaller earthquakes in and around the Kanto District. Actually three lithospheric slabs collide directly beneath the Kanto District with their own relative motions. The subduction process around the Kanto District is more complicated than the smooth descent beneath Northeast Japan. And the Kanto District is located at the transitional region between the different modes of the coupling of the descending plates with the overriding plates. The earthquakes beneath the Kanto District and vicinity are located at such various relative locations in the subduction zone as near the trench, along the plate boundary, within the descending slabs, behind the island arcs and at different depths. The focal mechanisms have close relations to their own relative locations in the subduction zone.

Spatial alignments and relative locations of subcrustal hypocenters in the intense clusters in and around the Kanto District will be covered in the present study by relating them to focal mechanisms.

2. Spatial distribution of subcrustal hypocenters in and around the Kanto District

The JMA hypocenter data cover a long period of several tens of years and a wide area including the Japan Trench and Izu-Bonin Islands, but the hypocenter locations, especially focal depths, are not very accurate. The ERI hypocenter data are more accurate than the JMA data and cover the smaller magnitudes down to about 2, but their data are limited only to the Kanto District and the short period of the last 10 years. Both the hypocenter data are not sufficient for detailed studies about features of earthquake occurrences in the Kanto District and vicinity, especially for the intense clusters of hypocenters.

Earthquakes which occurred from 1963 to 1980 were relocated by correcting the JMA travel-time data with the *Pn* station biases (MAKI, 1981a). Accuracies and problems in hypocenter locations are improved in these relocated hypocenters (MAKI, 1982a). These hypocenter data cover a long period of 18 years and a large area including the Japan Trench and the Izu-Bonin Islands. Focal depths are determined to the unit of 0.1 km, although the 10 or 20 km step is adopted in the JMA data (ICHIKAWA, 1965, 1978). Hypocenter locations and origin times are redetermined by using only the P arrival times observed at regional distances of 500 km or less. The ERI data are based on only the local observations and the origin times are preliminarily determined from the relation of S–P vs P times in both the JMA and ERI data.

The predominant inclined seismic zone from the east is shown on the depth distribution of small and micro earthquakes beneath the Kanto District by TSUMURA (1973). Other features in the depth distributions are the double-layered structure of the seismic zone of the Pacific Plate at intermediate-depths, another minor seismic zone inclined from the west, and the intense clusters of hypocenters at subcrustal depths. USAMI and WATANABE (1977) defined quantitatively 21 "earthquake nests" based on the distribution of earthquake numbers within the mesh of $2.5 \times 2.5\ \mathrm{km}^2$. And they estimated the possible ultimate magnitudes for each nest from the earthquake energy to be stored within the volume of the nest. MAKI and TSUMURA (1978, 1980) tried to enhance the spatial trends in hypocenter distributions by omitting isolated events, compensating dispersed events due to the location errors and ranking earthquake numbers within meshes by the logarithmic scale based on the statistical points. They also tried to interpret the spatial alignments of hypocenters by relating to focal mechanisms of relatively large earthquakes within the clusters. The most

accurate hypocenters in the Kanto District are obtained by the Joint Hypocenter Determination (JHD) method (MAKI, 1979). The intense clusters of hypocenters at depths from 40 to 60 km beneath the southwestern end of Ibaraki Prefecture are revealed to be separated from the gross inclined seismic zone of the descending Pacific Plate from the east. An inclined seismic zone from the west beneath the Kanto District was interpreted by the northeastern tongue of the Philippine Sea Plate (MAKI *et al.*, 1980; MAKI 1981b; MAKI and TSUMURA, 1980). Recently the active regions of subcrustal earthquakes are also interpteted by the acute intersection of the Northeast Honshu and Izu-Bonin slabs beneath the Kanto District (MAKI, 1984).

Epicenter distributions for every 40 km down to the depth of 120 km are compared in Fig. 2. These ranges of focal depth correspond to the crust, subcrust and uppermost mantle. The epicenter distribution of earthquakes which occurred at depths from 0 to 40 km is shown in Fig. 2a by circles classified by magnitudes. Some active regions can be picked out as, (1) the subduction zone along the Pacific coast of Northeast Honshu, where a planar pattern of hypocenter distribution is observed, (2) the inland region on the Japan Sea side, Chubu and Izu Islands, where epicenters show some linear alignments, and (3) an active zone along the 139°E line (MAKI, 1983a, b). The epicenter distribution of earthquakes which occurred at depths from 40 to 80 km is shown in Fig. 2b. Earthquakes are seldom observed in the inland regions at this depth range, and only the earthquakes in the subduction zone along the Pacific coast are observed, accompanying some intense clusters of hypocenters. Especially earthquakes beneath the Kanto District have a feature of strong concentration of hypocenters. The inclined seismic zone beneath Northeast Japan seems narrower than those beneath the Kanto District. Epicenters of earthquakes which occurred at depths from 80 to 120 km are shown in Fig. 2c. These earthquakes occur homogeneously within the slab of the Pacific Plate without clustering. Different features of hypocenter distributions are observed for these ranges of focal depth from 0 to 120 km in the Kanto District and vicinity.

Fig. 3 shows epicenter distributions of subcrustal earthquakes for depth intervals of 10 km. Clusters of hypocenters are located at different depths and locations with various sizes and trends in the spatial distribution. Fig. 3a represents the epicenter distribution of subcrustal earthquakes at depths from 40 to 50 km. Clusters of hypocenters are observed at the western end (on the western side of the 140°E line) of Ibaraki Prefecture ("a"), near Kasumigaura Lake and Choshi ("b") and Kashimanada

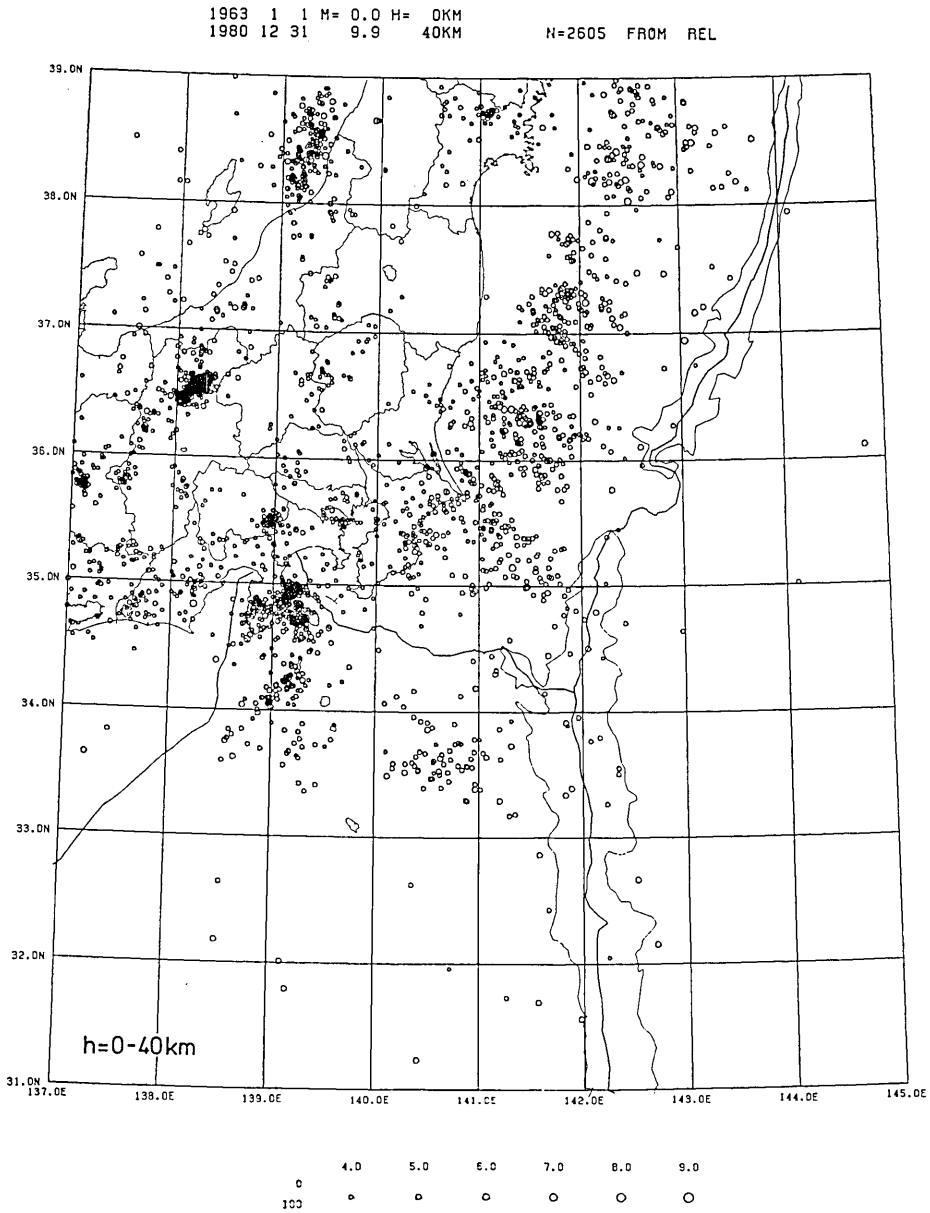
1963 1 1 M= 0.0 H= 0KM
1980 12 31 9.9 40KM
N=2605 FROM REL
39.0N
38.0N
37.0N
36.0N
35.0N
34.0N
33.0N
32.0N
31.0N
137.0E
138.0E
139.0E
140.0E
141.0E
142.0E
143.0E
144.0E
145.0E
h=0-40km
4.0
5.0
6.0
7.0
8.0
9.0
0
100

Fig. 2(a).

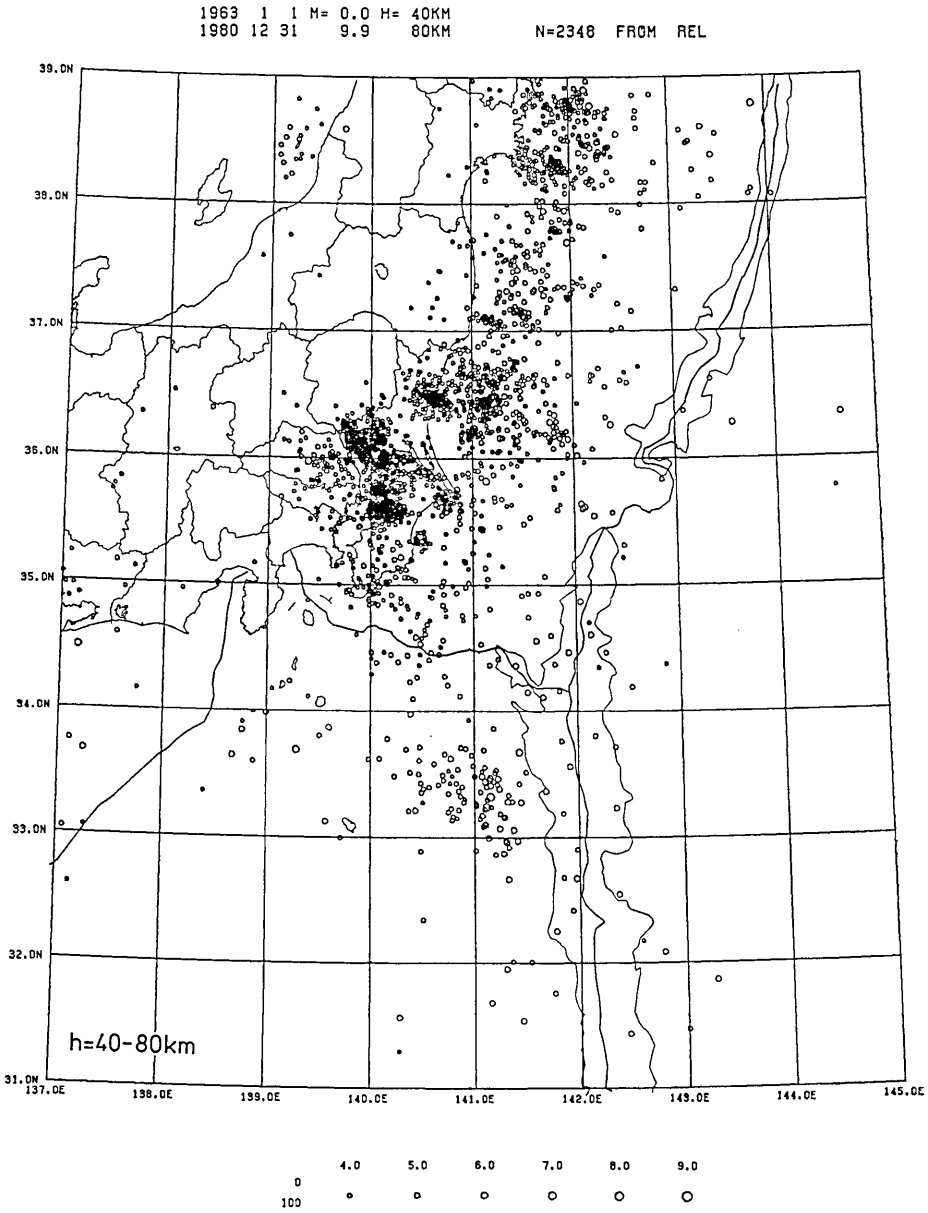
1963 1 1 M= 0.0 H= 40KM
1980 12 31 9.9 80KM
N=2348 FROM REL
39.0N
38.0N
37.0N
36.0N
35.0N
34.0N
33.0N
32.0N
31.0N
137.0E
138.0E
139.0E
140.0E
141.0E
142.0E
143.0E
144.0E
145.0E
h=40-80km
4.0
5.0
6.0
7.0
8.0
9.0
0
100

Fig. 2(b).

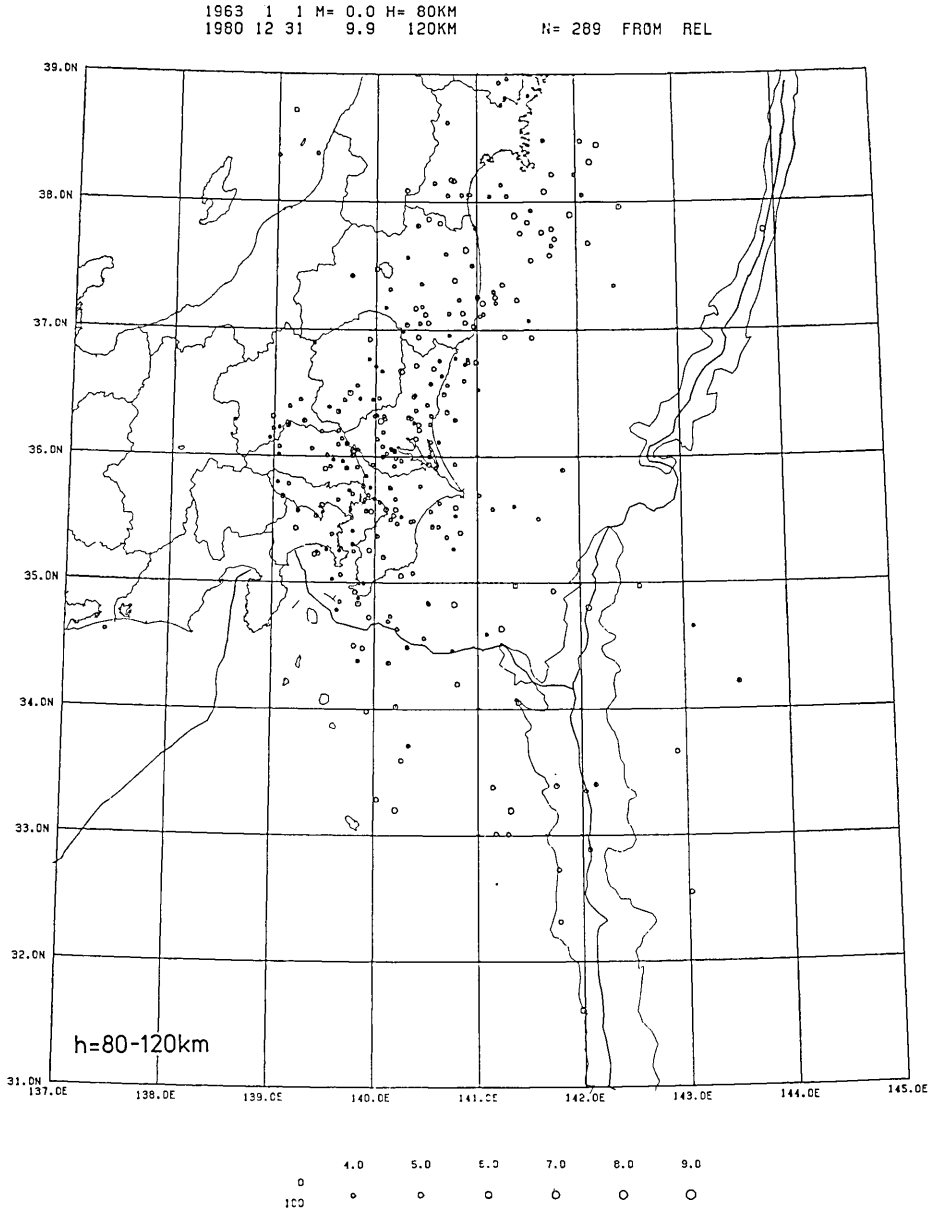

Fig. 2(c).

Fig. 2. Epicenter maps for three ranges of focal depth: (a) crustal earthquakes at depths from 0 to 40 km, (b) subcrustal earthquakes at depths from 40 to 80 km, and (c) intermediate-depth earthquakes at depths from 80 to 120 km. Hypocenters are located by correcting the JMA travel-time data of P wave with the Pn station biases (MAKI, 1981b). Epicenters are classified by earthquake magnitudes by JMA.

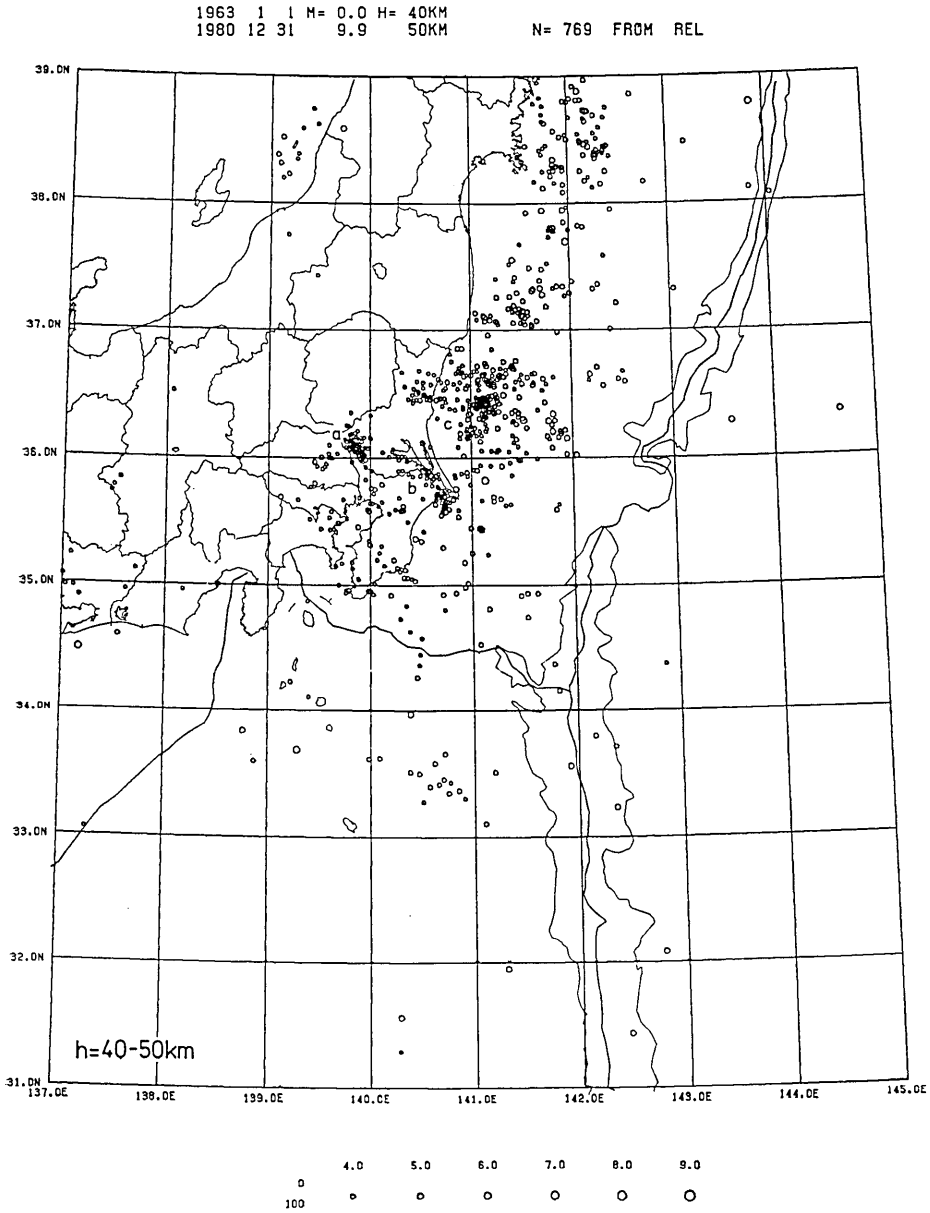
1963 1 1 M= 0.0 H= 40KM
1980 12 31 9.9 50KM
N= 769 FROM REL
39.0N
38.0N
37.0N
36.0N
35.0N
34.0N
33.0N
32.0N
31.0N
137.0E
138.0E
139.0E
140.0E
141.0E
142.0E
143.0E
144.0E
145.0E
a
b
c
h=40-50km
4.0
5.0
6.0
7.0
8.0
9.0
0
100

Fig. 3(a).

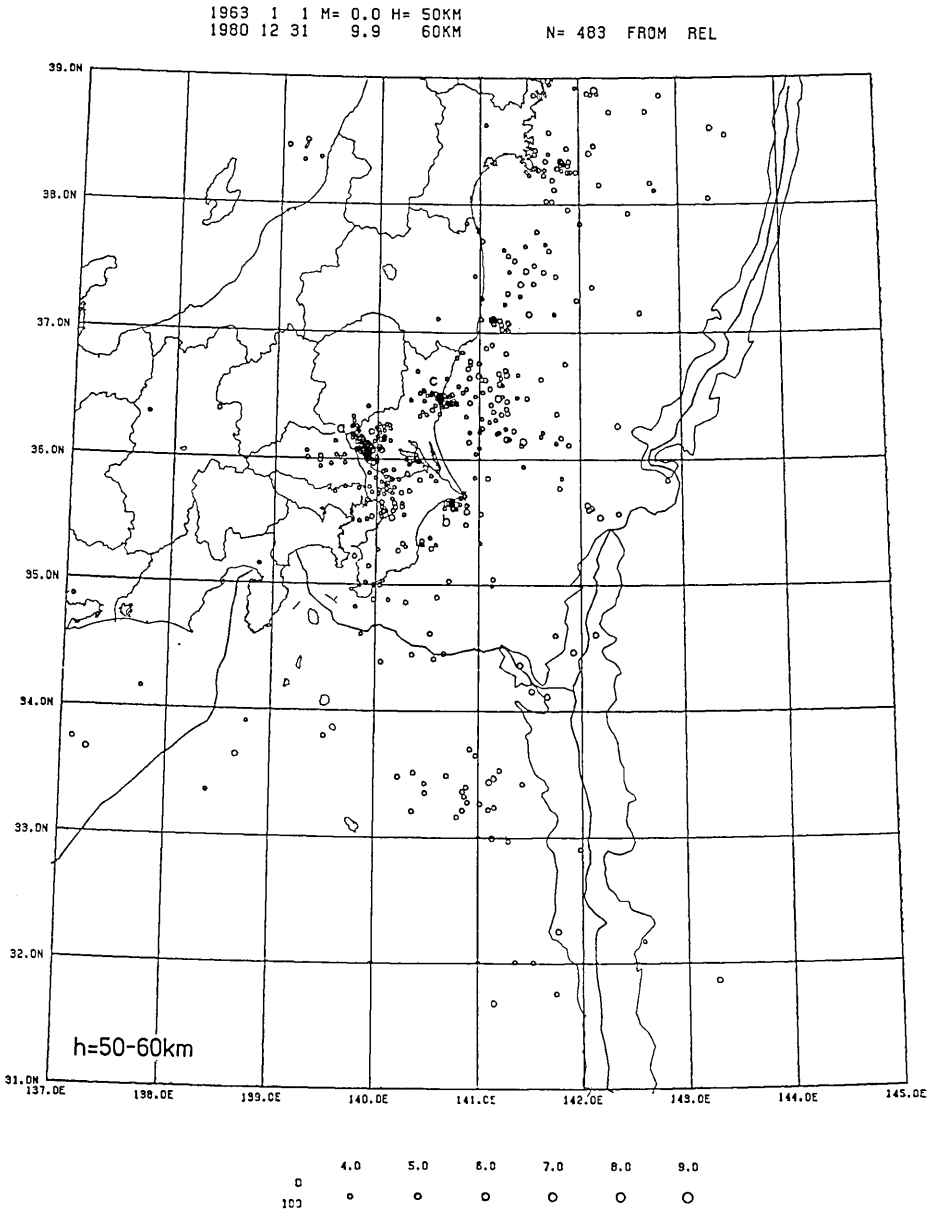
1963 1 1 M= 0.0 H= 50KM
1980 12 31 9.9 60KM
N= 483 FROM REL
39.0N
38.0N
37.0N
36.0N
35.0N
34.0N
33.0N
32.0N
31.0N
137.0E
138.0E
139.0E
140.0E
141.0E
142.0E
143.0E
144.0E
145.0E
h=50-60km
4.0
5.0
6.0
7.0
8.0
9.0
0
100

Fig. 3(b).

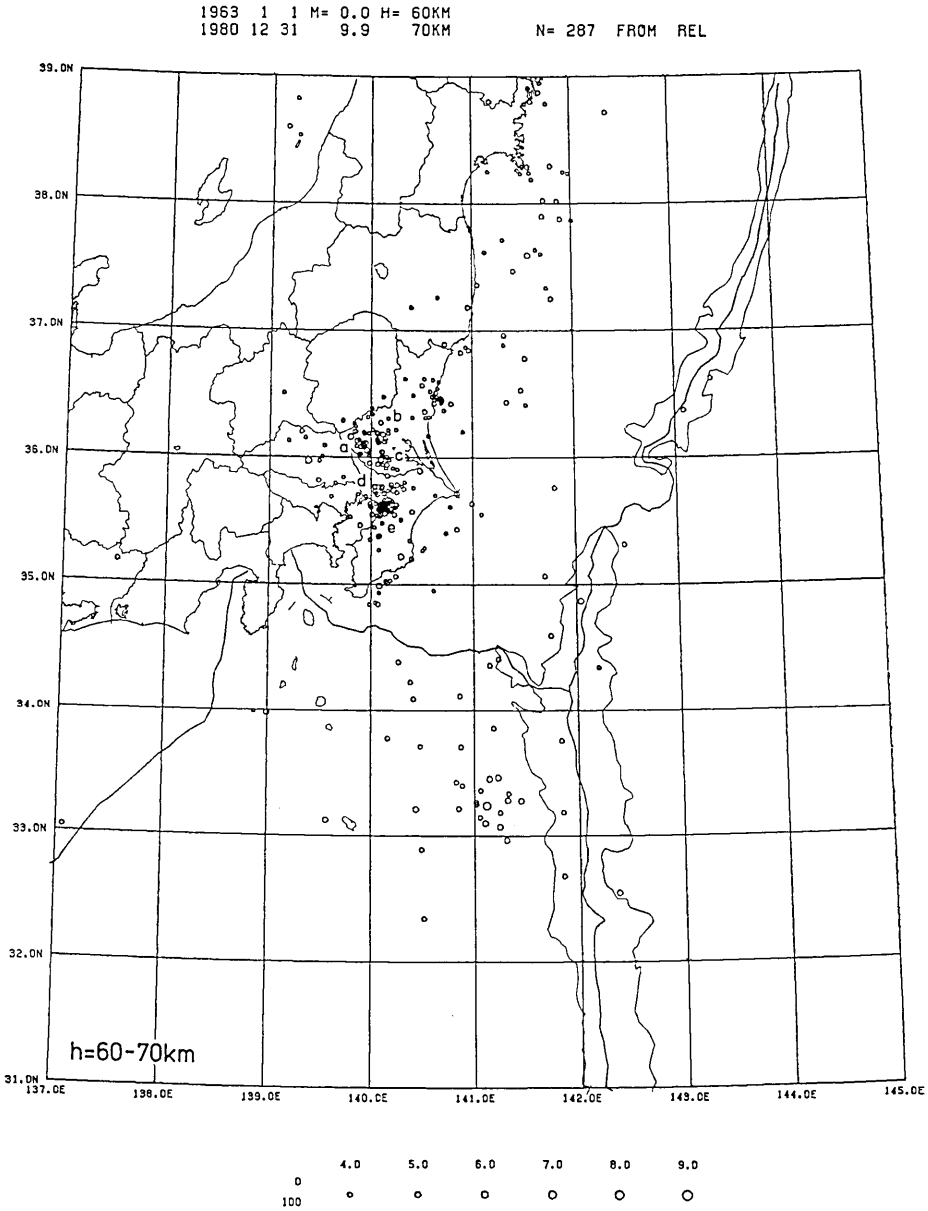
1963 1 1 M= 0.0 H= 60KM
1980 12 31 9.9 70KM
N= 287 FROM REL
39.0N
38.0N
37.0N
36.0N
35.0N
34.0N
33.0N
32.0N
31.0N
137.0E
138.0E
139.0E
140.0E
141.0E
142.0E
143.0E
144.0E
145.0E
h=60-70km
4.0
5.0
6.0
7.0
8.0
9.0
0
100

Fig. 3(c).

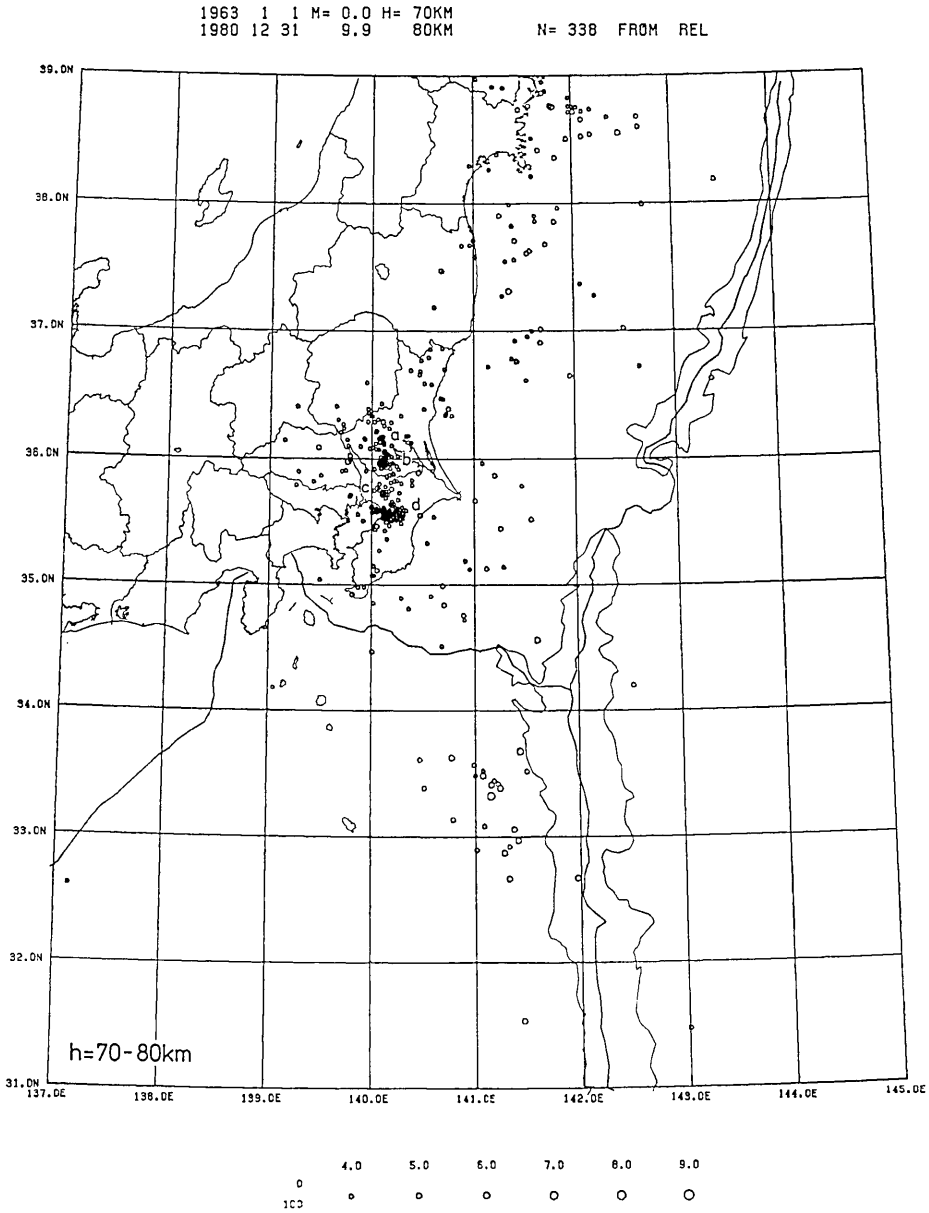

Fig. 3(d).

Fig. 3. Comparison of epicenter distributions of the relocated earthquakes for 10 km intervals of depth: (a) h=40-50 km, (b) h=50-60 km, (c) h=60-70 km and (d) h=70-80 km.

Table 1. Location and characteristcs of the intense clusters of subcrustal earthquakes in the Kanto District during the period from 1963 to 1980, derived from the relocated hypocenters by correcting the JMA travel-time data of P wave with the Pn station biases (MAKI, 1981a).

Region	Name	Location	Depth range (km)	Max. mag (JMA) 1963-1980	Trend in space	n	Focal mechanism solutions	Focal mechanism faulting
A	SW Ibaraki W	western part of SW Ibaraki	40-70	5.8	NW-SE	82	vertical T/P SW T	thrust N/NW
B	SW Ibaraki E	eastern part of SW Ibaraki	50-80	5.4	vertical	18	ditto	vertical slip NS
C	S Ibaraki	southern part of Ibaraki	50-80	5.2	vertical	15	ditto	ditto
D	N Chiba	northern part of Chiba	60-80	5.4	vertical	19	vertical T/P N-S T	ditto
E	M Chiba	middle part of Chiba	60-80	6.1	vertical	52	vertical T/P NW and SW T	ditto
F	Near Choshi	near Choshi	40-60	6.1	vertical	27	ditto	thrust NW
G	Kasumigaura	Kasumigaura Lake Tone River	40-50	5.4	vertical slow dipping	19	ditto	ditto
H	Nakaminato	near Nakaminato	40-60	5.2	slow dipping to W	33	vertical T N T	ditto
I	N Kashimanada	northern Kashimanada	40-60	5.8	slow dipping to W	19	vertical T N T	ditto
J	S Kashimanada	southern Kashimanada	40-60	6.0	slow dipping to W	22	vertical T N T	ditto

("c"). Earthquakes on the side of Northeast Honshu are less active and located in a narrower zone than in the Kanto District. Clustering hypocenters within a smaller volume at depths from 50 to 60 km are shown in Fig. 3b for earthquakes beneath the western end of Ibaraki Prefecture ("a"), near Choshi ("b") and in the northern part of Ibaraki Prefecture ("c"). Most earthquakes at depths from 60 to 70 km (Fig. 3c) are located in a limited region directly beneath the Kanto District and are separated into five smaller regions ("a" to "e"). For earthquakes at depths from 70 to 80 km the intense cluster of hypocenters (Fig. 3d) are located at four regions ("a" to "d") on the eastern side of the 140°E line. Deeper earthquakes at depths from 60 to 80 km beneath the middle part of Chiba Prefecture show an elongated area along the E-W striking plane.

Ten active regions (A to J) are defined based on the epicenter maps

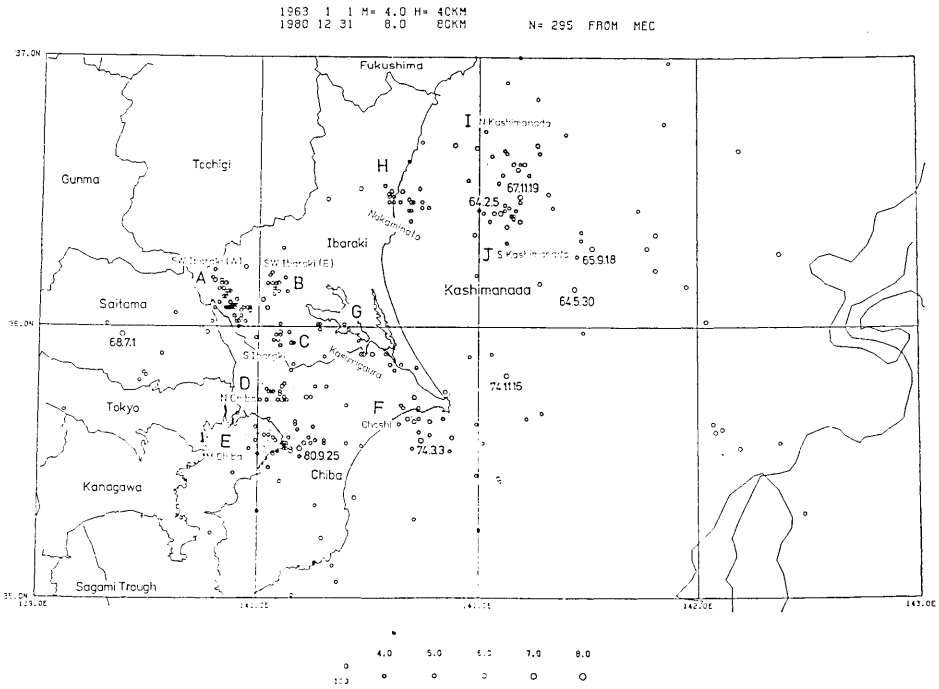

Fig. 4. Locations of intense clusters of subcrustal hypocenters in the Kanto District: A. western side of the 140°E line in the southwestern part of Ibaraki Prefecture (SW Ibaraki W), B. eastern side of the 140°E line in the southwestern part of Ibaraki Prefecture (SW Ibaraki E), C. southern part of Ibaraki Prefecture (S Ibaraki), D. northern part of Chiba Prefecture (N Chiba), E. middle part of Chiba Prefecture (M Chiba), F. near Choshi (Choshi), G. near Kasumigaura Lake and along Tonegawa River (Kasumigaura), H. near Nakaminato (Nakaminato), I. northern Kashimanada (N Kashimanada), and J. southern Kashimanada (S Kashimanada). Features of the hypocenter clusters are summarized in Table 1.

by referring to the earthquake nests by USAMI and WATANABE (1977). Their locations and features in the hypocenter distributions are summarized in Table 1 and are shown by shaded areas in Fig. 4, with subcrustal earthquakes at depths from 40 to 80 km with magnitudes of 4.0 or more. The dates of occurrence for these earthquakes are shown in this figure. Some isolated earthquakes with the larger magnitudes are separated from these active regions, as the Saitama Earthquake on Jul. 1, 1968 (M 6.1), and earthquakes east off Ibaraki Prefecture on Sep. 18, 1965 (M 6.7); May 30, 1964 (M 6.2) and Nov. 16, 1974 (M 6.1).

Depth distributions of the relocated hypocenters are shown for several sections around the active regions beneath the western part of Ibaraki and Chiba Prefectures. Hypocenters used here are limited to those relocated using 10 or more travel-time data. Fig. 5 shows the E-W section (30 km width) between points A (139.7°E, 36.1°N) and B (140.3°E, 36.1°N) beneath the southwestern part of Ibaraki Prefecture. Hypocenters located on the western side of the 140°E line show an inclined pattern to the west, but the ones on the eastern side show a rather vertical alignment. Fig. 6 shows the E-W section (20 km width) between points A (139.9°E, 35.6°N)

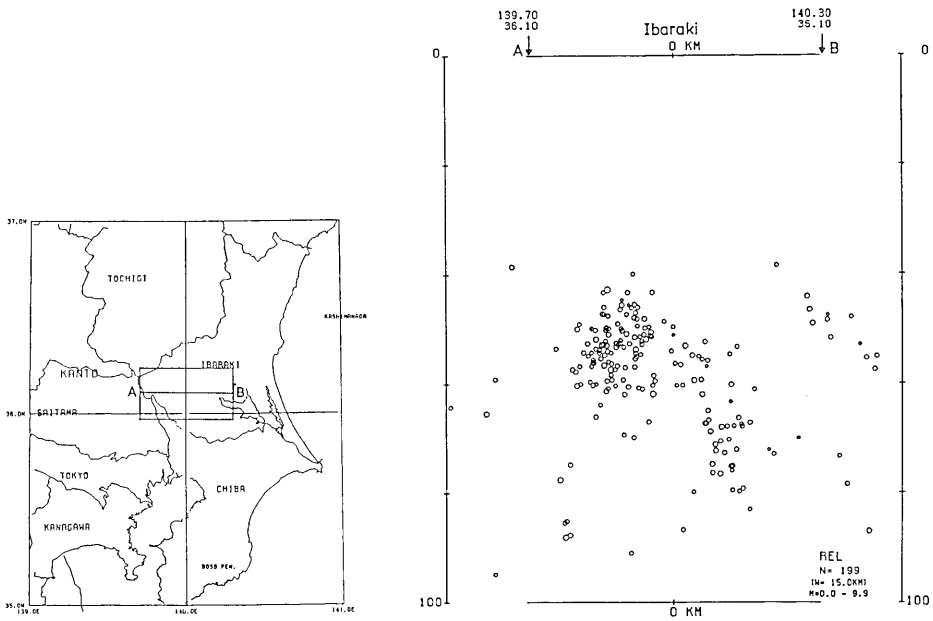

Fig, 5. Depth distribution of the relocated hypocenters along the E-W section (30 km width) between points A (139.7°E, 36.1°N) and B (140.3°E, 36.1°N) beneath the southwestern part of Ibaraki Prefecture. Location of the section is shown on the left.

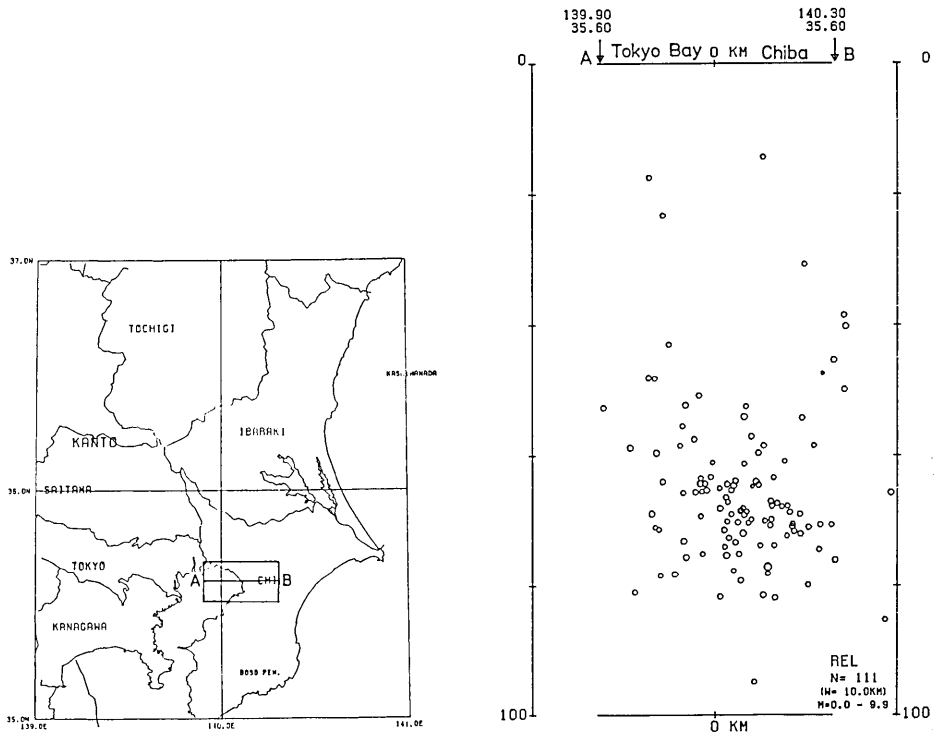

Fig. 6. Depth distribtion of the relocated hypocenters along the E-W section (10 km width) between points A (139.9°E, 35.6°N) and B (140.3°E, 35.6°N) beneath the middle part of Chiba Prefecture.

and B (140.3°E, 35.6°N) beneath the middle part of Chiba Prefecture. An inclined pattern towards the west can not be observed for this section. The relative location of the hypocenter cluster beneath the middle part of Chiba Prefecture seems to be identical to the one beneath the eastern side of the 140°E line due to the same depth and the vertical alignment in the spatial distribution. Fig. 7 shows the N-S section (50 km width) between points A (140.0°E, 36.5°N) and B (140.0°E, 35.5°N) beneath the western part of Ibaraki and Chiba Prefectures. A northward plunging of the seismic zone is observed at the shallower depths from 40 to 60 km beneath the southwestern part of Ibaraki Prefecture. Earthquakes located at the deeper part from 50 to 80 km did not show such an inclined pattern, but a concentration at depths from 60 to 75 km. Fig. 8 shows the depth distribution of hypocenters along the E-W section (30 km width) between points A (140.9°E, 36.6°N) and B (141.3°E, 36.6°N) beneath the northern part of Kashimanada. Hypocenters along this section show a very thin seismic zone of 10 km inclined slowly to the west.

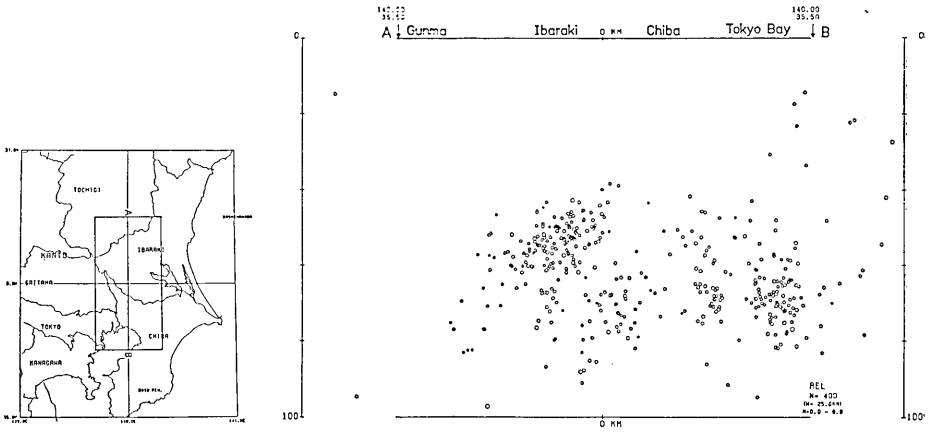

Fig. 7. Depth distribution of the relocated hypocenters along the N-S section (50 km width) between points A (140.0°E, 36.5°N) and B (140.0°E, 35.5°N) beneath the southwestern part of Ibaraki Prefecture and the middle part of Chiba Prefecture.

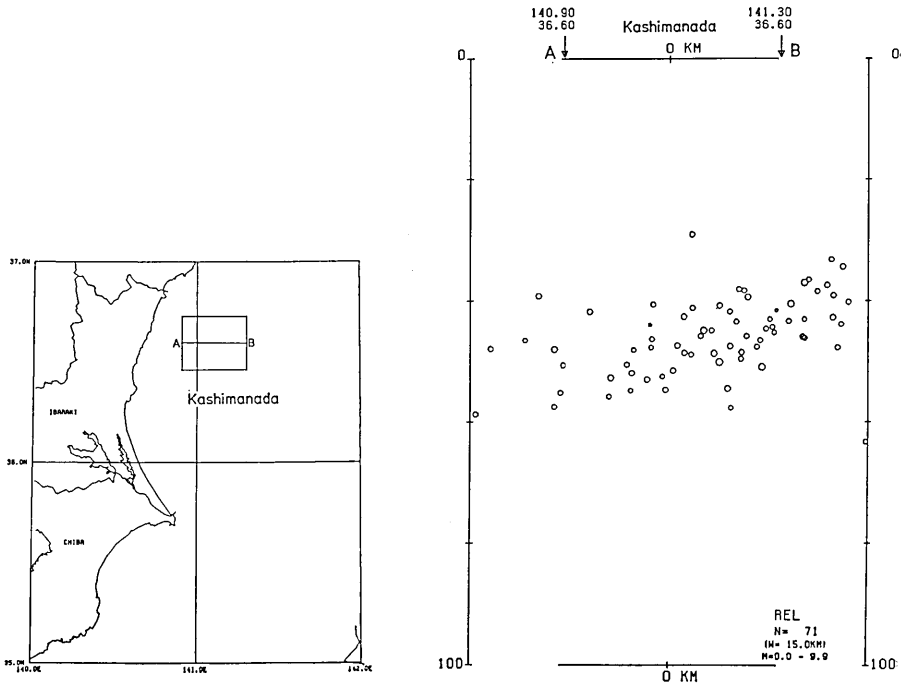

Fig. 8. Depth distribution of the relocated hypocenters along the E-W section (30 km width) between points A (140.9°E, 36.6°N) and B (141.3°E, 36.6°N) beneath the northern part of Kashimanada, east off Ibaraki Prefecture.

Clusters of subcrustal earthquakes at some locations and depths are observed from the relocated hypocenters. These clusters of hypocenters show a northwest linear alignment of epicenters of earthquakes which occurred at depths from 40 to 60 km beneath the western end of Ibaraki Prefecture, the vertical alignment of hypocenters at depths from 50 to 80 km on the eastern side of the 140°E line beneath the southwestern part of Ibaraki Prefecture and the northern and middle part of Chiba Prefecture, and a slowly dipping seismic zone east off Ibaraki Prefecture.

3. Determination of fault-plane solutions of subcrustal earthquakes

In the previous study focal mechanisms were determined by a reference method for earthquakes which occurred beneath the Kanto District during the period from June of 1971 to March of 1977 (MAKI *et al.*, 1980). Differences or similarities of focal mechanisms between earthquakes or source regions were not derived sufficiently in an objective sense. Recently problems in the trial-and-error graphical methods for mechanism determination have been solved by a new numerical method (MAKI, 1982b). Observed first-motion data of P wave are compared with the theoretical radiation pattern for numerous tentative sets of principal axes (P and T), which are homogeneously arranged on the focal sphere. Inconsistent data for more probable sets of P and T axes with scores over 75% are summarized for individual stations. By discarding stations with less reliability the most probable solutions with scores of 95% or more are obtained. The tentative sets (n=6156) of principal axes are made for intervals of 10° for azimuth and dip angles. For cases with too many possible solutions larger intervals of 15° are again used for azimuth and dip angles (n=2275). By the numerical method multiple solutions can be obtained even if located separately from others. Various possible solutions are selected for cases with too many solutions.

Fault-plane solutions satisfying 10 or more first-motion data are adopted in the present study. For earthquakes which occurred at depths from 40 to 80 km with magnitudes of 5.0 or more during the period from 1963 to 1979, fault-plane solutions have been obtained for 154 earthquakes (MAKI, 1983d) from the first-motion data of BISC (Bulletin of the International Seismological Centre), ISS (International Seismological Summary) and JMA. But useful solutions were not obtained for the following three earthquakes with magnitudes of 5 or more which occurred on (1) Apr. 25, 1963 (20h19m 19.4s, 31.68°N, 141.16°E, h=50.4 km, M 5.0), (2) Sep. 11, 1965 (14h21m20.6s,

33.98°N, 139.00°E, h=6.2 km, M 5.0) and (3) Jun. 26, 1974 (02h39m56.3s, 34.56°N, 141.16°E, h=78.6 km, M 5.2).

In the present study solutions of focal mechanism are obtained for subcrustal earthquakes which occurred in 1980 and with magnitudes down to 4.0 using the first-motion data from BISC (the first-motion data are compiled for earthquakes from 1971 to 1978 in a magnetic tape). Fault-plane solutions (n=704), which satisfy the first-motion data of 10 or more with scores of 95% or more are obtained for 487 out of 1029 subcrustal earthquakes which occurred during the period from 1963 to 1980 with magnitudes of 4.0 or more. Forty-nine earthquakes are excluded due to the less than 10 bits of first-motion data satisfying solutions. In these fault-plane solutions the orthogonal relation between the principal axes and poles of nodal planes are held within 0.25°, except the following three earthquakes which have a difference of angular distance larger than 0.25° but smaller than 0.30° from the orthogonal relation, (1) Apr. 5, 1964 (10h44m49s, 36.16°N, 140.04°E, h=54.8 km, M 4.9), (2) Mar. 2, 1968 (09h40m 55s, 35.66°N, 140.73°E, h=59.5 km, M 4.7) and (3) Sep. 25, 1980 (02h59m48s, 35.57°N, 140.21°E, h=68.0 km, M 5.3).

Alternative solutiohs should be also adopted for some earthquakes due to many possible solutions which are distributed over a wide region or which are separately located. Confidence regions of fault-plane solutions are shown by the equal-area projection on the left-hand side of Fig. 9 for an earthquake which occurred directly beneath the Japan Trench on Feb. 28, 1967, (h=76.3 km, M 5.3; number of first-motion data n=39). Scores of 95% or more are obtained for 286 tentative solutions. Another solution of strike-slip (Fig. 9d) is also possible besides the vertical slip along the N-S plane (Fig. 9b, c). *T* axes are located in a small area striking north-west, but P and N axes are mixed. Multiple solutions are also given for an earthquake which occurred beneath the Japan Trench near the Boso triple junction on Mar. 13, 1972 (h=44.1 km, M 5.7; Fig. 10; n=100). For this earthquake principal axes (P and T) are not mixed, but each axis shows a large possible area.

Some types of focal mechanism will be shown for some earthquakes. Fig. 11 shows a thrust type of focal mechanism with the horizontal NW-SE compression for an earthquake which occurred beneath the middle part of Chiba Prefecture on Sep. 25, 1980 (h=77.0 km, M 6.1). Fig. 12 shows another type of thrust with the horizontal N-S compression for an earthquake which occurred beneath the western end of Ibaraki Prefecture on Aug. 4, 1974 (h=42.8 km, M 5.8). These earthquakes have nearly vertical T axes and variable azimuths of P axes. Fig. 13 shows a normal fault

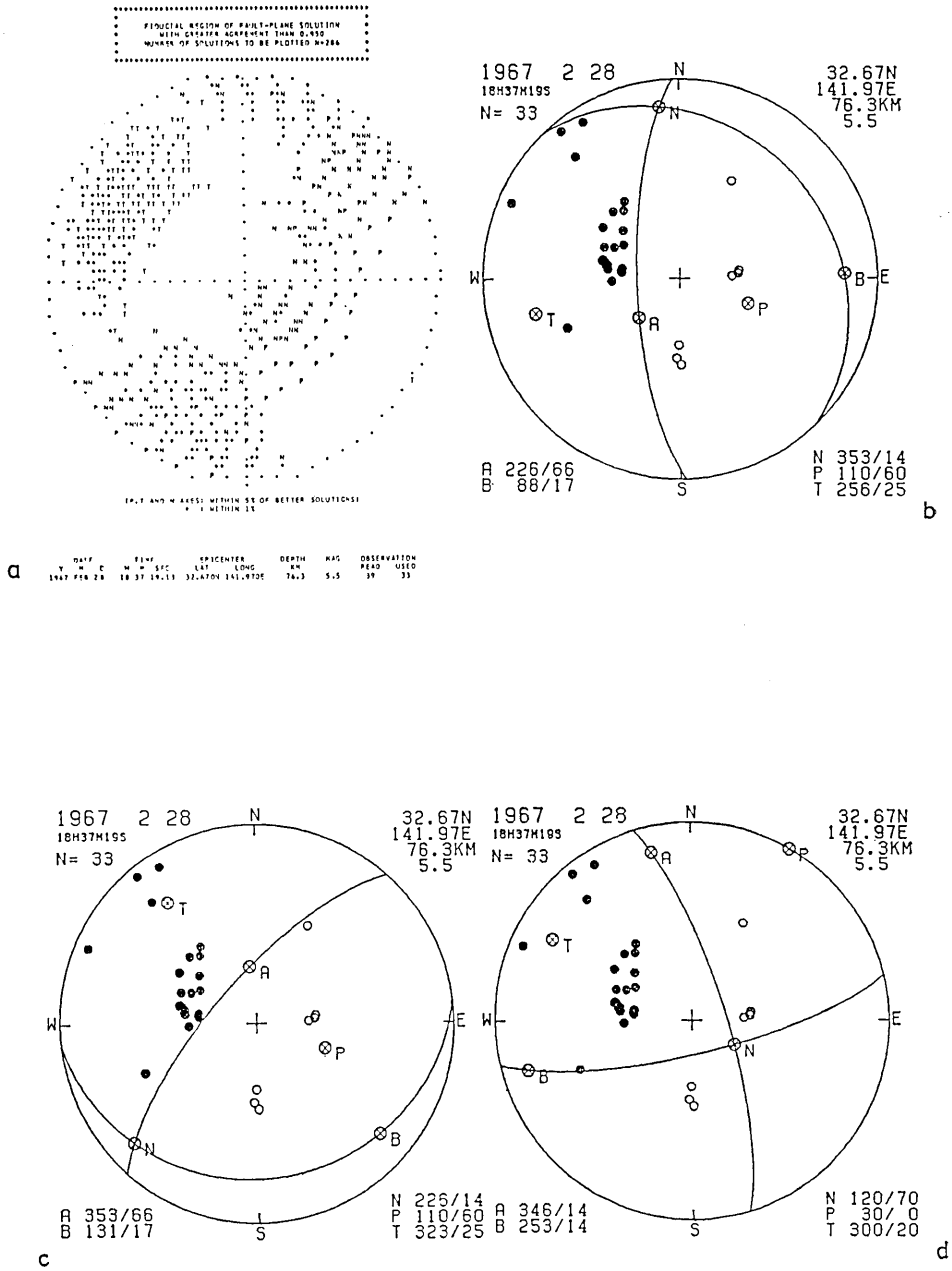

Fig. 9. Confidence region of fault-plane solutions (a) and multiple solutions (b to d) for a subcrustal earthquake which occurred on Feb. 28, 1967, beneath the Izu-Bonin Trench (h=76.3 km, M5.5) with a lower number of first-motion data (n=33). Solutions for axes of maximum pressure and tension and null vector with scores greater than 99% are shown by asterisks ("*") and with scores from 95 to 99% by letters "P", "T" and "N". Empty and solid circles denote first motions of dilatation and compression. Multiple solutions (b to d) are equally possible with the same score.

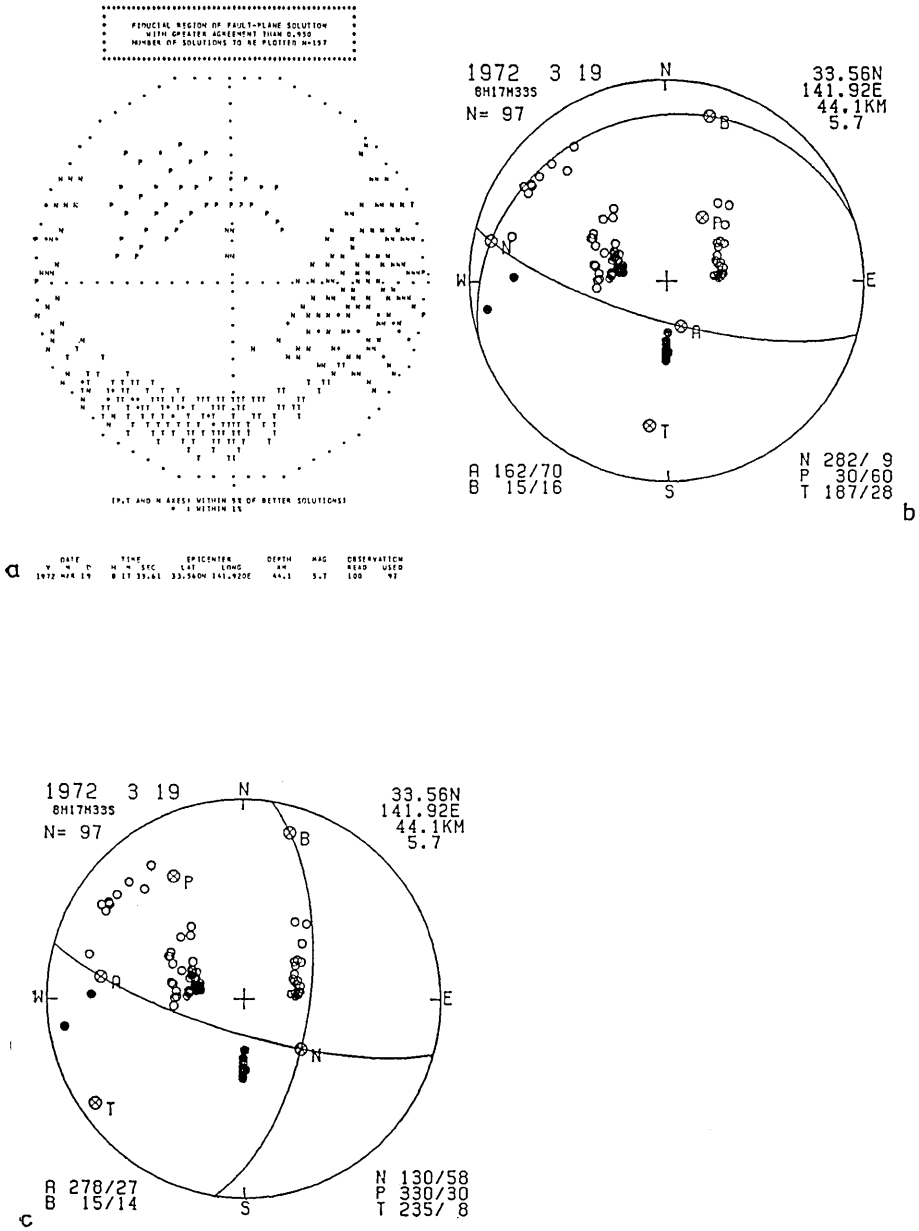

Fig. 10. Confidence region of fault-plane solutions (a) and two multiple solutions (b and c) for a subcrustal earthquake which occurred on Mar. 19, 1972 south of the Boso triple junction (h=44.1 km, M5.7) with a number of first-motion data (n=97).

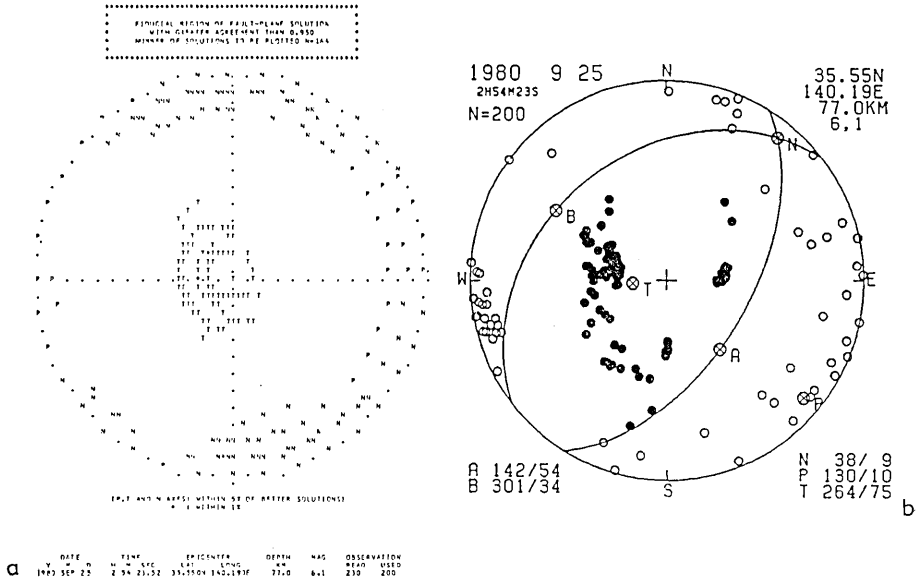

Fig. 11. Confidence region of fault-plane solutions (a) and the best-suited solution of the reverse fault with the NW-SE compression (b) for a subcrustal earthquake which occurred on Sep. 25, 1980 beneath the middle part of Chiba Prefecture (h=77.0 km, M6.1).

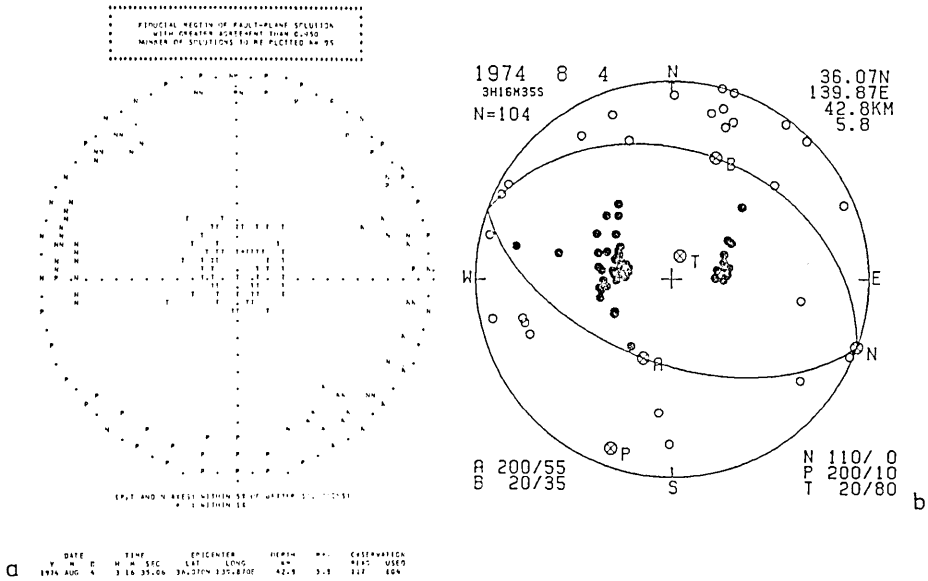

Fig. 12. Confidence region of fault-plane solutions (a) and the best-suited solution of the reverse fault with the nearly N-S compresion (b) for a subcrustal earthquake which occurred on Aug. 4, 1974 beneath the western end of SW Ibaraki Prefecture (h=42.8 km, M5.8).

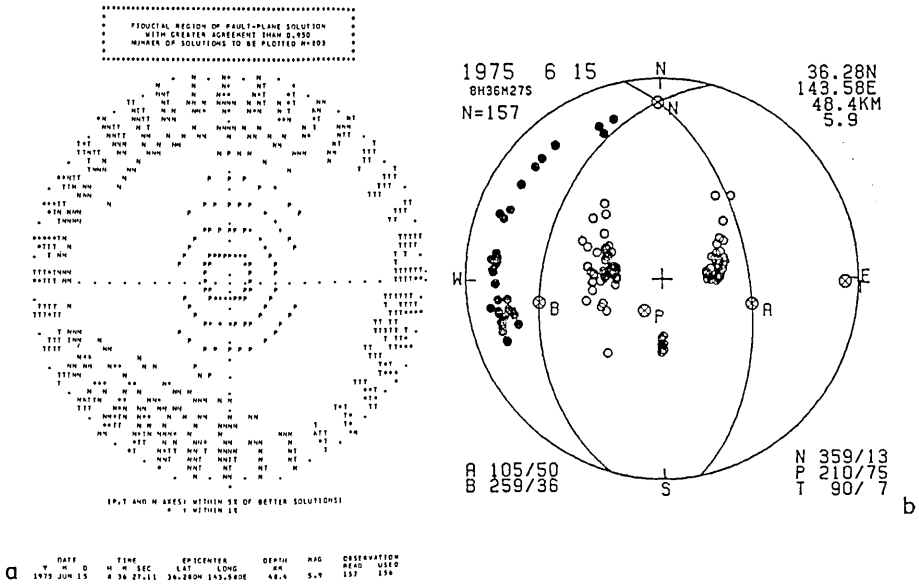

Fig. 13. Confidence region of fault-plane solutions (a) and the best-suited solution of the normal fault with the horizontal E-W extension (b) for a subcrustal earthquake which occurred on June 15, 1975 outside the Japan Trench (h=48.4 km, M5.9).

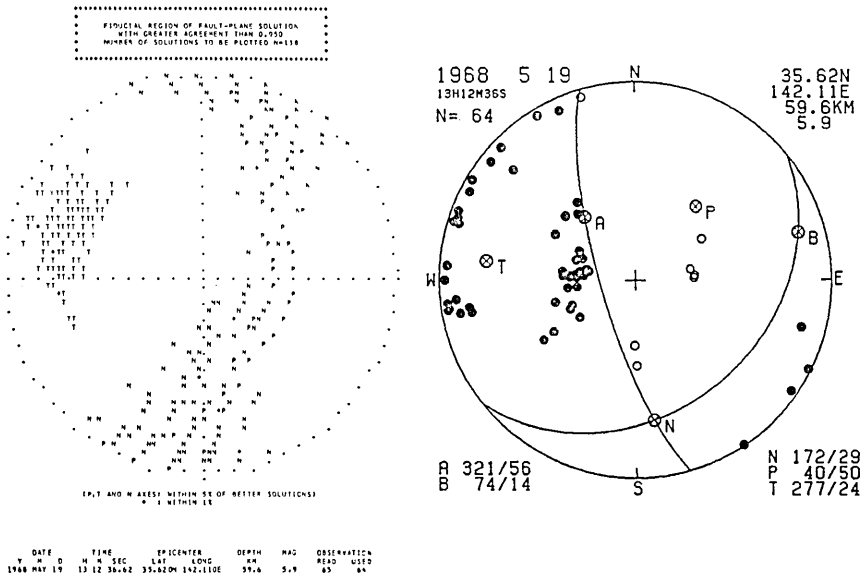

Fig. 14. Confidence region of fault-plane solutions (a) and the best-suited solution of the western side sinking along the vertical N-S plane (b) for a subcrustal earthquake which occurred on May 19, 1968 directly inside the Japan Trench (h=59.6 km, M5.9).

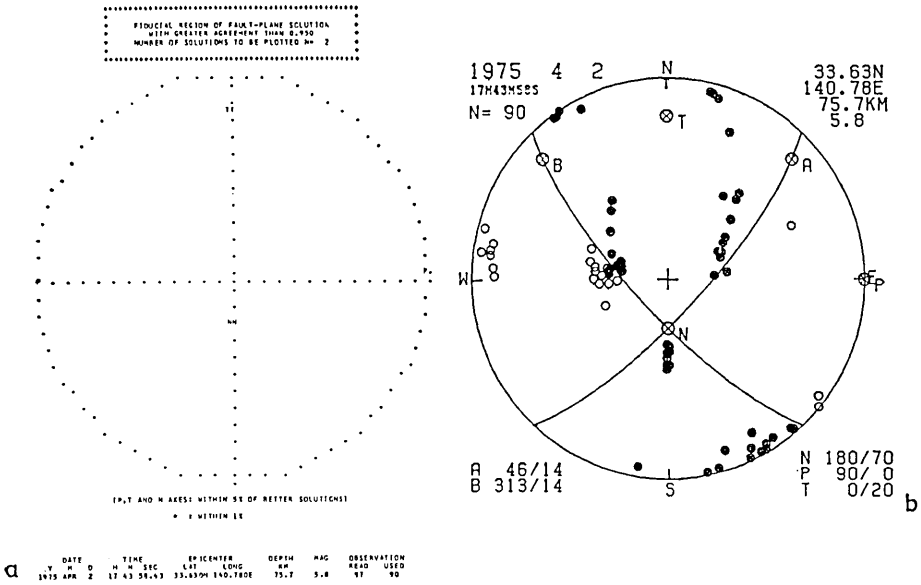

Fig. 15. Confidence region of fault-plane solutions (a) and the best-suited solution of the strike-slip with the E-W compression (b) for a subcrustal earthquake which occurred on Apr. 2, 1975 south of the Boso triple junction (h=75.7 km, M5.8).

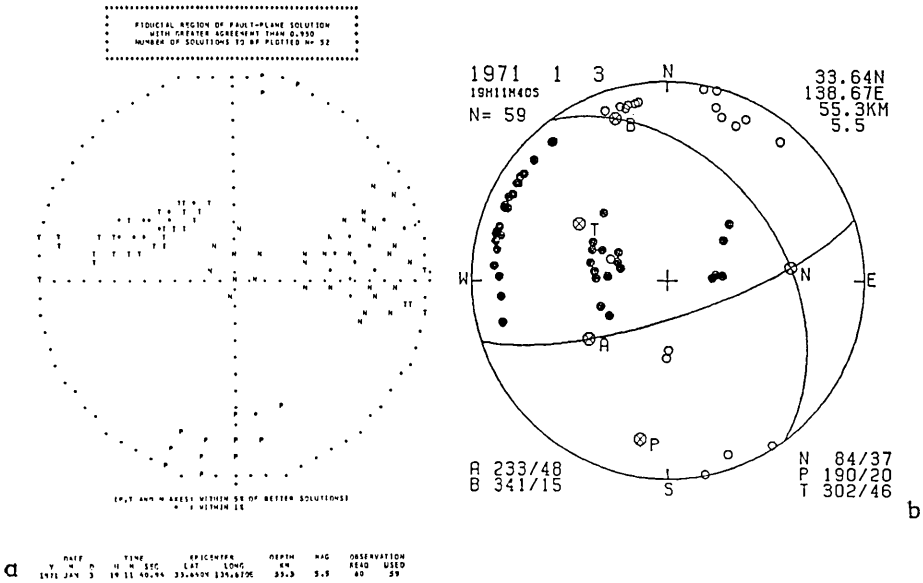

Fig. 16. Confidence region of fault-plane solutions (a) and the best-suited solution of the strike-slip with the E-W extension (b) for a subcrustal earthquake which occurred on Jan. 3, 1971 west of Hachijojima Island (h=55.3 km, M5.5).

with the horizontal E-W extension for an earthquake which occurred seawards from the Japan Trench on June 15, 1975 (h=48.4 km, M 5.9). Fig. 14 shows a solution with the vertical nodal plane striking N-S for an earthquake which occurred on the land side directly near the Japan Trench on May 19, 1968 (h=59.5 km, M 5.9). These types of focal mechanisms denote the compound process of the outward bending and detachment of the Pacific Plate around the Japan Trench. A strike-slip with the E-W compression is uniquely determined (Fig. 15) for an earthquake which occurred near the Boso triple junction on Apr. 2, 1975 (h=75.7 km, M 5.8). Fig. 16 shows a strike-slip with an E-W extension for an earthquake which occurred behind the Izu-Bonin Islands on Jan. 3, 1971 (h=55.3 km, M 5.5).

Fault-plane solutions of subcrustal earthquakes are listed in the Appendix. Origin times, epicenters and focal depths are redetermined by correcting the JMA travel times with the Pn station biases (MAKI, 1981a).

Table 2. Number of earthquakes which are relocated, whose focal mechanism are determined in the present study and published in the ICHIKAWA-JMA catalogues.

year	earthquakes relocated	mechanism in this study	Ichikawa-JMA catalogue
1963	39	4	3
1964	66	26	5
1965	60	20	7
1966	61	29	3
1967	59	26	8
1968	63	20	3
1969	52	16	3
1970	50	22	10
1971	63	25	11
1972	87	42	22
1973	71	37	20
1974	71	26	18
1975	52	26	8
1976	30	19	10
1977	45	36	24
1978	97	48	11
1979	41	27	10
subtotal	1007	449	176
1980	22	38	not published
total	1029	487	176

Angles in the solutions are denoted in the unit of tenths of a degree for the orthogonal relation of poles of nodal planes. Numbers of first-motion data are also given in the last two columns for the read (all) and used ones. Table 2 summarizes the annual numbers of earthquakes, (a) relocated by MAKI (1981a), (b) for which fault-plane solutions can be obtained in the present study, and (c) included in the Ichikawa and JMA catalogues. Fault-plane solutions in the present study are obtained for 45% of the subcrustal earthquakes (n=1029) which occurred at depths from 40 to 80 km during the period of 17 years from 1963 to 1979. The number of earthquakes in the present study amounts to the 2.8 times more than the earthquakes in the Ichikawa and JMA catalogues. Some fault-plane solutions in the Ichikawa and JMA catalogues are determined by a fewer number of first-motion data than in the present study, as for earthquakes which occurred on Sep. 18, 1965 (M 6.7); Nov. 19, 1967 (M 6.0); Dec. 4, 1972 (M 7.2) and Feb. 20, 1978 (M 6.7).

Fig. 17 shows a summary of 704 fault-plane solutions for 487 subcrustal earthquakes including multiple solutions. Principal axes (P, T and N) are denoted by empty and solid circles and crosses on the left-hand

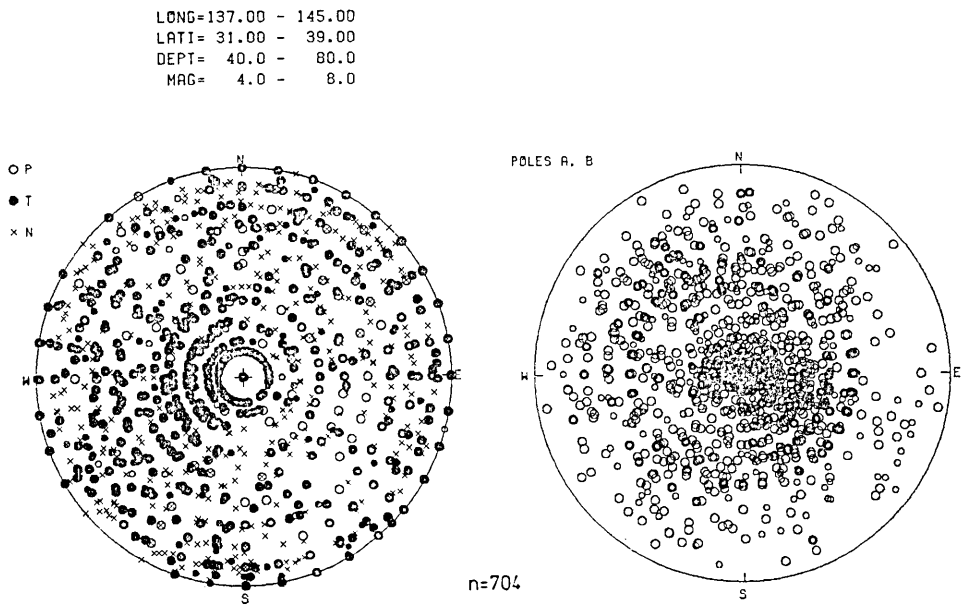

Fig. 17. Summary of fault-plane solutions (n=704) for subcrustal earthquakes (n=487) in the Kanto District and vicinity, (a) principal axes on the left-hand side by empty and solid circles and by crosses for P, T ahd N axes, and (b) poles of nodal planes on the right-hand side. Multiple solutions are shown by smaller symbols.

side, and poles of nodal planes on the right-hand side. Although a variety of focal mechanisms are observed, the nearly vertical T axes plunging to the west and the vertical pole are predominant.

4. Spatial variation of focal mechanisms of subcrustal earthquakes

Focal mechanisms of earthquakes in and around the Kanto District show the regional variations (MAKI *et al.*, 1980; MAKI, 1981b, 1983a, b, d, 1984), and these variations are caused by the complicated process of the plate convergence and intersection of the arc systems. The subcrustal earthquakes beneath the Kanto District especially show the intense clusters of hypocenters at certain depths and locations. The intense clusters of hypocenters at depths around 60 km beneath Ibaraki and Chiba Prefectures have been interpreted by the collision of the Philippine Sea Plate with the descending Pacific Plate (MAKI *et al.*, 1978, 1980; MAKI and TSUMURA, 1980; MAKI, 1981b). The intense activity of earthquakes beneath the Kanto District is also interpreted by the acute intersection of the Northeast Honshu and Izu-Bonin slabs (MAKI, 1984). Using a number of fault-plane solutions for subcrustal earthquakes, the spatial variation of focal mechanisms will be derived from individual solutions of the larger earthquakes and from the classified types of fault-plane solutions with relation to the epicenter and depth distributions of the relocated hypocenters.

The geographical distribution of schematic diagrams of focal mechanisms is shown in Fig. 18 for 27 out of 60 subcrustal earthquakes with magnitudes of 5.5 or more. Representations for other earthquakes are omitted due to their near locations and similar focal mechanisms. Dates of earthquake occurrences are denoted beside the schematic diagrams. Empty and shaded areas denote dilatational and compressional areas of first-motions, respectively. A thrust type of focal mechanism with an almost horizontal NW-SE compression is observed for earthquakes located along the subduction zone of Northeast Honshu on Nov. 19, 1973 and Aug. 15, 1963, east off the Kanto District on Sep. 18, 1965; May 30, 1964; Nov. 16, 1974; Mar. 3, 1974; May 8, 1980; Nov. 19, 1967 and Feb. 5, 1964, and near the Izu-Bonin Trench on Feb. 29, 1972; Dec. 4, 1972 and Nov. 27, 1965. This type of focal mechanism means the relative motion of the Pacific Plate with the Eurasian and Philippine Sea Plates. Another thrust type of focal mechanism with the N-S compression is observed for earthquakes on July 1, 1968 and Aug. 4, 1974 (Fig. 12), which are located within the contact region of the acute intersection of the Notheast Honshu and Izu-

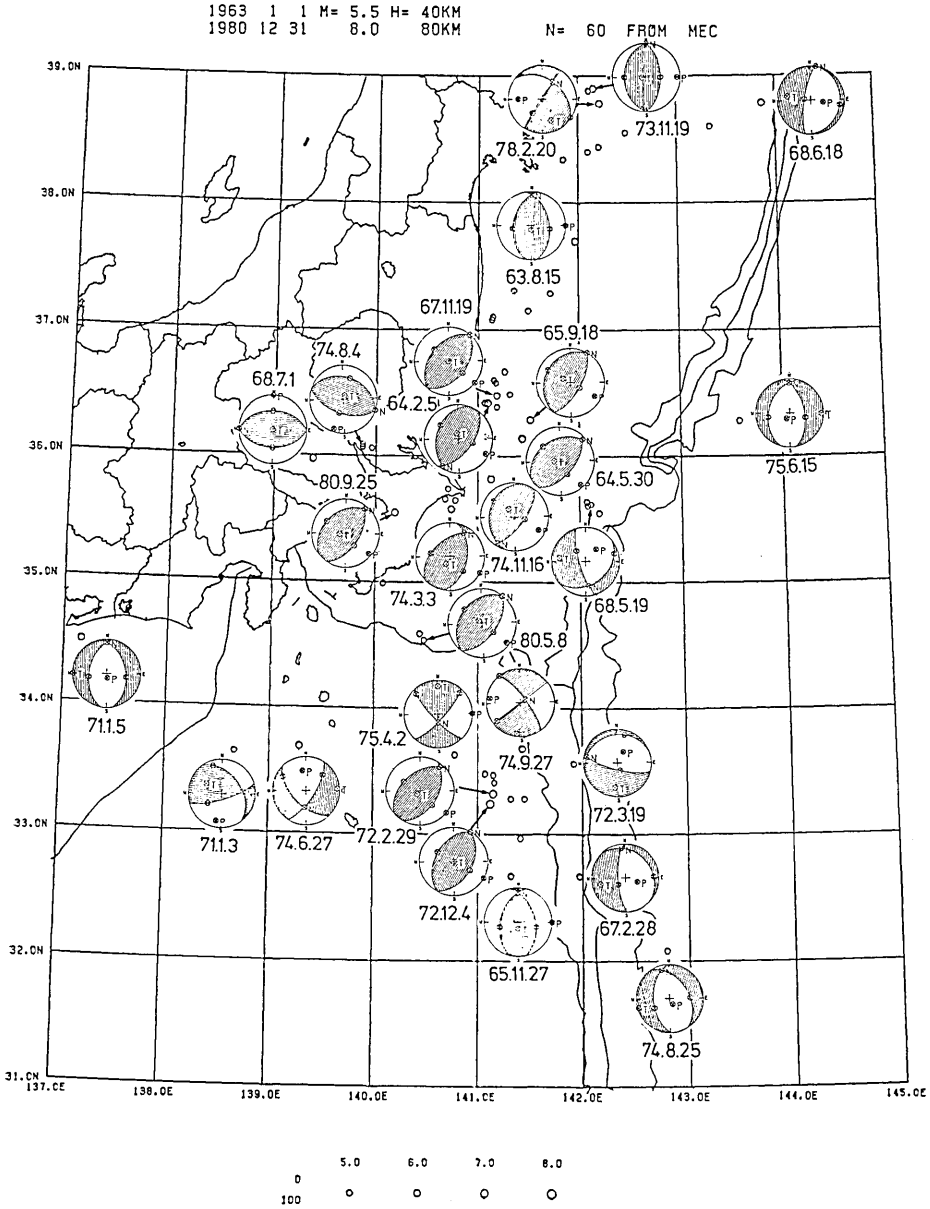

Fig. 18. Regional variation of focal mechnisms for the larger (M≧5.5) subcrustal earthquakes in and around the Kanto District. Focal mechanisms are represented by schematic diagrams of the equal-area projection of lower focal hemisphere. Empty and shaded areas denote dilatational and compressional areas of first motion.

Bonin slabs beneath the Kanto District and vicinity. A thrust type with the horizontal NW-SE compression for an earthquake on Sep. 25, 1980 (Fig. 11) is also noticeable due to its deeper location (h=77.0 km) which is separated from the subduction zone.

A horizontal E-W extension is observed for earthquakes located outside the Japan Trench on Aug. 25, 1974 and June 15, 1975 (Fig 13). This type of focal mechanism is produced by the bending due to the subduction of the Pacific Plate near the trench. The vertical slip with the western side sinking along the trench axis is observed for earthquakes located in the inside directly near the Japan Trench on June 18, 1968; May 19, 1968 (Fig. 14) and for one of the multiple solutions of an earthquake on Feb. 28, 1967 (Fig. 9b). This type of focal mechanism suggests the preference of the detachment due to the weight of the lithospheric plate (KANAMORI, 1971a, b, 1977) to the simple flexture beneath the trench (CHEN and FORSYTH, 1978; CHAPPLE and FORSYTH, 1879). On the other hand a type of transverse slip along the E-W nodal plane perpendicular to the trench axis is observed for an earthquake on Mar. 19, 1972 as one of the multiple solutions (Fig. 10b). Earthquakes on Sep. 27, 1974 and Apr. 2, 1975 (Fig. 15) show a strike-slip with a horizontal E-W compression and they are related to the horizontal relative motion along the Sagami Trough. An E-W extension is observed for earthquakes on June 27, 1974 and Jan. 3, 1971 (Fig. 16) west of Hachijojima Island. Such an E-W extension is related to the process of back-arc spreading (UYEDA and KANAMORI, 1979).

The spatial distribution of focal mechanisms is also discussed from the geographical distribution of mechanism types, which are systematically classified based on azimuths and dip angles of principal axes (P, T and N) as shown in Fig. 19. Reverse faults are identified by angles of T axes steeper than 45°, and they are separated into two types based on azimuths of P axes, namely the NW-SE and NE-SW compression. The reverse faults are predominantly observed for 409 (55%) of 704 total solutions, and most of these types (n=283, 70%) are produced by the NW-SE compression. The predominance of reverse faults are noticeable in comparison to other ranges of focal depths, such as the strike-slips for crustal earthquakes (MAKI, 1983a, b), normal faults of the "down-dip compression" for the mantle earthquakes (MAKI, 1983d) and the normal faults and strike-slips for the intermediate-depth earthquakes (MAKI, 1984). For the subcrustal earthquakes the normal faults are observed for 122 solutions, which are equally separated into two types with the NW-SE and NE-SW extension. Strike-slips are observed for 154 solutions which are equally classified into two types with NW-SE and NE-SW compressions. The epicenter

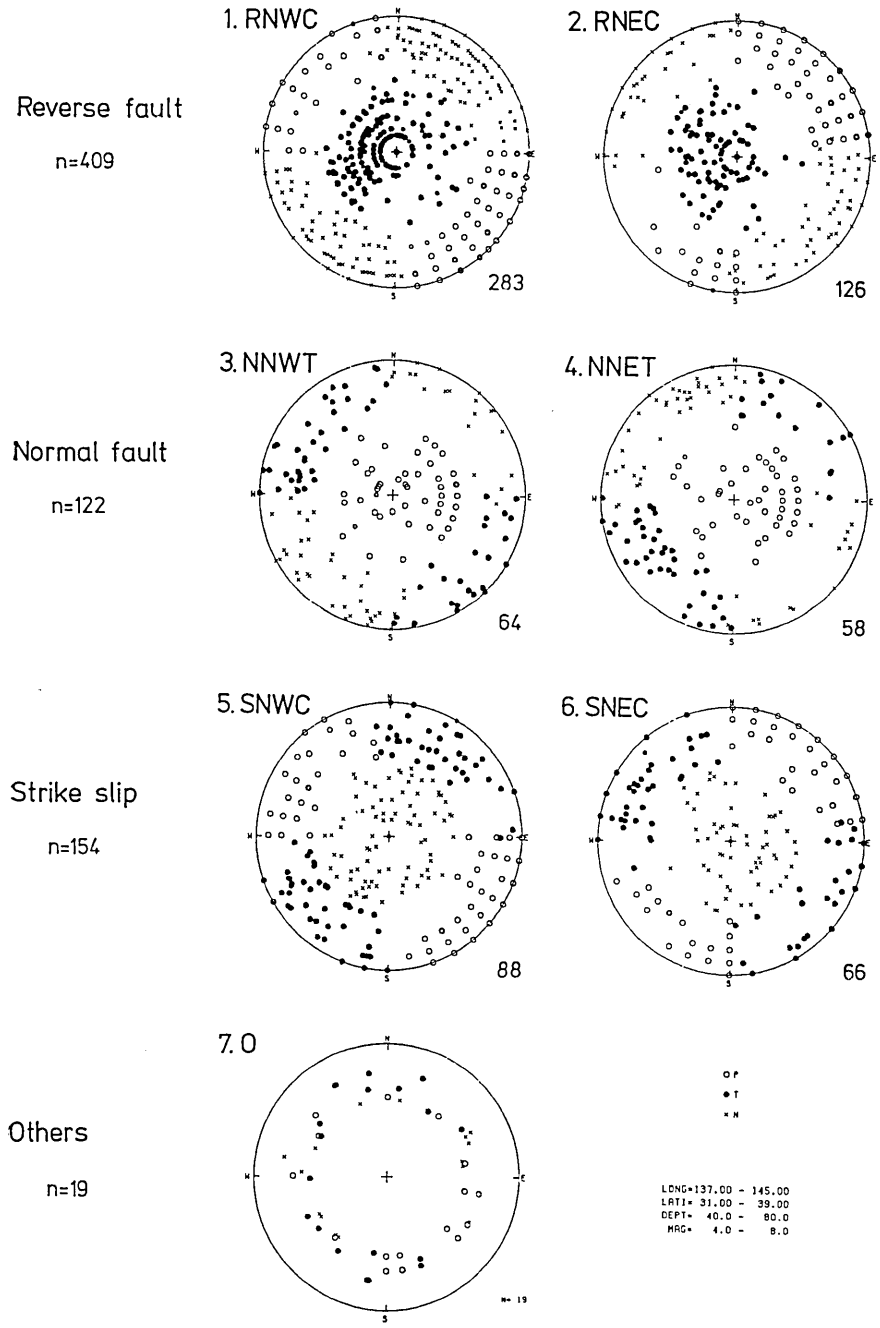

Fig. 19. Classification of fault-plane solutions into seven types: (1) RNWC: reverse fault with a NW-SE compression (n=283), (2) RNEC: reverse fault with a NE-SW compression (n=126), (3) NNWT: normal fault with a NW-SE extension (n=64), (4) NNET: normal fault with a NE-SW extension (n=58), (5) SNWC: strike-slip with a NW-SE compression (n=88), (6) SNEC: strike-slip with a NE-SW compression (n=66), and (7) O: others (n=19). Types of reverse and normal faults and strike-slips are systematically classified based on dip angles of P, T and N axes, and each type is separated into two types by azimuths of P and T axes.

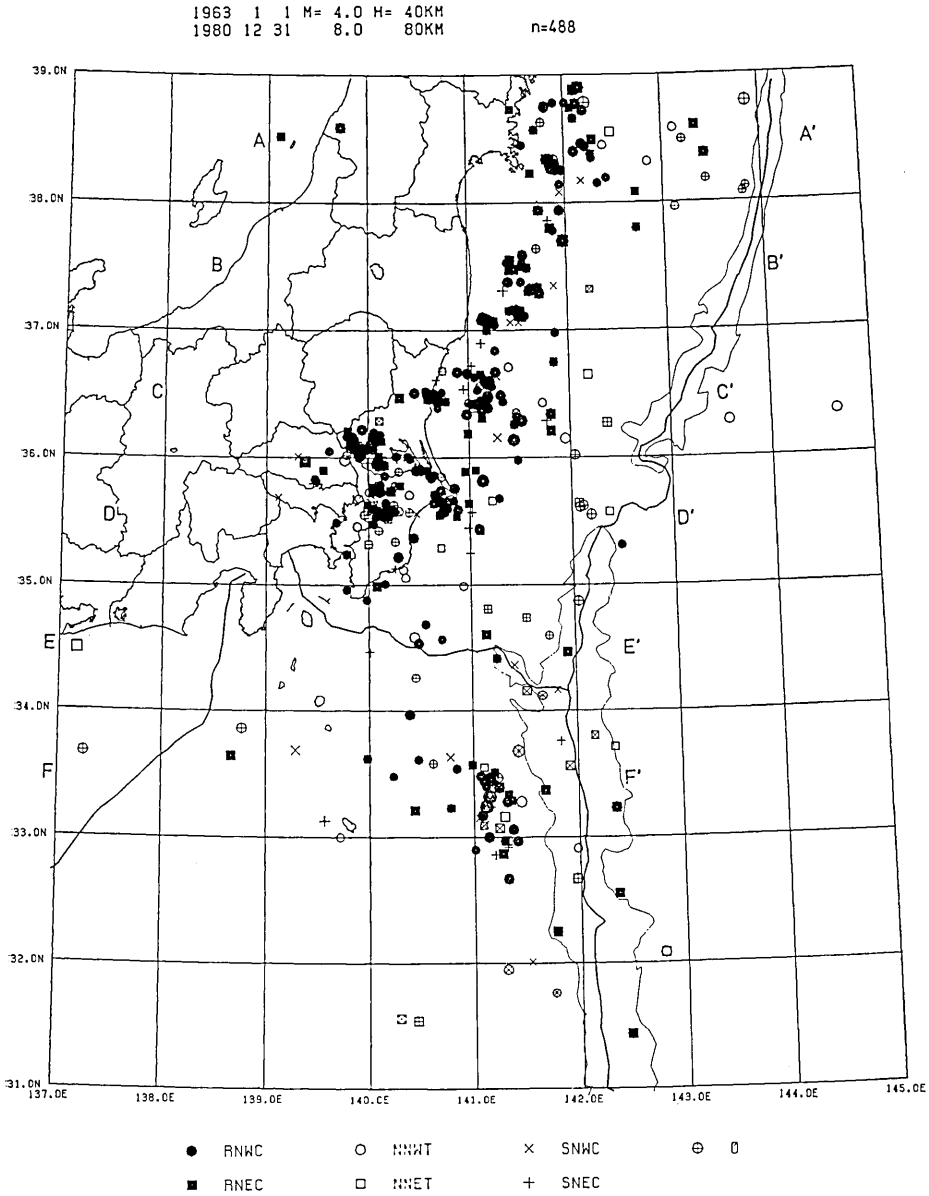

Fig. 20. Geographical distribution of fault types of subcrustal earthquakes. Solid and empty circles and crosses denote reverse and normal faults and strike-slips, respectively. Circles and squares for reverse and normal faults show azimuths of NW-SE and NE-SW for P or T axes, and strike-slips are also separated by azimuths of P axes. Epicenters for earthquakes with multiple solutions are shown by duplicated symbols.

distribution of mechanism types is shown in Fig. 20. Solid, empty and cross symbols denote reverse and normal faults and strike-slips, and two types with variable azimuths of P or T axes are denoted by circles and squares for reverse or normal faults. Reverse faults are predominantly observed along the coastal region on the Pacific side of Northeast Japan and the Kanto District, and normal faults are seen near the Japan Trench. Some earthquakes of the strike-slip tend to be located in front of the descending slab.

Depth distributions of mechanism types along the E-W sections are shown in Fig. 21 for only hypocenters at depths from 40 to 80 km. Equal-area projections of the northern focal hemisphere are also shown for only the relatively large earthquakes by schematic diagrams. Hatched and empty areas denote dilatational and compressional areas of first-motion. Mechanism types are shown by the same symbols used in Fig. 20. The reverse faults are predominantly observed along the inclined seismic zone (Fig. 21c, d). The E-W extension is observed for an earthquake which occurred on June 18, 1968 beneath the Japan Trench (arrowheads in Fig. 21a). Another type of the E-W extension is also observed for earthquakes on June 27, 1974 in the back-arc region of the Izu-Bonin Islands (Fig. 21e, f) and an earthquake off the Aichi Prefecture on Jan. 5, 1971. The strike-slip is observed for earthquakes located within the descending slab on Feb. 20, 1978 (Fig. 21a) and Sep. 27, 1974 (Fig. 21f).

The thrust type of focal mechanism along the upper boundary of the inclined seismic zone is predominant for subcrustal earthquakes along the coastal region on the Pacific side of Northeast Japan and the Kanto District. The thrust type of focal mechanism is also observed for earthquakes far east of Hachijojima Island along the Izu-Bonin Trench. Different relative locations of active regions from the trench axis and different levels of earthquake activity are observed between Northeast Japan and the Izu-Bonin Islands. These contrasts can be interpreted by the difference in the coupling of the Pacific Plate with the overriding plates (UYEDA and KANAMORI, 1979). The intense clusters of earthquakes beneath the Kanto District are located within the intesecting region of the Northeast Honshu and Izu-Bonin slabs (MAKI, 1984).

Two types of focal mechanisms near the Japan Trench, namely the horizontal E-W extension outside the Japan Trench and the vertical slip with the western side sinking along the N-S plane inside the Japan Trench, suggest the subduction process which consists of the bending before the trench and the vertical failure of the lithospheric slabs directly beneath the trench axis. The process of back-arc spreading in the Izu-Bonin Islands

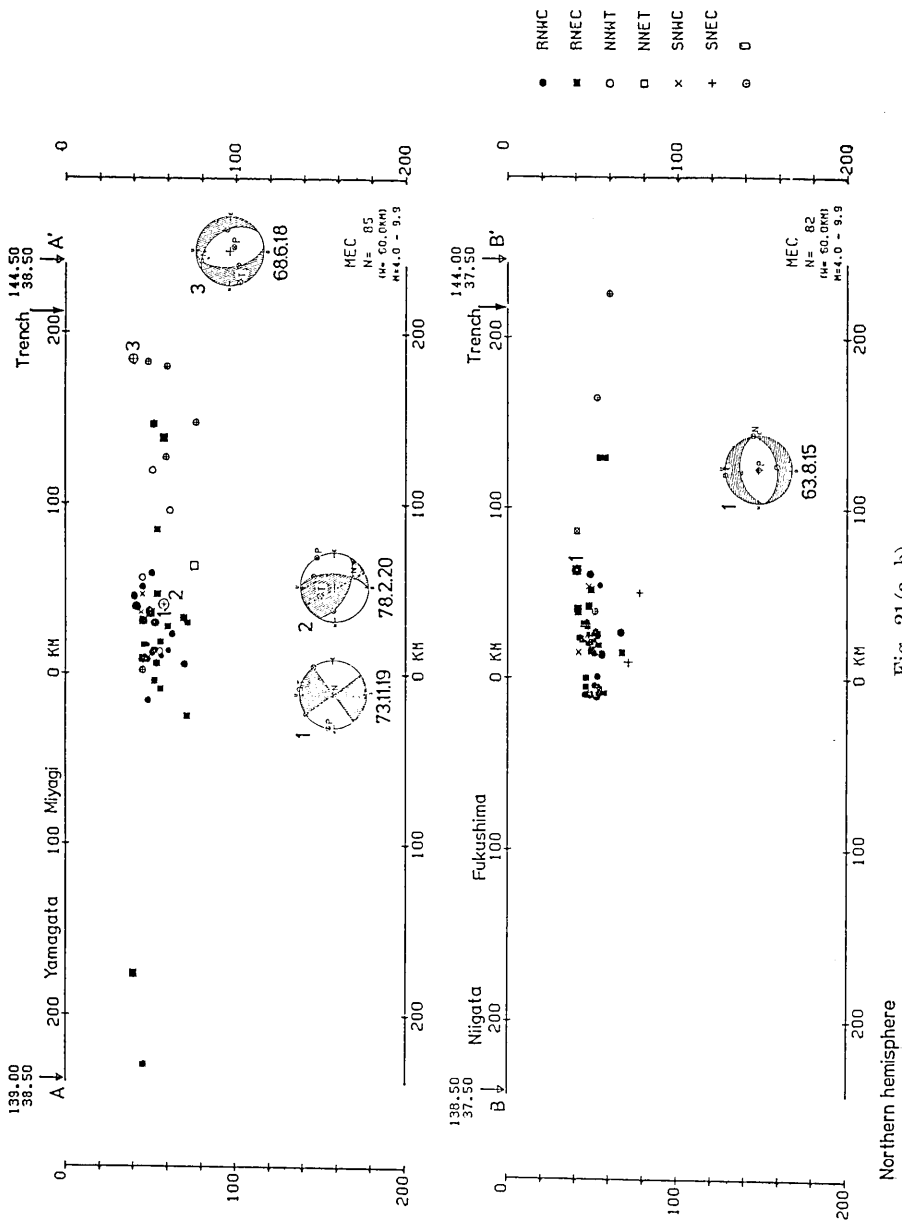
RNHC
RNEC
NNHT
NNET
SNHC
SNEC
Trench
144.50
38.50
A'
A
139.00
38.50
Yamagata
Miyagi
0 KM
MEC
N= 85
(H= 60.0KM)
M=4.0 - 9.9
68.6.18
73.11.19
78.2.20
Trench
144.00
37.50
B'
B
138.50
37.50
Niigata
Fukushima
MEC
N= 82
(H= 60.0KM)
M=4.0 - 9.9
63.8.15
Northern hemisphere

Fig. 21 (a, b)

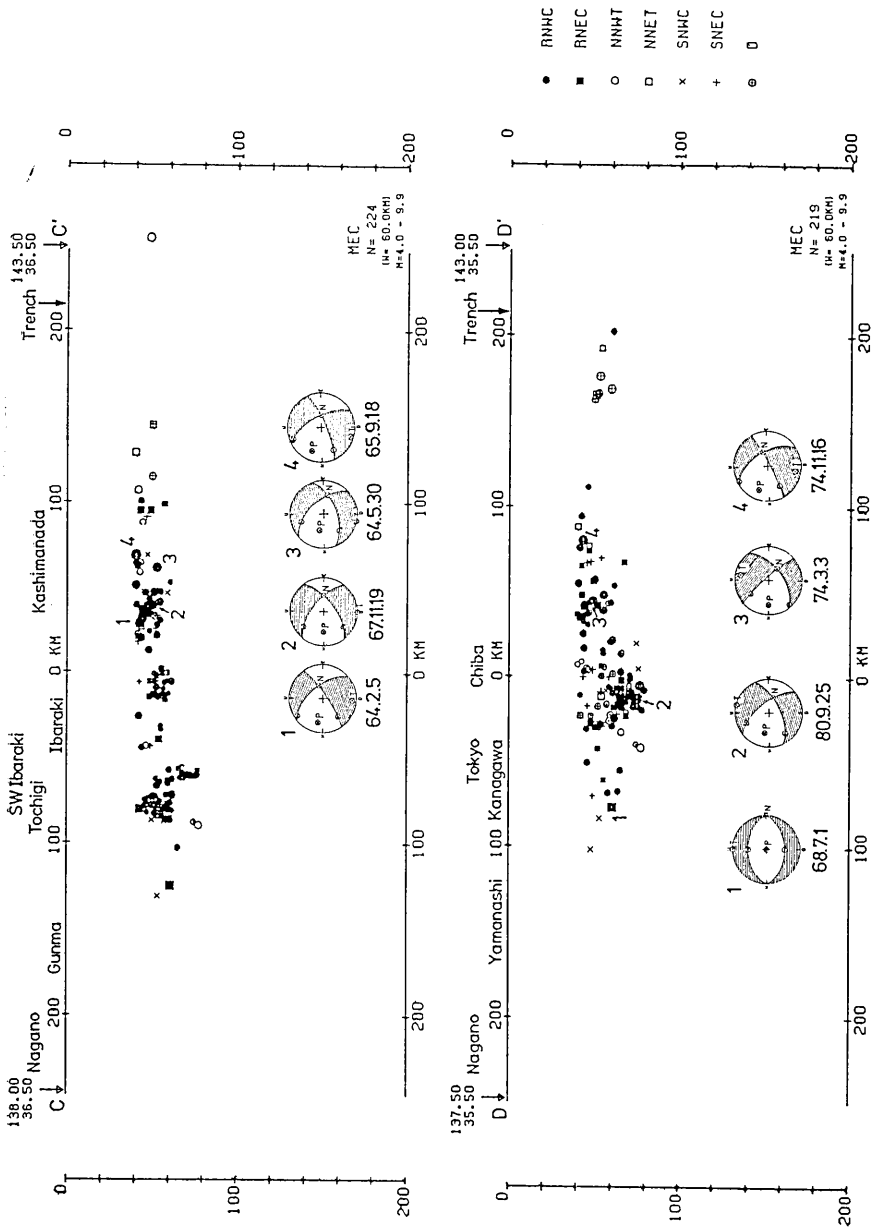
ANWC
ANEC
NNWT
NNET
SNWC
SNEC
138.00
36.50
Nagano
C
Gunma
SW Ibaraki
Tochigi
Ibaraki
0 KM
Kashimanada
Trench
143.50
36.50
C'
MEC
N= 224
(H= 60.0KM)
M=4.0 - 9.9
64.2.5
67.11.19
64.5.30
65.9.18
137.50
35.50
Nagano
D
Yamanashi
Tokyo
Kanagawa
Chiba
0 KM
Trench
143.00
35.50
D'
MEC
N= 219
(H= 60.0KM)
M=4.0 - 9.9
68.7.1
80.9.25
74.3.3
74.11.16
Northern hemisphere

Fig. 21 (c, d)

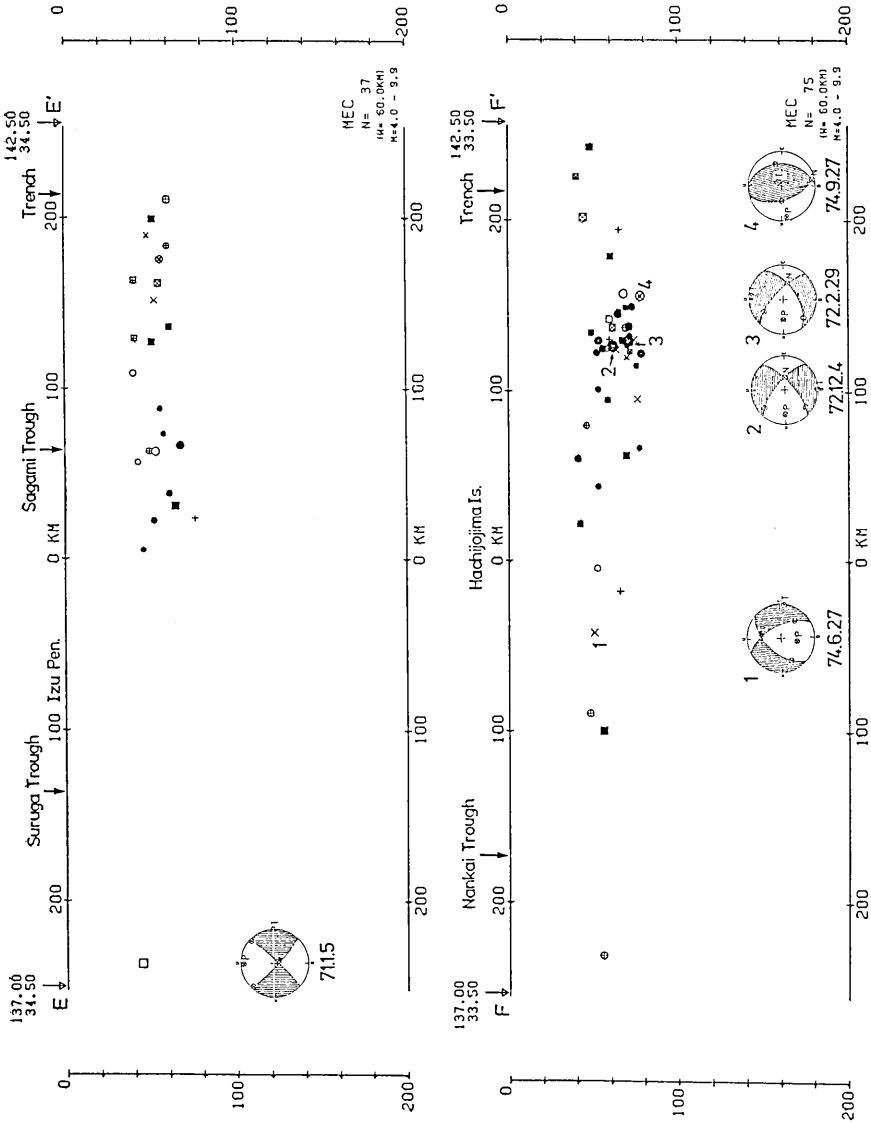

Fig. 21 (e, f)

Fig. 21. Depth distributions of fault types of subcrustal earthquakes along the E–W sections between latitudes of, (a) 39.0°N and 38.0°N, (b) 38.0°N and 37.0°N, (c) 37.0°N and 36.0°N, (d) 36.0°N and 35.0°N, (e) 35.0°N and 34.0°N, and (f) 34.0°N and 33.0°N. Focal mechanisms are shown for only the larger earthquakes (M≧5.0) by schematic diagrams of the equal-area projection of the northern focal hemisphere.

is also observed from the E-W extension for earthquakes located west of Hachijojima Island.

The stress regime around the trench has been interpreted by the bending of the lithospheric plate (CHEN and FORSYTH, 1978; CHAPPLE and FORSYTH, 1979) and by the detachment due to the weight (KANAMORI, 1971a, b, 1977). Two types of focal mechanism obtained in the present study, namely the horizontal extension outside the trench and the vertical slip with the western side sinking along the N-S plane near the trench axis, support both hypotheses. The nearly horizontal E-W extension for earthquakes in the back-arc region of the Izu-Bonin Islands is consistent with the stress regime due to the back-arc spreading (UYEDA and KANAMORI, 1979; UYEDA and MCCABE, 1983). The process of the back-arc opening has been interpreted by the different stages of the evolutional development of the island arcs (KANAMORI, 1971a, b, 1977) and by the model of the anchored slab in the deep interior (UYEDA and KANAMORI, 1978).

5. Causes of the intense clusters of subcrustal hypocenters

The intense clusters of subcrustal hypocenters beneath the Kanto District have been considered to be caused by the collision of the Philippine Sea Plate with the Pacific Plate (MAKI *et al.*, 1978, 1980; MAKI and TSUMURA, 1980; MAKI, 1981b). But other clusters of subcrustal earthquakes can be observed in other regions located far from the colliding region, especially on the side of Northeast Japan. It is questionable that the minor seismic zone inclined from the west represents the sinking of the Philippine Sea Plate to the east, because it cannot be identified for all parts beneath the Kanto District. The intense clusters of hypocenters are located in the contact region of the acute intersection of the Northeast Honshu and Izu-Bonin slabs (MAKI, 1984). In the present chapter focal mechanisms of earthquakes in the active regions are studied by relating to the systematic trends in the spatial distribution of hypocenters.

Fault-plane solutions of subcrustal earthquakes in the ten active regions are summarized in Fig. 22 (a to j). Principal axes (P, T and N axes) are represented by empty and solid circles and crosses on the left-hand side, and poles of nodal planes are denoted by empty circles on the right-hand side. Numbers of fault-plane solutions are also given for each active region. The nearly vertical T axes plunging to the west are commonly observed for all the active regions. Some different patterns are observed for some active regions, namely the SW T axes in the southwestern end of Ibaraki Prefecture (A), the horizontal N-S T axes in the northern part

A. SW Ibaraki (W)
62

B. SW Ibaraki (E)
18

C. S Ibaraki
15

D. N Chiba
19

E. M Chiba
52

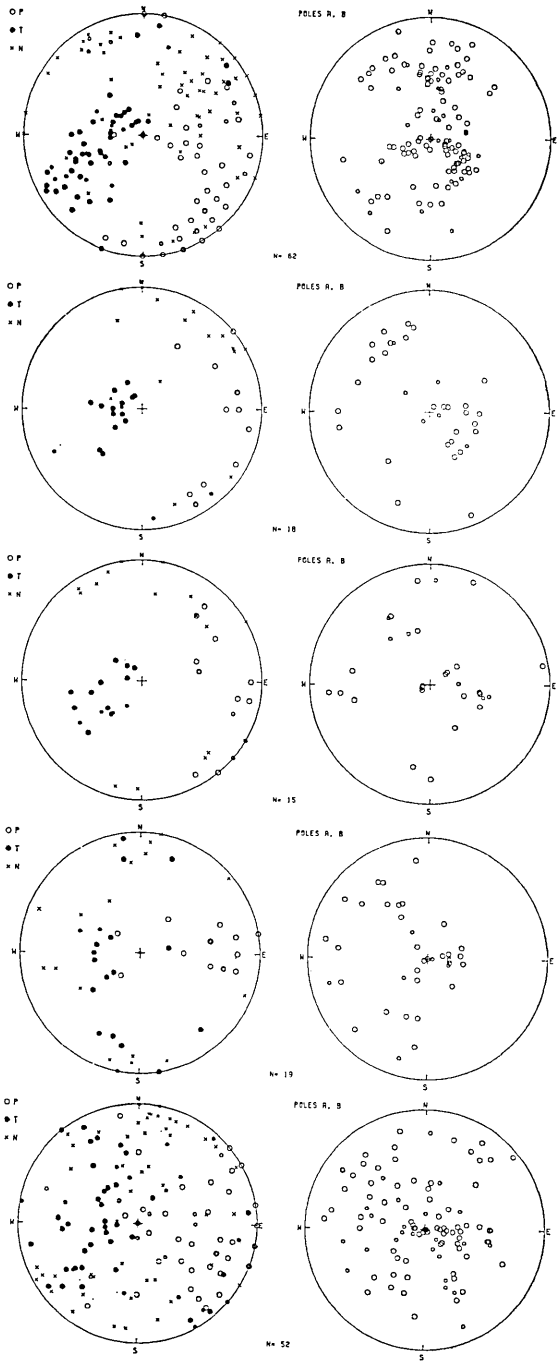

Fig. 22(a)

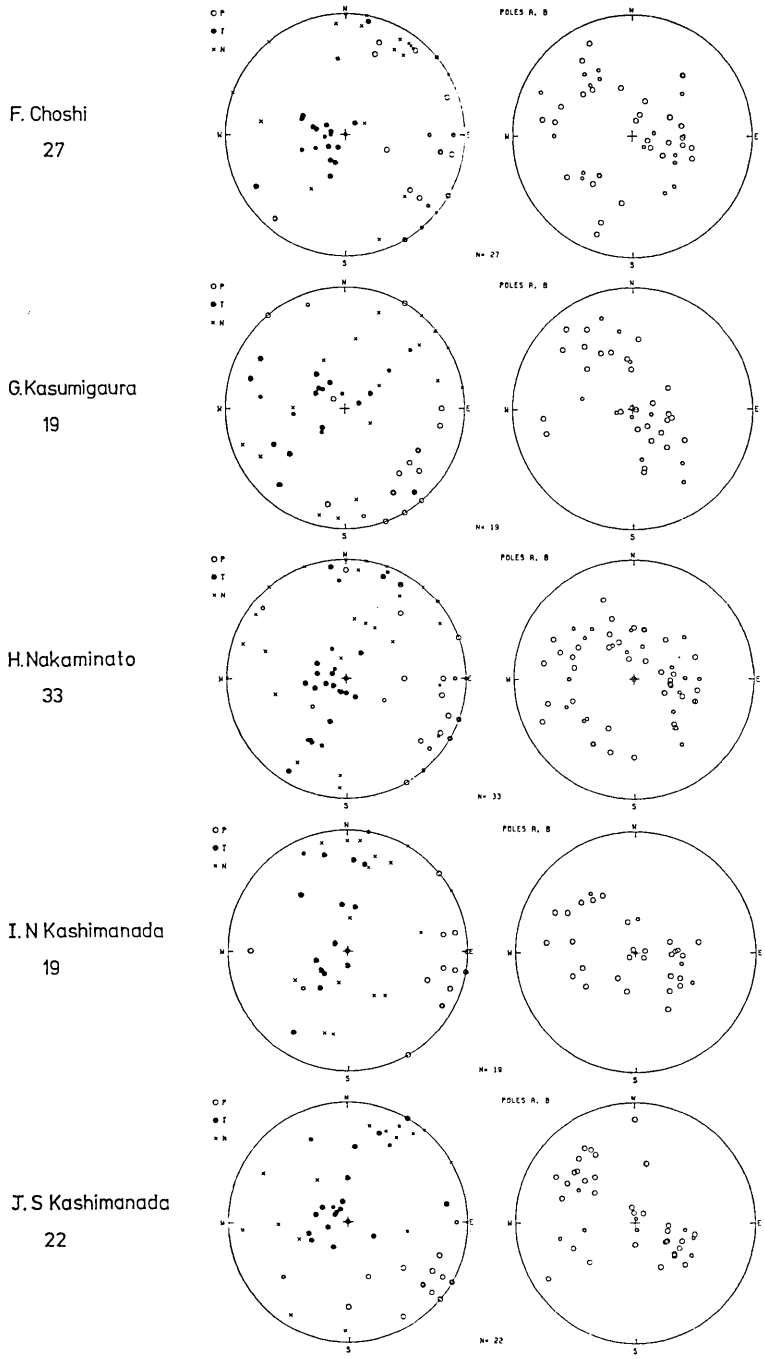

Fig. 22(b)

Fig. 22. Comparison of fault-plane solutions of subcrustal earthquakes within the 10 intense clusters of hypocenters in the Kanto District. Principal axes are shown on the left-hand side by empty and solid circles and crosses. Poles of nodal planes are shown on the right-hand side. Numbers mean fault-plane solutions obtained for each cluster.

of Chiba Prefecture (D), and the NW T axes in the middle part of Chiba Prefecture (E). Normal faults are also seen in the southwestern end of Ibaraki Prefecture (A) and the middle part of Chiba Prefecture (E). The northward T axes are seen for earthquakes in Nakaminato (H) and Kashimanada (I and J). The reverse faults of the vertical T axis are related to the relative motion of the descending Pacific Plate with the overriding plates. T axes plunging to the west and the almost vertical poles of nodal planes plunging to the east denote the western side sinking along the vertical N-S plane. Numbers and features of fault-plane solutions for each active region are summarized in Table 1.

Spatial distributions of focal mechanisms are represented in Fig. 23 (a to d) by schematic diagrams for the relatively large earthquakes and classified types of fault-plane solution for the 10 km intervals of depth from 40 to 80 km. For a depth range from 40 to 50 km (Fig. 23a) reverse faults are observed in Kashimanada (I and J), Kasumigaura (G), Choshi (F) and the SW Ibaraki regions (A and B). An earthquake on Mar. 27, 1973 near the Japan Trench shows a type of normal fault. The reverse faults are also predominant for depths from 50 to 60 km in Northern Kashimanada, Nakaminato, Choshi and the SW Ibaraki regions (Fig. 23b). Earthquakes located far east off Choshi and near the Japan Trench on Apr. 22, 1966 and May 19, 1968 show the western side sinking along the vertical N-S plane. Earthquakes at depths from 60 to 80 km are located in a limited area directly beneath the Kanto District. Most earthquakes at these depths show a reverse fault with an E-W compression (July 27, 1971; Mar. 30, 1975; Sep. 20, 1967; Oct. 18, 1972; Nov. 10, 1967). Other reverse faults have P axes with variable azimuths, namely the N-S P axis for an earthquake on July 1, 1968 and the NW-SE P axis on Sep. 25, 1980. The reverse fault with the E-W compression at depths from 70 to 80 km located on the eastern side of the 140°E line is interpreted by the western side sinking along the vertical N-S plane.

Depth distributions of mechanism types are shown along the same E-W and N-S sections of Figs. 5 to 7 together with schematic diagrams of the equal-area projection of the northern and eastern focal hemisphere. Fig. 24 shows the depth distribution of mechanism types of subcrustal earthquakes ($n=97$) along the E-W sections (width 30 km) between points A (139.7°E, 36.1°N) and B (140.3°E, 36.1°N) beneath the western part of Ibaraki Prefecture. Equal-area projections of the northern focal hemisphere are shown by schematic diagrams for the relatively large earthquakes ($M \geqq 5.0$). A separation of hypocenters into two groups is observed, namely the inclined seismic zone to the west at the shallower

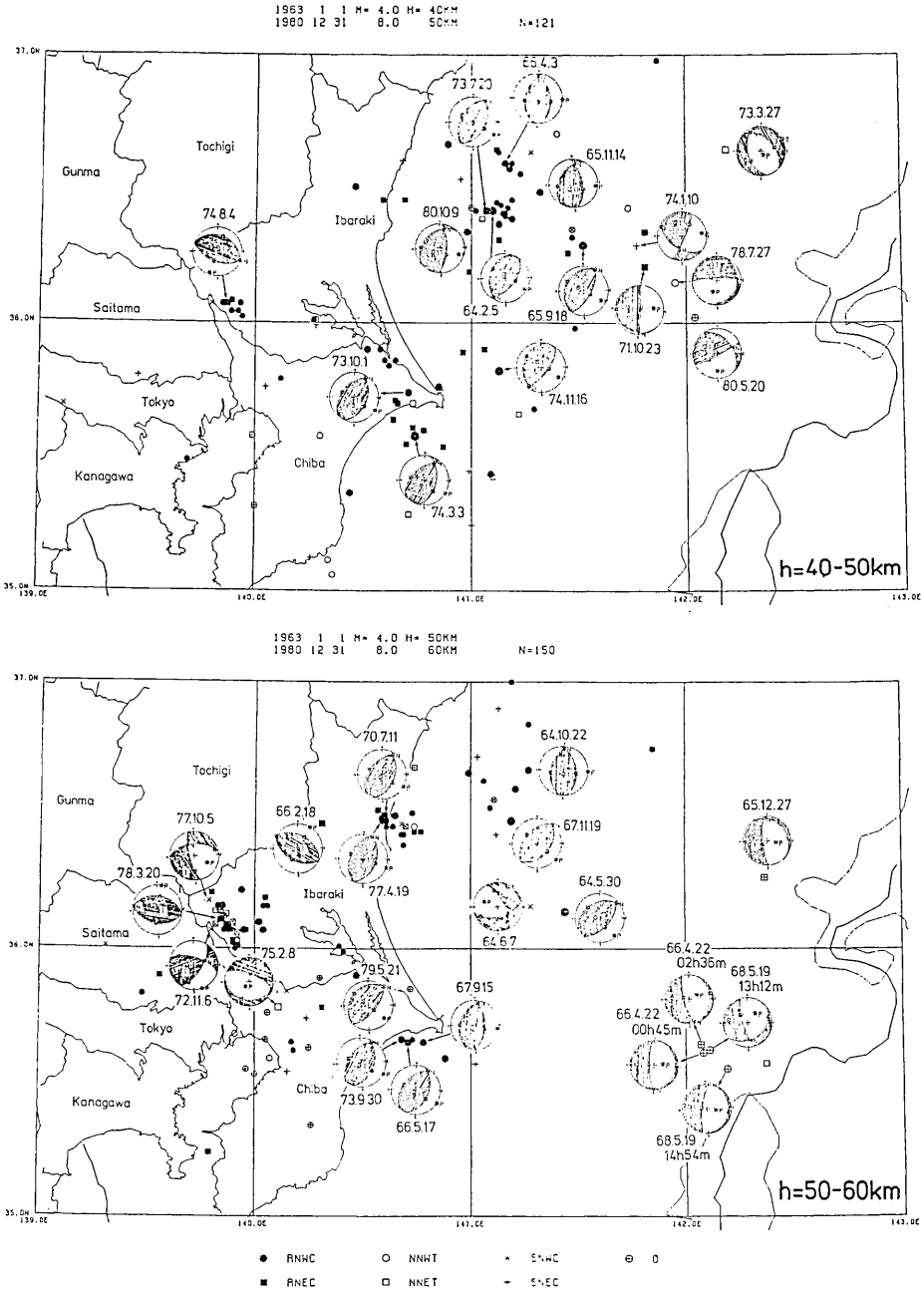
1963 1 1 M= 4.0 H= 40KM
1980 12 31 8.0 50KM N=121
Gunma
Tochigi
Ibaraki
Saitama
Tokyo
Kanagawa
Chiba
74.8.4
73.7.20
65.4.3
73.3.27
65.11.14
74.1.10
80.10.9
78.7.27
64.2.5
65.9.18
71.10.23
73.10.1
74.11.16
80.5.20
74.3.3
h=40-50km
1963 1 1 M= 4.0 H= 50KM
1980 12 31 8.0 60KM N=150
70.7.11
64.10.22
66.2.18
65.12.27
77.10.5
67.11.19
78.3.20
77.4.19
64.5.30
64.6.7
75.2.8
66.4.22
02h36m
68.5.19
13h12m
79.5.21
67.9.15
72.11.6
66.4.22
00h45m
73.9.30
66.5.17
68.5.19
14h54m
h=50-60km
RNHC
NNHT
SNHC
RNEC
NNET
SNEC

Fig. 23(a, b)

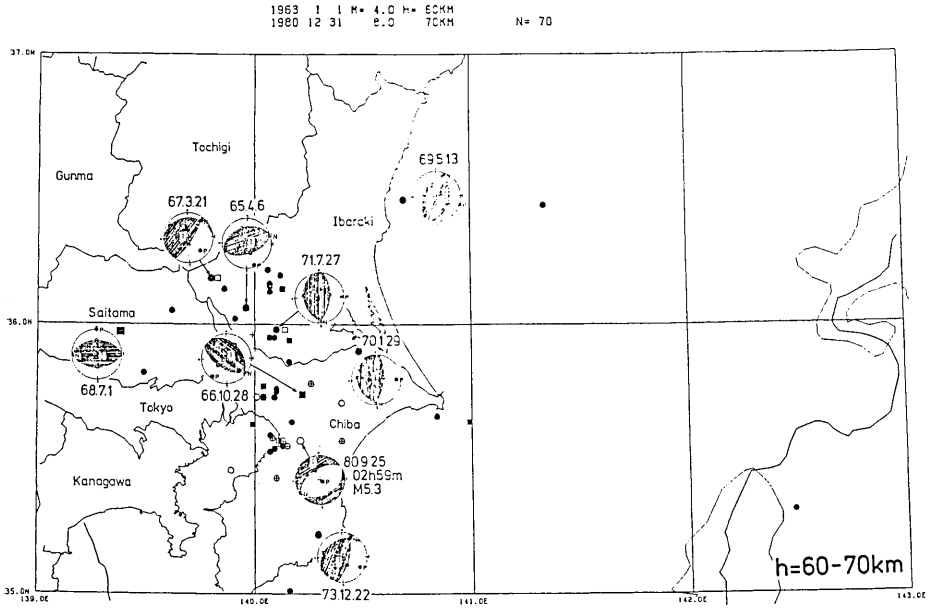

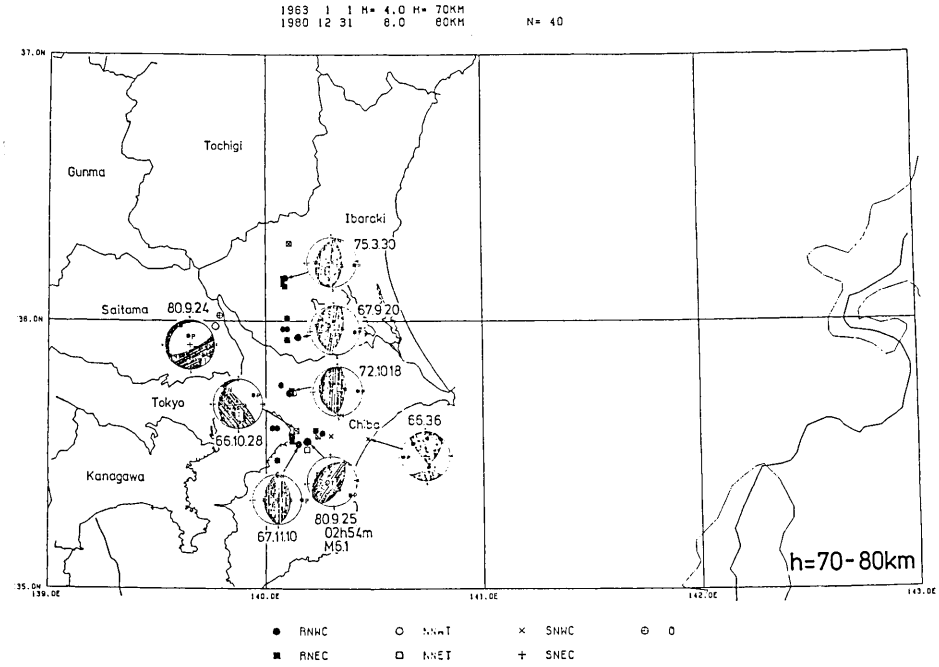

Fig. 23(c, d)

Fig. 23. Epicenter distributions of fault types and mechanism diagrams of subcrustal earthquakes for every 10 km of focal depths in the Kanto District: (a) h=40-50 km, (b) h=50-60 km, (c) h=60-70 km and (d) h=70-80 km. Epicenters are classified by mechanism types, and focal mechanisms are shown beside epicenters for some earthquakes by schematic diagrams of the lower focal hemisphere.

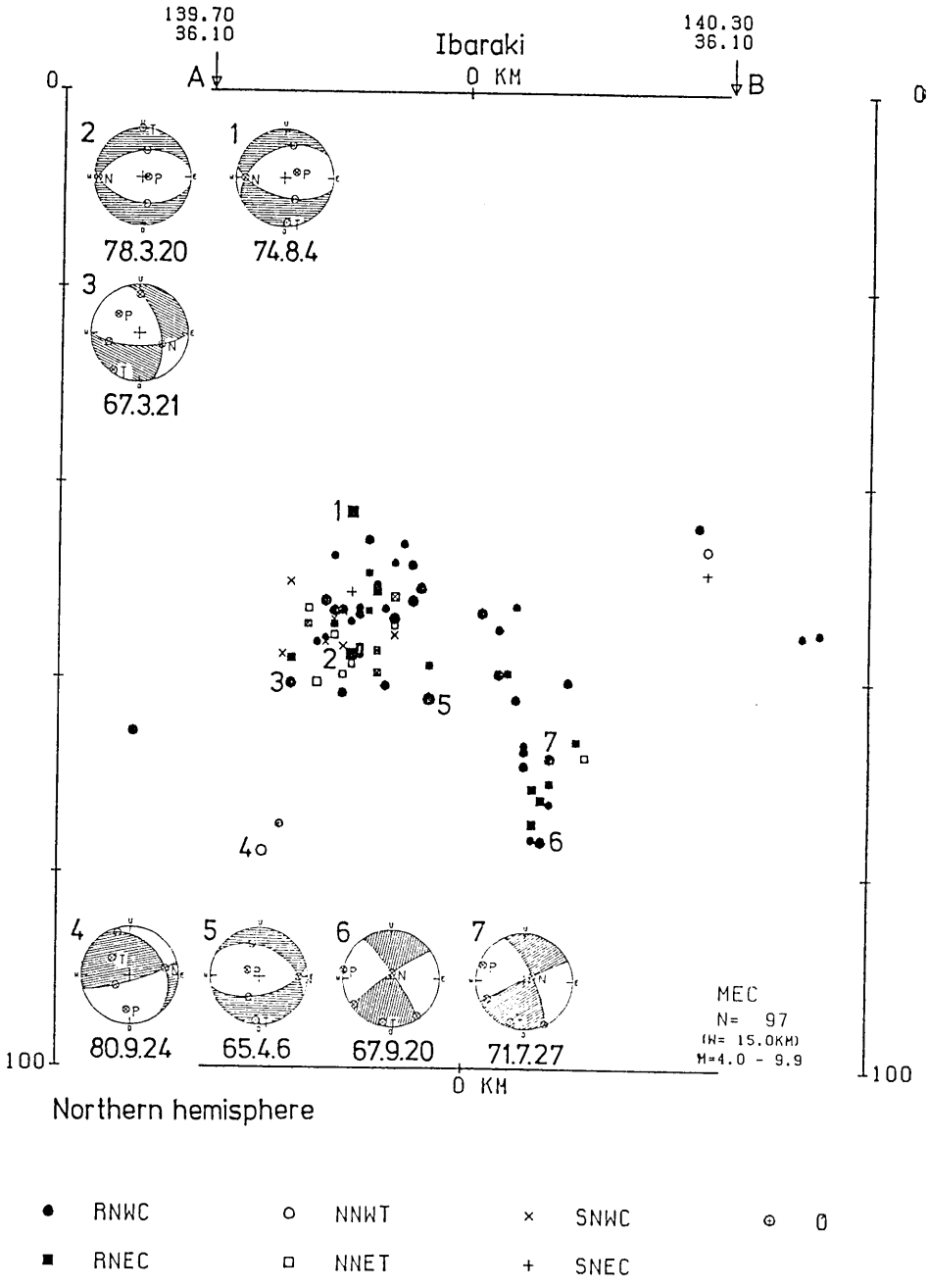

Fig. 24. Depth distribution of mechanism types of subcrustal earthquakes along the E-W section between points A (139.7°E, 36.1°N) and B (140.3°E, 36.1°N) beneath the southwestern part of Ibaraki Prefecture (width 30 km). Focal mechanisms are denoted for some earthquakes by schematic diagrams of the northern focal hemisphere.

depths from 40 to 60 km and a vertical alignment at the deeper part from 50 to 80 km on the eastern side of the 140°E line. The reverse faults of the deeper earthquakes on Sep. 20, 1967 and July 27, 1971 show a consistency between the almost vertical nodal plane plunging to the east and the vertical alignment of hypocenters. Fig. 25 shows the depth distribution along the E-W section (width 20 km) between points A (139.9°E, 35.6°N) and B (140.3°E, 35.6°N) beneath the middle part of Chiba Prefecture. No systematic trends are observed for the spatial distribution of hypocenters and focal mechanisms. A feature of the western side sinking is observed for the largest earthquake which occurred at the bottom of clustering hypocenters on Sep. 25, 1980 (M 6.1). Fig. 26 shows the depth distribution of mechanism types along the N-S section (width 50 km) between points A (140.0°E, 36.5°N) and B (140.0°E, 35.5°N) beneath the western part of Ibaraki and Chiba Prefectures. For this section schematic diagrams of the eastern focal hemisphere are represented. Some larger earthquakes located at depths from 40 to 60 km beneath the southwestern part of Ibaraki Prefecture show the reverse fault with a nodal plane dipping to the west (Aug. 4, 1974; Mar. 20, 1978; Apr. 6, 1965; Mar. 21, 1967). The reverse fault of the deeper earthquakes on Mar. 30, 1975; July 27, 1971; Sep. 20, 1967; Oct. 18, 1972; Nov. 10, 1967; Oct. 8, 1968 and Sep. 25, 1980 are characterized by the horizontal eastward P axis and the western side sinking along the vertical N-S plane. The normal faults with the almost vertical P axis are observed for earthquakes on Sep. 24, 1980 and Feb. 8, 1975. A systematic difference is observed between the subcrustal earthquakes at the shallower depths on the western side of the 140°E line beneath the southwestern end of Ibaraki Prefecture and those at the deeper part on the eastern side of the 140°E line beneath the western part of Ibaraki and Chiba Prefectures.

The intense clusters of subcrustal hypocenters are located at their own relative locations and they show particular types of focal mechanisms. Earthquakes in the offshore region are located along the inclined seismic zone of the thickness 10 km, and then they show the reverse fault with the slowly dipping plane to the west. The systematic differences in the spatial alignment of hypocenter distribution and focal mechanisms are observed for two groups of hypocenters beneath the southwestern part of Ibaraki Prefecture. The shallower earthquakes at depths from 40 to 60 km beneath the southwestern end of Ibaraki Prefecture (on the western side of the 140°E line) show a linear alignment of epicenters with the northwest dipping of hypocenters and they show the focal mechanism of the reverse faults with the N-S and NW-SE compressions. The deeper earth-

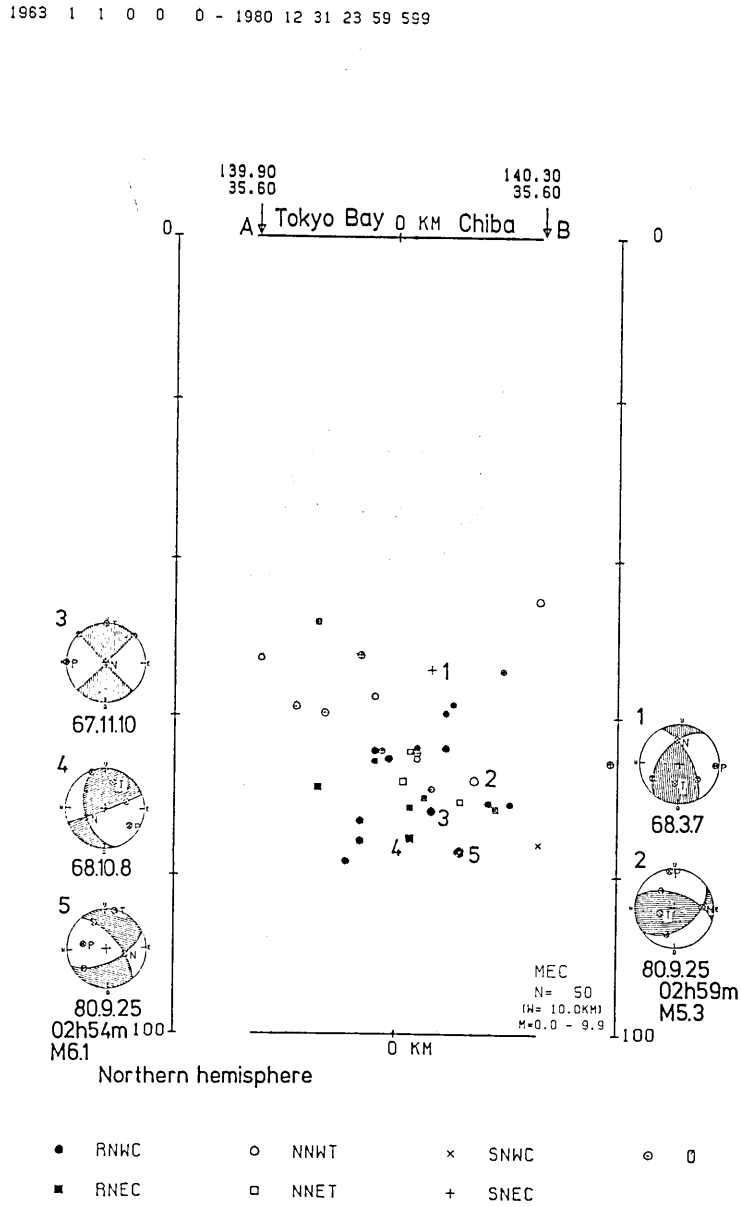

Fig. 25. Depth distribution of mechanism types of subcrustal earthquakes along the E-W section between points A (139.9E, 35.6°N) and B (140.3°E, 35.6°N) beneath the middle part of Chiba Prefecture (width 30 km).

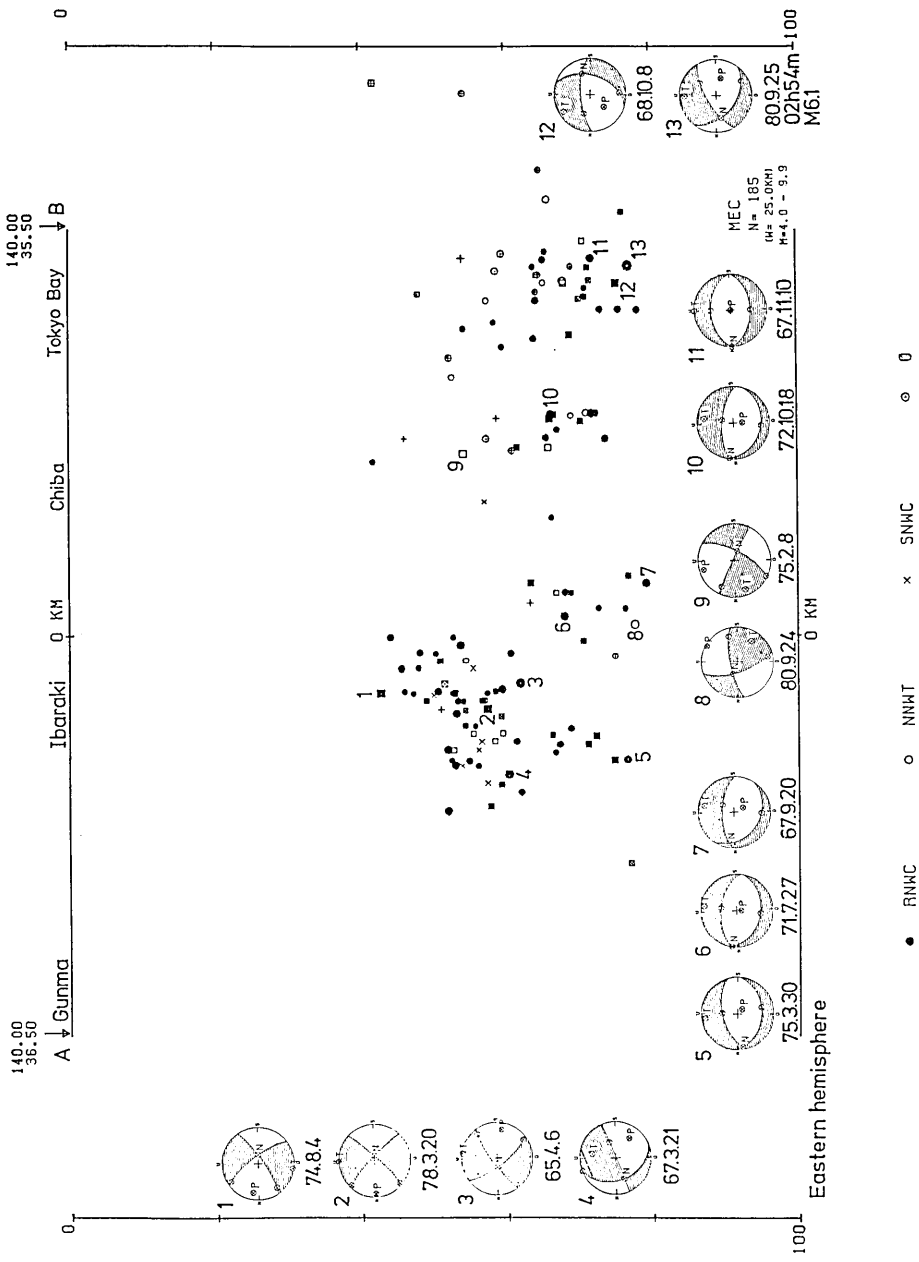

Fig. 26. Depth distribution of mechanism types of subcrustal earthquakes along the N-S section between points A (140.0°E, 36.5°N) and B (140.0°E, 35.5°N) beneath the western part of Ibaraki and Chiba Prefecture (width 50 km).

quakes at depths from 50 to 80 km beneath the southwestern part of Ibaraki Prefecture and northern part of Chiba Prefecture (on the eastern side of the 140°E line) show rather a vertical alignment within the slab and show the focal mechanism of the vertical slip along the N-S striking plane. Earthquakes located beneath the middle part of Chiba Prefecture show a somewhat confused pattern on the hypocenter distribution and show the mixed types of focal mechanisms.

The intense clusters of the subcrustal earthquakes are generated by two kinds of mechanisms due to their relative locations and focal mechanisms, namely (1) the relative motions of the descending Pacific Plate with the overriding plates, and (2) the vertical slip with the western side sinking along the N-S plane within the descending slab of the Pacific Plate.

6. Discussion and conclusion

The epicenter distributions for three ranges of focal depth are compared using the precisely relocated hypocenters by correcting the JMA travel-time data with the Pn station biases (MAKI, 1981a). The subcrustal earthquakes at depths from 40 to 80 km in and around the Kanto District show more intense clusters of hypocenters than other depths of the crust (h=0-40 km) and intermediate-depths (h=80-120 km). These intense clusters of subcrustal hypocenters are located at their own depths in front of the subducted slab of the Pacific Plate. The depth distributions of the relocated hypocenters are shown for several sections around the intense clusters beneath the Kanto District. The upper boundary of the descending Pacific Plate is identified by the very thin seismic zone of 10 km width inclined from the east beneath Kashimanada, east off Ibaraki Prefecture. The shallower earthquakes at depths down to 40 km beneath the western end of Ibaraki Prefecture show the linear alignment of epicenters and dipping plane to the northwest. The deeper earthquakes at depths from 50 to 80 km beneath the western part of Ibaraki and Chiba Prefectures (on the eastern side of the 140°E line) show rather a vertical alignment. Some of the relatively large earthquakes are not located within the active regions, so-called "earthquake nests", so far as the period studied here.

Seven hundred and four fault-plane solutions, satisfying 10 or more first-motion data, are obtained for 487 subcrustal earthquakes which occurred during the period from 1963 to 1980 with magnitudes of 4.0 or more in and around the Kanto District. The reverse faults are predominantly observed for 55% of all the fault-plane solutions compared to other depth ranges with the predominant normal faults and strike-slips.

Especially the reverse fault with the NW-SE compression is obtained for 40%. The focal mechanisms obtained here suggest a complicated pattern of earthquake-generating stress at the subcrustal depths in and around the Kanto District. Some types of focal mechanisms are observed; the horizontal E-W extension for earthquakes outside the Japan Trench, the western side sinking along the nearly vertical plane parallel to the trench axis for earthquakes directly inside the Japan Trench, the strike-slip with the E-W compression near the Boso triple junction, and the horizontal E-W extension in the back-arc region of the Izu-Bonin Islands. A consistency between the planar alignment of hypocenters and the reverse fault with the E-W or NW-SE compression is observed in the offshore regions of Kashimanada, east off Ibaraki Prefecture. The shallower earthquakes beneath the western end of Ibaraki Prefecture show the reverse fault with the N-S compression. Deeper earthquakes beneath the western part of Ibaraki and Chiba Prefectures show a focal mechanism of the western side sinking along the almost vertical N-S plane. The subduction process of the Pacific Plate is observed for the coastal region in Northeast Japan and the Kanto District from the hypocenter distribution of subcrustal earthquakes and their fault-plane solutions of the reverse type. The northwest warping of the seismic zone is observed beneath the Kanto District. The upper boundary of the gross seismic zone of the descending Pacific Plate inclined to the west are identified from the very thin seismic zone of 10 km.

In the previous study the intense clusters of hypocenters beneath the southwestern end of Ibaraki Prefecture have been interpreted by the relative motion of the Pacific Plate with the overriding plate (MAKI *et al.*, 1978, 1980; MAKI, 1981b; MAKI and TSUMURA, 1978). The deeper clusters of hypocenters beneath the middle part of Chiba Prefecture were explained by the collision of the Pacific Plate with the northeastern end of the Philippine Sea Plate. The minor seismic zone inclined from the west can be observed for micro and small earthquakes by the recent high-sensitivity seismograph network, but this seismic zone is not clearly observed as a planar pattern for the larger earthquakes and over all the region beneath the Kanto District. The intense activity of earthquakes beneath the Kanto District has been explained by the acute intersection of the Northeast Honshu and Izu-Bonin slabs (MAKI, 1984). More precise locations of hypocenters and studies of focal process are required to clarify the cause of clustering earthquakes beneath the Kanto District. Some relative locations of hypocenters with respect to region and depth suggest the feature of the subduction process of the lithospheric plate, and the fine structure of the spatial distribution

and focal mechanisms are useful for studies of these features. Especially the stress regimes around the trench and in the back-arc region are to be solved based on the spatial distributions and focal mechanisms of earthquakes occurring in these regions.

Acknowledgments

The author acknowledges Prof. Tokuji Utsu for reviewing the manuscript. He also thanks the members of Seminar on Dec. 6, 1983 for their helpful comments. He thanks the Seismological Section of JMA for the use of the Data File of the travel-times. Computations and drafting were made by using the IBM 4341 of the Earthquake Prediction Data Center, Earthquake Research Institute, University of Tokyo.

References

CHAPPLE, W.M. and D.W. FORSYTH, 1979, Earthquakes and bending of plates at trenches, *Journ. Geophys. Res.*, 84, 6729-6749.

CHEN, T. and D.W. FORSYTH, 1978, A detailed study of two earthquakes seaward of the Tonga Trench: Implications for mechanical behavior of the oceanic lithosphere, *Journ. Geophys. Res.*, 83, 4995-5003.

HASEGAWA, A., N. UMINO and A. TAKAGI, 1978a, Double-planed structure of the deep seismic zone in the northeastern Japan arc, *Tectonophysics*, 47, 43-58.

HASEGAWA, A., N. UMINO and A. TAKAGI, 1978b, Double-planed deep seismic zone and upper-mantle structure in the Northeastern Japan Arc, *Geophys. Journ. Roy. astr. Soc.*, 54, 281-296.

ICHIKAWA, M., 1965, Automatic data processing of seismological observations in the Japan Meteorological Agency and a few comments on the results obtained, *Paper Meteor. Geophys.*, JMA, 16, 90-103 (in Japanese).

ICHIKAWA, M., 1971, Reanalyses of mechanism of earthquakes which occurred in and near Japan, and statistical studies on the nodal plane solutions obtained, 1926-1968, *Geophys. Mag.*, 35, 207-274.

ICHIKAWA, M., 1978, Focal depth determined by JMA and some related problems, *Quart. Journ. Seism.*, JMA, 45, 29-35 (in Japanese).

ICHIKAWA, M., 1979, Some problems in the focal mechanism in and near Japan, *Geophys. Mag.*, 39, 1-22.

JMA (Japan Meteorological Agency), 1976 to 1982, List of nodal plane solutions for earthquakes occurring in 1973 to 1979, in "The Seismological Bulletin of the Japan Meteorological Agency".

KANAMORI, H., 1971a, Seismological evidence for a lithospheric normal faulting—The Sanriku earthquake of 1933, *Phys.Earth Planet. Inter.*, 4, 289-300.

KANAMORI, H., 1971b, Great earthquakes at island arcs and the lithosphere, *Tectonophysics*, 12, 187-198.

KANAMORI, H., 1977, Seismic and aseismic slip along subduction zones and their tectonic implications, in "*Island Arcs, Deep Sea Trenches and Back-Arc Basins*", Maurice Ewing Ser., vol. 1, edited by M. TALWANI and W.C. PITMAN III, AGU, Washington, D.C., pp. 162-174.

MAKI, T., 1979, Joint hypocenter determination of earthquakes in the Kanto District

Read on May 4, 1979, at the semi-annual meeting of the Seismological Society of Japan.

MAKI, T., 1981a, Regional variation of Pn residuals and its application to relocation of earthquakes in and around the Kanto District, *Bull. Earthq. Res. Inst., Univ. Tokyo*, 56, 309-346.

MAKI, T., 1981b, Earthquake mechanisms of subcrustal earthquakes beneath the Kanto District, *Memoirs Gol. Soc. Japan*, 20, 259-200 (in Japanese).

MAKI, T., 1982a, Effect of observational conditions on hypocenter location of intermediate-depth earthquakes in Central Japan, *Bull. Earthq. Res. Inst.*, Univ. Tokyo, 57, 49-82.

MAKI, T., 1982b, Numerical estimation of confidence region of fault-plane solutions, *Bull. Earthq. Res. Inst., Univ. Tokyo*, 57, 193-220.

MAKI, T., 1983a, An active zone and focal machanisms of shallow earthquakes in the Kanto District, *Journ. Japan Soci. Natural Disast. Science*, 2, 16-32 (in Japanese),

MAKI, T., 1983b, Distribution and focal mechanisms of shallow earthquakes in the Kanto District—An active zone and seismic gaps along the 139°E line—, Read on Apr. 26 1983, at the semi-annual meeting of the Seismological Society of Japan.

MAKI, T., 1983c, Extended travel-time tables of the JMA standard model of the crust and upper mantle structure beneath the Japanese Islands, *Bull. Earthq. Res. Inst., Univ. Tokyo*, 58, 311-387.

MAKI, T., 1983d, Spatial variation of earthquake-generating stresses in and around the Kanto District, Central Japan, *Bull. Earthq. Res. Inst., Univ. Tokyo*, 58, 591-646.

MAKI, T., 1984, Focal mechanisms and spatial distribution of intermediate-depth earthquakes beneath the Kanto District and vicinity with relation to the double seismic zone, *Bull. Earthq. Res. Inst., Univ. Tokyo*, 59, 1-51.

MAKI, T., A. HORIE and I. KAWASAKI, 1978, Earthquake mechanisms beneath the Kanto District and vicinity, (2) the southwestern part of Ibaraki Prefecture and middle part of Chiba Prefecture, Read on Oct. 11, 1978 at the semi-annual meeting of the Seismological Society of Japan.

MAKI, T., I. KAWASAKI and A. HORIE, 1980, Earthquake mechanisms associated with the conjunction of the sinking plates beneath the Kanto District, Central Japan, *Bull. Earthq. Res. Inst., Univ. Tokyo*, 55, 577-600.

MAKI, T. and K. TSUMURA, 1978, On the enhancement of the seismic trends by the use of the spatial distribution of small earthquakes in the Kanto District, Read on Oct. 11, 1978, at the semi-annual meeting of the Seismological society of Japan.

MAKI, T. and K. TSUMURA, 1980, On seismic fault-systems derived from the spatial distribution and mechanisms of the earthquakes in the Kanto District, *Journ. Anal. Res. Data Natur. Disast.*, 7, 47-60 (in Japanese).

TSUMURA, K., 1973, Microearthquake activity in the Kanto District, *in* Publication for the 50th anniversary of the Great Kanto Earthquake, 1923", Earthq. Res. Inst., Univ. Tokyo, 67-87 (in Japanese).

USAMI, T. and T. WATANABE, 1977, Definition and characteristics features of a seismically active region (earthquake nest) in the Kanto District, *Bull. Earthq. Res. Inst., Univ. Tokyo*, 52, 379-406 (in Japanese).

UYEDA, S. and H. KANAMORI, 1979, Back-arc opening and the mode of subduction, *Journ. Geophys. Res.*, 84, 1049-1061.

UYEDA, S. and R. MCCABE, 1983, A possible mechanism of episodic spreading of the Philippine Sea, in "*Accretion Tectonics in the Circum-Pacific Regions*", edited by M. HASHIMOTO and S. UYEDA, 291-306.

関東地方の地殻下地震の発震機構と震源分布
—とくに活動域について—

東京大学地震研究所　牧　正

関東地方周辺の地殻下地震は特定の地域・深さで著しい集中の活動を示す．これらの活動域の地震について震源配列，相対位置，発震機構がしらべられた．地殻下地震は東北日本・伊豆小笠原島弧の接合部に集中している傾向がみられ，とくに東北日本側で活発であると共に地震面が北西に彎曲を示す．活動度のもっとも高い茨城県南西部の地殻下地震は深さ・位置の異なる2つの活動域に分けられる．東経140°線の西側の活動域は深さ40～60 km で北西に傾むき下がる配列を示し，東経140°線の東側では深さ 60～80 km でむしろ鉛直の配列を示す．

1963-1980 年，マグニチュード4以上の地震の約半分の地震（1029個のうち487 個）について，10個以上の初動データを満足するメカニズム解（704 個）を求めることができた．これらの解の内55%が逆断層型でとくに関東地方や東北日本側で卓越し，伊豆諸島では他のタイプのメカニズムもあらわれる．関東地方では南北圧力の逆断層型がみられ，東北日本・伊豆小笠原弧のスラブの接合に伴なう地震面の北西への彎曲に関わるものと思われる．日本海溝の外側では水平の東西張力，海溝内側では鉛直面に沿う西落ちの縦ずれのメカニズムがみられる．東西張力のメカニズムは伊豆・小笠原諸島の西側にもみられ，房総ジャンクション南方では横ずれ型のメカニズムがみられる．これらの複雑な特徴は3つのプレートの収束と東北日本・伊豆小笠原弧のスラブの接合及び背弧拡大などの附加的過程によるものと考えられる．

茨城県南西部の2つの活動域の内，西側の活動域の地震は北西—南東（及至南—北）の圧力をもつ逆断層型で，東側の地震は鉛直面に沿う西落ちの縦ずれ型のメカニズムが卓越している．従って茨城県南西部の2つの地殻下地震の活動域は，①東経140° 線の西側＝彎曲する東北日本弧のスラブ上面に沿う逆断層地震，②東経140° 線の東側＝太平洋プレートのスラブ内のやや深い震源で西落ちの鉛直縦ずれ型の地震に分けられる．後者は千葉県中部の深さ 60-80 km の活動域にも共通する．

Appendix

List of fault-plane solutions by the numerical method (MAKI, 1983b) of subcrustal earthquakes which occurred in and around the Kanto District during the period from 1963 to 1980 with magnitudes of 4.0 or more. Hypocenters and origin times are determined by correcting the JMA travel times with the *Pn* station biases (MAKI, 1981a). Earthquake magnitudes are taken from JMA. Fault-plane solutions are given by dip direction (dd) and dip angles (d) for poles of nodal planes (X and Y) and principal axes (P, T and N). Numbers of first-motion data are given for the read (all) and used ones in the last two columns. Azimuth and dip angles are given in the unit of tenths of a degree for the orthogonal relation of the double-couple model.

Eq	Date y m d	Time h m s	Latit deg	Long deg	Dep km	Mag	Pole-X dd	d	Pole-Y dd	d	B-axis dd	d	P-axis dd	d	T-axis dd	d	Number read	used
1	63 525	113738	33.86	138.77	47.2	5.1	319.6	42.4	86.6	33.4	198.5	29.5	30.0	60.0	291.3	5.0	13	12
							80.9	20.7	179.1	20.7	310.0	60.0	40.0	0.0	130.0	30.0	13	12
2	63 8 4	204314	35.37	140.44	43.9	5.1	202.7	32.8	317.3	32.8	80.0	40.0	170.0	0.0	260.0	50.0	29	26
3	63 815	151131	37.70	141.97	40.7	6.6	99.9	44.1	260.2	44.1	0.0	10.0	90.0	0.0	180.0	80.0	123	103
							9.9	44.1	170.2	44.1	270.0	10.0	0.0	0.0	90.0	80.0	123	103
4	631224	215545	36.07	140.04	59.4	5.2	162.0	54.0	321.5	34.3	58.3	9.9	150.0	10.0	284.6	75.9	31	27
5	64 126	74854	36.63	141.06	53.0	4.6	165.4	21.2	258.0	6.6	4.5	67.7	120.0	10.0	213.6	19.7	11	10
							142.6	51.0	283.4	32.1	26.4	19.7	120.0	10.0	235.5	67.7	11	10
6	64 2 5	203015	36.42	141.10	44.1	6.0	108.0	54.0	308.5	34.3	211.8	9.9	120.0	10.0	345.4	75.9	70	57
7	64 3 4	437 2	37.06	141.43	41.8	4.5	43.5	34.3	307.8	8.3	206.1	54.5	350.0	30.0	90.3	17.2	14	12
8	64 3 5	164239	35.71	140.65	40.1	4.4	58.0	54.0	258.5	34.3	161.8	9.9	70.0	10.0	295.4	75.9	13	12
							142.0	54.0	301.5	34.3	38.3	9.9	130.0	10.0	264.6	75.9	13	12
9	64 313	43213	35.90	141.06	46.9	4.4	92.0	54.0	251.5	34.3	348.3	9.9	80.0	10.0	214.6	75.9	12	12
10	64 325	114321	36.37	141.13	45.2	5.3	138.9	41.6	281.1	41.6	30.0	20.0	120.0	0.0	210.0	70.0	37	31
11	64 4 5	104449	36.16	140.04	54.8	4.9	166.1	63.7	322.3	24.6	56.6	9.4	150.0	20.0	302.7	67.7	23	20
12	64 417	115825	36.51	140.73	52.4	4.6	159.0	60.0	294.8	22.5	32.9	18.8	130.0	20.0	263.2	62.0	26	23
13	64 525	427 8	37.47	141.42	67.5	4.5	24.9	73.1	172.7	14.5	265.0	8.7	0.0	30.0	160.6	58.5	10	10
14	64 530	233043	36.14	141.44	52.8	6.2	152.0	54.0	311.5	34.3	48.3	9.9	140.0	10.0	274.6	75.9	108	102
15	64 6 7	234930	36.16	141.28	58.7	5.4	346.4	33.3	241.7	21.1	125.3	49.0	290.0	40.0	26.5	7.6	35	34
16	64 616	143927	38.59	139.73	40.1	5.2	30.0	45.0	210.0	45.0	300.0	0.0	30.0	0.0	210.0	90.0	12	12
							135.0	45.0	315.0	45.0	45.0	0.0	135.0	0.0	315.0	90.0	12	12
17	64 622	112038	36.22	139.94	51.9	5.1	14.9	73.1	162.7	14.5	255.0	8.7	350.0	30.0	150.6	58.5	34	26
18	64 7 9	21 2 8	34.16	141.52	54.8	5.4	144.6	7.1	235.4	7.1	10.0	80.0	100.0	0.0	190.0	10.0	34	32
							219.6	58.2	11.2	28.6	108.3	12.7	340.0	70.0	201.8	15.2	34	32
19	64 730	164122	35.73	140.04	66.6	4.5	142.8	46.5	41.5	10.6	301.9	41.6	80.0	40.0	190.4	22.5	17	14
							15.4	74.5	274.0	3.1	183.2	15.2	80.0	40.0	289.5	46.0	17	14
20	64 8 7	17 5 1	37.38	141.54	53.1	4.7	77.4	51.0	296.6	32.1	193.6	19.7	100.0	10.0	344.5	67.7	18	17
21	6410 1	414 9	36.09	139.87	51.0	4.9	217.5	27.0	322.6	27.0	90.0	50.0	180.0	0.0	270.0	40.0	21	21
22	641014	12 453	33.23	142.36	48.2	5.1	44.5	43.1	195.5	43.1	300.0	15.0	30.0	0.0	120.0	75.0	16	16
							135.0	45.0	315.0	45.0	45.0	0.0	135.0	0.0	315.0	90.0	16	16
23	641022	185437	36.67	141.27	50.9	5.5	99.9	44.1	260.2	44.1	0.0	10.0	90.0	0.0	180.0	80.0	41	39
24	641114	145645	36.50	140.65	52.6	5.1	101.1	41.6	318.9	41.6	210.0	20.0	120.0	0.0	30.0	70.0	28	27
25	641115	95537	36.16	139.85	52.9	5.1	150.0	65.0	330.0	25.0	60.0	0.0	150.0	20.0	330.0	70.0	28	27
26	641121	13442	36.01	139.31	53.6	4.9	196.8	14.0	103.2	14.0	330.0	70.0	150.0	20.0	240.0	0.0	21	21
27	641124	35530	36.43	141.12	52.8	4.6	126.5	34.3	222.2	8.3	324.0	54.5	180.0	30.0	79.7	17.2	19	15

Eq	Date y m d	Time h m s	Latit deg	Long deg	Dep km	Mag	Pole-X dd	Pole-X d	Pole-Y dd	Pole-Y d	B-axis dd	B-axis d	P-axis dd	P-axis d	T-axis dd	T-axis d	Number read	Number used
28	641217	113318	35.31	142.48	60.5	4.9	220.9	62.1	111.1	10.2	16.1	25.7	270.0	30.0	139.1	48.6	14	11
29	641221	81444	36.52	140.57	57.7	4.6	18.0	54.0	218.5	34.3	121.8	9.9	30.0	10.0	255.4	75.9	11	11
							67.4	51.0	286.6	32.1	183.6	19.7	90.0	10.0	334.5	67.7	11	11
							130.0	55.0	310.0	35.0	40.0	0.0	130.0	10.0	310.0	80.0	11	11
30	641224	183823	36.08	139.88	53.3	4.6	156.1	63.7	312.3	24.4	46.5	9.4	140.0	20.0	292.7	67.7	13	11
31	65 124	65113	36.66	140.99	52.7	5.2	150.0	45.0	330.0	45.0	60.0	0.0	150.0	0.0	330.0	90.0	40	37
32	65 314	21 414	37.07	141.26	46.1	4.5	3.9	63.7	207.8	24.4	113.5	9.4	20.0	20.0	227.3	67.7	11	10
							142.6	51.0	283.4	32.1	26.4	19.7	120.0	10.0	235.5	67.7	11	10
33	65 4 6	143159	36.06	139.96	61.9	5.5	160.0	55.0	340.0	35.0	70.0	0.0	160.0	10.0	340.0	80.0	93	87
34	65 413	05038	36.01	139.92	53.7	5.1	172.6	51.0	313.4	32.1	56.4	19.7	150.0	10.0	265.5	67.7	35	28
35	65 413	125022	36.06	139.92	51.5	4.5	204.3	62.0	71.1	20.0	334.0	18.8	100.0	60.0	235.9	22.5	14	13
							291.2	28.0	21.7	0.8	113.2	62.0	340.0	20.0	242.9	18.8	14	13
36	65 422	75246	37.86	141.82	77.8	4.7	338.7	34.8	234.9	19.0	121.7	49.0	20.0	10.0	281.7	39.3	14	12
37	65 519	113221	36.02	139.79	74.9	4.3	256.9	55.4	157.2	6.6	62.8	33.8	310.0	30.0	189.2	41.6	11	10
38	65 712	11519	36.20	140.06	62.0	4.9	169.0	60.0	304.8	22.5	42.9	18.8	140.0	20.0	273.2	62.0	20	20
39	65 718	165745	35.24	139.79	52.2	4.4	42.0	54.0	201.5	34.3	298.3	9.9	30.0	10.0	164.6	75.9	13	12
							336.1	63.7	132.3	24.4	226.6	9.4	320.0	20.0	112.7	67.7	13	12
40	65 830	058 2	35.86	140.65	45.8	4.6	83.9	63.7	287.8	24.4	193.5	9.4	100.0	20.0	307.3	67.7	15	14
41	65 9 3	3 3 9	35.76	140.07	73.7	4.6	129.0	60.0	264.8	22.5	2.9	18.8	100.0	20.0	233.2	62.0	22	20
42	65 9 3	92118	35.77	140.04	61.6	4.5	96.1	63.7	252.3	24.4	346.6	9.4	80.0	20.0	232.7	67.7	14	14
43	65 911	42552	37.31	141.36	71.1	5.5	183.2	42.0	83.5	10.7	342.2	46.0	230.0	20.0	124.0	37.2	38	33
44	65 918	12117	36.29	141.52	40.4	6.7	120.0	65.0	300.0	25.0	30.0	0.0	120.0	20.0	300.0	70.0	141	130
45	65 918	54236	36.32	141.47	40.4	4.8	140.8	68.3	265.6	12.8	359.7	17.2	100.0	30.0	244.0	54.5	15	14
46	6510 9	222340	34.37	141.41	52.5	5.2	51.6	35.0	317.9	5.2	220.6	54.5	100.0	20.0	358.8	28.0	27	26
47	651114	145412	36.49	141.32	40.5	5.6	122.6	51.0	263.4	32.1	6.4	19.7	100.0	10.0	215.5	67.7	77	68
48	651126	91714	31.95	141.30	44.7	5.2	14.0	10.6	106.0	10.6	240.0	75.0	330.0	0.0	60.0	15.0	17	14
							270.0	15.0	90.0	75.0	180.0	0.0	270.0	60.0	90.0	30.0	17	14
49	651127	174218	32.67	141.32	70.6	5.5	150.0	45.0	330.0	45.0	60.0	0.0	150.0	0.0	330.0	90.0	55	52
							104.5	43.1	255.5	43.1	0.0	15.0	90.0	0.0	180.0	75.0	55	52
50	651227	13 721	36.27	142.37	50.1	5.1	65.0	0.0	335.0	0.0	200.0	90.0	20.0	0.0	110.0	0.0	17	17
							232.5	70.8	85.4	16.3	352.5	9.9	100.0	60.0	257.2	28.0	17	17
51	66 1 8	17 051	36.41	141.15	47.3	4.8	330.0	35.0	150.0	55.0	60.0	0.0	150.0	10.0	330.0	80.0	14	13
							78.0	54.0	278.5	34.3	181.8	9.9	90.0	10.0	315.4	75.9	14	13
52	66 111	23 616	33.67	137.25	55.2	5.4	1.2	28.0	91.7	0.8	183.2	62.0	50.0	20.0	312.9	18.8	38	34
							307.5	70.8	94.6	16.3	187.5	9.9	80.0	60.0	282.8	28.0	38	34
53	66 113	224222	36.08	139.89	49.0	4.3	42.2	54.8	282.0	19.5	181.2	28.0	80.0	20.0	319.4	54.5	10	10
							192.6	51.0	333.4	32.1	76.4	19.7	170.0	10.0	285.5	67.7	10	10

Eq	Date y m d	Time h m s	Latit deg	Long deg	Dep km	Mag	Pole-X dd	Pole-X d	Pole-Y dd	Pole-Y d	B-axis dd	B-axis d	P-axis dd	P-axis d	T-axis dd	T-axis d	Number read	Number used
54	66 117	84157	36.90	141.13	50.6	4.8	106.4	33.3	1.7	21.1	245.3	49.0	50.0	40.0	146.5	7.6	15	14
							271.7	27.4	174.1	14.3	59.4	58.5	220.0	30.0	315.0	8.7	15	14
55	66 124	8 913	35.59	140.88	50.3	5.0	146.1	63.7	302.3	24.4	36.6	9.4	130.0	20.0	282.7	67.7	28	27
56	66 218	92753	36.47	140.31	54.1	5.1	30.0	45.0	210.0	45.0	300.0	0.0	30.0	0.0	210.0	90.0	53	47
57	66 3 6	161534	35.56	140.47	74.8	4.8	314.0	28.1	51.1	13.0	163.3	58.5	270.0	10.0	5.7	29.5	22	20
58	66 314	1538 3	36.60	141.21	54.5	5.0	116.1	63.7	272.3	24.4	6.6	9.4	100.0	20.0	252.7	67.7	38	35
59	66 4 3	74321	38.46	142.18	49.6	5.3	100.2	44.1	299.9	44.1	200.0	10.0	110.0	0.0	20.0	80.0	51	49
60	66 4 3	134338	36.58	141.18	48.7	5.8	99.9	44.1	260.2	44.1	0.0	10.0	90.0	0.0	180.0	80.0	115	107
61	66 416	191321	34.87	142.04	60.1	5.2	356.8	14.0	263.2	14.0	130.0	70.0	40.0	0.0	310.0	20.0	43	39
							306.2	73.9	107.3	15.3	198.7	5.0	100.0	60.0	291.5	29.5	43	39
62	66 422	04522	35.61	142.08	52.0	5.8	346.5	34.3	82.2	8.3	184.0	54.5	40.0	30.0	299.7	17.2	45	39
							286.2	73.9	87.3	15.3	178.7	5.0	80.0	60.0	271.5	29.5	45	39
63	66 422	23648	35.64	142.07	50.7	5.5	287.5	70.8	74.6	16.3	167.5	9.9	60.0	60.0	262.8	28.0	27	23
							235.4	21.2	328.0	6.6	74.5	67.7	190.0	10.0	283.6	19.7	27	23
64	66 5 9	2 329	35.76	140.05	46.1	4.3	125.0	0.0	35.0	0.0	260.0	90.0	80.0	0.0	170.0	0.0	14	12
65	66 5 9	115749	38.52	139.12	45.9	4.7	320.0	25.0	140.0	65.0	50.0	0.0	140.0	20.0	320.0	70.0	13	10
							29.9	44.1	190.2	44.1	290.0	10.0	20.0	0.0	110.0	80.0	13	10
							80.0	55.0	260.0	35.0	350.0	0.0	80.0	10.0	260.0	80.0	13	10
66	66 517	959 4	35.65	140.71	51.8	5.1	129.9	44.1	290.2	44.1	30.0	10.0	120.0	0.0	210.0	80.0	68	61
							220.0	55.0	40.0	35.0	130.0	0.0	220.0	10.0	40.0	80.0	68	61
67	66 523	14316	36.54	140.95	41.8	4.6	12.6	27.0	267.5	27.0	140.0	50.0	50.0	0.0	320.0	40.0	11	11
68	66 6 3	233657	35.73	140.13	71.1	4.8	19.6	42.4	146.6	33.4	258.5	29.5	90.0	60.0	351.3	5.0	19	16
69	66 718	133921	38.34	141.90	55.5	4.8	280.0	85.0	100.0	5.0	10.0	0.0	100.0	50.0	280.0	40.0	29	24
70	66 829	5 333	35.46	139.89	65.9	4.7	147.8	47.2	20.3	29.4	272.8	28.0	70.0	60.0	177.5	9.9	19	16
71	6610 2	202040	36.40	141.16	43.9	4.8	132.0	54.0	291.5	34.3	28.3	9.9	120.0	10.0	254.6	75.9	11	11
72	661028	222029	35.74	140.22	66.1	5.0	232.0	54.0	31.5	34.3	128.3	9.9	220.0	10.0	354.6	75.9	43	39
73	661031	4 416	35.64	140.64	43.4	4.8	58.0	54.0	258.5	34.3	161.8	9.9	70.0	10.0	295.4	75.9	23	21
							320.0	45.0	140.0	45.0	50.0	0.0	140.0	0.0	320.0	90.0	23	21
74	6611 8	221518	35.01	140.16	60.9	4.5	280.0	55.0	100.0	35.0	190.0	0.0	280.0	10.0	100.0	80.0	10	10
							350.0	55.0	170.0	35.0	260.0	0.0	350.0	10.0	170.0	80.0	10	10
75	661119	141956	37.55	141.43	49.4	5.3	0.0	45.0	180.0	45.0	90.0	0.0	0.0	0.0	0.0	90.0	63	59
							120.0	45.0	300.0	45.0	30.0	0.0	120.0	0.0	300.0	90.0	63	59
76	661126	142514	35.64	140.17	64.0	4.8	164.9	73.1	312.7	14.5	45.0	8.7	140.0	30.0	300.6	58.5	14	12
77	661126	163834	35.58	140.26	71.0	4.2	327.4	51.0	186.6	32.1	83.6	19.7	350.0	10.0	234.5	67.7	10	10
78	661214	20 424	36.07	139.80	50.0	4.9	159.1	20.7	60.9	20.7	290.0	60.0	110.0	30.0	200.0	0.0	42	30

Eq	Date y m d	Time h m s	Latit deg	Long deg	Dep km	Mag	Pole-X dd	d	Pole-Y dd	d	B-axis dd	d	P-axis dd	d	T-axis dd	d	Number read	used
79	661227	102217	37.10	141.15	48.3	5.5	119.9	44.1	280.2	44.1	20.0	10.0	110.0	0.0	200.0	80.0	71	60
80	67 213	2021 9	36.13	139.86	61.4	4.9	350.0	45.0	170.0	45.0	80.0	0.0	170.0	0.0	350.0	90.0	39	35
81	67 222	1747 1	35.13	140.26	43.5	4.6	325.4	7.1	234.6	7.1	100.0	80.0	10.0	0.0	280.0	10.0	14	13
82	67 228	183719	32.67	141.97	76.3	5.5	346.8	14.0	253.2	14.0	120.0	70.0	30.0	0.0	300.0	20.0	39	33
							226.6	66.7	88.2	17.8	353.4	14.5	110.0	60.0	256.3	25.7	39	33
							353.4	66.7	131.8	17.8	226.6	14.5	110.0	60.0	323.7	25.7	39	33
83	67 3 2	171744	35.60	140.05	75.6	4.9	136.1	63.7	292.3	24.4	26.6	9.4	120.0	20.0	272.7	67.7	40	40
84	67 321	65449	36.17	139.80	60.4	5.1	180.8	68.3	305.6	12.8	39.7	17.2	140.0	30.0	284.0	54.5	52	50
85	67 4 7	832 9	35.76	140.85	40.6	5.3	194.0	10.6	286.0	10.6	60.0	75.0	150.0	0.0	240.0	15.0	27	27
							150.0	45.0	330.0	45.0	60.0	0.0	150.0	0.0	330.0	90.0	27	27
86	67 515	112732	32.25	141.77	56.3	5.4	235.4	7.1	144.6	7.1	10.0	80.0	190.0	10.0	280.0	0.0	49	48
							220.9	46.5	346.2	28.7	94.3	29.5	190.0	10.0	296.7	58.5	49	48
87	67 516	142128	34.88	139.98	51.9	4.5	351.3	34.8	95.1	19.0	208.3	49.0	310.0	10.0	48.3	39.3	13	12
							298.0	54.0	138.5	34.3	41.8	9.9	310.0	10.0	175.4	75.9	13	12
88	67 517	42450	31.76	141.75	54.4	4.9	102.8	67.5	10.7	0.8	280.4	22.5	170.0	40.0	31.9	41.6	45	35
							314.0	28.1	51.1	13.0	163.3	58.5	270.0	10.0	5.7	29.5	45	35
89	67 517	183442	38.15	142.34	45.7	4.8	57.5	81.1	297.1	4.5	206.5	7.6	110.0	40.0	305.3	49.0	11	10
90	67 522	114214	35.82	139.49	64.1	4.5	327.4	51.0	186.6	32.1	83.6	19.7	350.0	10.0	234.5	67.7	27	23
91	67 7 2	10 616	36.46	140.70	52.5	4.4	165.9	14.1	75.9	0.1	345.4	75.9	120.0	10.0	211.8	9.9	11	11
							49.6	42.4	176.6	33.4	288.5	29.5	120.0	60.0	21.3	5.0	11	11
92	67 7 2	1638 5	32.55	142.37	62.3	5.1	21.1	41.6	238.9	41.6	130.0	20.0	40.0	0.0	310.0	70.0	15	14
93	67 8 3	211256	36.04	139.89	45.6	4.5	136.1	63.7	292.3	24.4	26.6	9.4	120.0	20.0	272.7	67.7	11	11
							192.6	51.0	333.4	32.1	76.4	19.7	170.0	10.0	285.5	67.7	11	11
94	67 8 9	1 559	37.07	141.15	45.7	4.7	147.9	54.8	268.0	19.5	8.8	28.0	110.0	20.0	230.6	54.5	12	12
95	67 830	11 612	35.59	140.07	64.3	4.7	280.0	45.0	100.0	45.0	10.0	0.0	100.0	0.0	280.0	90.0	31	27
96	67 830	17 942	36.14	140.08	71.2	4.8	80.0	65.0	260.0	25.0	350.0	0.0	80.0	20.0	260.0	70.0	47	38
97	67 915	92838	35.65	140.78	55.4	5.6	112.0	54.0	271.5	34.3	8.3	9.9	100.0	10.0	234.6	75.9	76	68
98	67 920	93242	35.94	140.15	79.3	5.2	83.9	63.7	287.8	24.4	193.5	9.4	100.0	20.0	307.3	67.7	61	55
99	671010	1547 0	36.65	141.12	47.4	4.9	96.1	63.7	252.3	24.4	346.6	9.4	80.0	20.0	232.7	67.7	32	29
100	6711 2	41722	37.15	141.52	44.4	5.0	30.0	45.0	210.0	45.0	300.0	0.0	30.0	0.0	210.0	90.0	32	31
							119.9	44.1	280.2	44.1	20.0	10.0	110.0	0.0	200.0	80.0	32	31
101	6711 8	105612	35.44	141.09	41.4	5.0	286.1	63.7	82.3	24.4	176.5	9.4	270.0	20.0	62.7	67.7	13	11
102	671110	31935	35.54	140.15	71.9	5.3	90.0	45.0	270.0	45.0	0.0	0.0	90.0	0.0	270.0	90.0	87	80
103	671119	54238	36.02	139.90	50.3	4.3	179.1	62.1	289.0	10.2	23.9	25.7	130.0	30.0	260.9	48.6	13	13
104	671119	21 7 0	36.48	141.19	50.1	6.0	130.0	45.0	310.0	45.0	40.0	0.0	130.0	0.0	310.0	90.0	137	125
105	671217	44413	35.64	140.99	67.5	4.5	341.1	60.0	205.2	22.5	107.1	18.8	10.0	20.0	236.8	62.0	12	12

Eq	Date y m d	Time h m s	Latit deg	Long deg	Dep km	Mag	Pole-X dd	Pole-X d	Pole-Y dd	Pole-Y d	B-axis dd	B-axis d	P-axis dd	P-axis d	T-axis dd	T-axis d	Number read	Number used
106	68 112	11241	34.12	141.67	55.9	5.0	171.7	27.4	74.1	14.3	319.4	58.5	120.0	30.0	215.0	8.7	27 /	23
							65.4	48.4	332.8	2.3	240.8	41.6	120.0	30.0	7.2	33.8	27 /	23
107	68 118	25619	35.78	140.26	60.9	4.7	104.6	7.1	195.4	7.1	330.0	80.0	60.0	0.0	150.0	10.0	17 /	13
							159.9	47.6	358.5	40.9	260.3	9.4	60.0	80.0	169.7	3.4	17 /	13
108	68 123	204515	35.76	140.10	65.6	4.7	154.6	41.3	62.2	2.7	329.1	48.6	100.0	30.0	206.1	25.7	27 /	23
							75.1	73.1	287.3	14.5	195.0	8.7	100.0	30.0	299.4	58.5	27 /	23
109	68 219	234825	38.25	141.97	56.1	4.6	80.2	44.1	279.9	44.1	180.0	10.0	90.0	0.0	0.0	80.0	17 /	14
							230.8	68.3	355.6	12.8	89.7	17.2	190.0	30.0	334.0	54.5	17 /	14
110	68 226	5 031	37.59	141.56	66.7	5.4	129.9	44.1	290.2	44.1	30.0	10.0	120.0	0.0	210.0	80.0	104 /	97
111	68 3 6	91233	36.07	139.95	50.6	5.2	172.6	51.0	313.4	32.1	56.4	19.7	150.0	10.0	265.5	67.7	37 /	33
112	68 3 7	115443	35.54	140.15	54.1	5.1	42.6	27.0	297.5	27.0	170.0	50.0	80.0	0.0	350.0	40.0	47 /	42
113	68 321	94055	35.66	140.73	59.5	4.7	154.9	73.1	302.7	14.5	35.0	8.7	130.0	30.0	290.0	58.5	20 /	19
114	68 4 7	114742	38.31	141.89	51.2	4.9	85.1	73.1	297.3	14.5	205.0	8.7	110.0	30.0	309.4	58.5	30 /	23
115	68 421	1734 0	38.60	143.34	58.1	5.8	206.6	37.8	333.4	37.8	90.0	30.0	180.0	0.0	270.0	60.0	103 /	91
116	68 5 7	225530	35.95	140.07	66.9	4.2	202.7	81.6	72.9	5.4	342.3	6.4	80.0	50.0	247.0	39.3	10 /	10
117	68 519	131236	35.62	142.11	59.6	5.9	344.6	21.2	252.0	6.6	145.5	67.7	30.0	10.0	296.4	19.7	65 /	64
							321.1	56.5	74.0	14.5	172.4	29.5	40.0	50.0	277.3	24.4	65 /	64
118	68 519	1454 5	35.55	142.19	52.8	5.5	344.6	7.1	75.4	7.1	210.0	80.0	30.0	10.0	300.0	0.0	36 /	34
							100.0	15.0	280.0	75.0	10.0	0.0	100.0	60.0	280.0	30.0	36 /	34
119	68 618	35724	38.78	143.87	40.3	6.0	324.6	21.2	232.0	6.6	125.5	67.7	10.0	10.0	276.4	19.7	44 /	42
							100.0	15.0	280.0	75.0	10.0	0.0	100.0	60.0	280.0	30.0	44 /	42
120	68 7 1	194512	35.97	139.38	60.8	6.1	0.0	45.0	180.0	45.0	270.0	0.0	0.0	0.0	180.0	90.0	177 /	154
121	68 922	2241 0	35.34	140.26	54.4	4.7	339.1	20.7	240.9	20.7	110.0	60.0	20.0	0.0	290.0	30.0	13 /	11
							260.2	44.1	99.9	44.1	0.0	10.0	180.0	80.0	270.0	0.0	13 /	11
122	6810 7	44025	31.56	140.29	41.7	5.2	67.4	72.5	274.0	15.7	181.9	7.4	285.0	60.0	87.8	28.9	37 /	35
							1.0	31.6	96.7	9.1	200.9	56.8	315.0	15.0	53.5	28.9	37 /	35
123	6810 8	95041	35.57	140.12	75.3	5.3	100.8	68.3	225.6	12.8	319.7	17.2	60.0	30.0	204.0	54.5	59 /	53
124	681028	234039	33.46	141.15	66.9	5.3	80.0	45.0	260.0	45.0	350.0	0.0	80.0	0.0	260.0	90.0	65 /	65
							140.0	45.0	320.0	45.0	50.0	0.0	140.0	0.0	320.0	90.0	65 /	65
125	681031	164017	38.38	142.29	45.5	4.7	355.4	21.2	88.0	6.6	194.5	67.7	310.0	10.0	43.6	19.7	11 /	10
126	69 115	1 2 0	37.52	141.55	53.1	4.9	90.0	45.0	270.0	45.0	0.0	0.0	90.0	0.0	270.0	90.0	33 /	30
							138.0	54.0	338.5	34.3	241.8	9.9	150.0	10.0	15.4	75.9	33 /	30
							20.0	35.0	200.0	55.0	110.0	0.0	200.0	10.0	20.0	80.0	33 /	30
127	69 328	12 713	33.48	140.23	52.5	4.9	86.8	14.0	353.2	14.0	220.0	70.0	130.0	0.0	40.0	20.0	26 /	23
							349.1	20.7	250.9	20.7	120.0	60.0	300.0	30.0	30.0	0.0	26 /	23
							300.0	75.0	120.0	15.0	210.0	0.0	300.0	30.0	120.0	60.0	26 /	23
							30.8	68.3	155.6	12.8	249.7	17.2	350.0	30.0	134.0	54.5	26 /	23

Eq	Date y m d	Time h m s	Latit deg	Long deg	Dep km	Mag	Pole-X dd	Pole-X d	Pole-Y dd	Pole-Y d	B-axis dd	B-axis d	P-axis dd	P-axis d	T-axis dd	T-axis d	Number read	Number used
128	69 425	122928	35.66	140.05	52.3	4.5	18.7	34.8	274.9	19.0	161.7	49.0	60.0	10.0	321.7	39.3	13	11
							282.8	46.5	181.5	10.6	81.9	41.6	220.0	40.0	330.4	22.5	13	11
129	69 513	353 1	34.96	139.79	45.6	4.3	320.0	35.0	140.0	55.0	50.0	0.0	140.0	10.0	320.0	80.0	13	11
130	69 513	231943	36.46	140.69	61.2	5.2	119.9	44.1	280.2	44.1	20.0	10.0	110.0	0.0	200.0	80.0	41	37
131	69 515	1056 9	34.99	140.08	64.4	5.6	50.2	44.1	249.9	44.1	150.0	10.0	60.0	0.0	330.0	80.0	13	12
132	69 522	204049	36.48	140.59	57.7	4.4	159.9	44.1	320.2	44.1	60.0	10.0	150.0	0.0	240.0	80.0	12	12
							268.7	34.8	164.9	19.0	51.7	49.0	310.0	10.0	211.7	39.3	12	12
133	69 611	14140	38.73	141.46	71.6	4.5	92.6	81.1	212.9	4.5	303.5	7.6	40.0	40.0	204.7	49.0	11	11
134	69 623	1457 8	37.31	141.62	45.2	5.2	40.0	45.0	220.0	45.0	310.0	0.0	40.0	0.0	220.0	90.0	59	56
							119.9	44.1	280.2	44.1	20.0	10.0	110.0	0.0	200.0	80.0	59	56
135	69 8 6	174022	32.01	141.53	56.4	4.7	214.0	28.1	311.1	13.0	63.3	58.5	170.0	10.0	265.7	29.5	14	11
136	69 821	222155	36.43	141.00	41.6	4.7	67.2	46.5	168.5	10.6	268.1	41.6	130.0	40.0	19.6	22.5	11	10
							284.6	41.3	192.2	2.7	99.1	48.6	230.0	30.0	336.1	25.7	11	10
137	69 828	45056	34.74	141.53	40.5	4.8	33.4	66.7	171.8	17.8	266.6	14.5	150.0	60.0	3.7	25.7	21	21
							190.9	20.7	289.1	20.7	60.0	60.0	240.0	30.0	150.0	0.0	21	21
138	69 913	2019 1	33.76	141.84	65.0	4.9	255.4	21.2	348.0	6.6	94.5	67.7	210.0	10.0	303.6	19.7	22	17
139	6910 3	21 319	35.32	140.00	42.0	4.5	105.3	53.4	7.0	6.1	272.6	35.9	40.0	40.0	158.3	29.5	15	13
							104.6	7.1	195.4	7.1	330.0	80.0	60.0	0.0	150.0	10.0	15	13
							7.3	81.6	137.1	5.4	227.7	6.4	130.0	50.0	323.0	39.3	15	13
							189.8	49.3	352.4	39.4	89.6	8.7	300.0	80.0	180.4	5.0	15	13
140	691113	32323	35.45	140.99	45.5	4.9	134.1	14.1	44.1	0.1	314.6	75.9	180.0	10.0	88.3	9.9	30	24
141	691116	25018	36.56	141.23	48.5	4.6	300.0	35.0	120.0	55.0	30.0	0.0	120.0	10.0	300.0	80.0	11	11
142	70 129	15 321	35.90	140.48	60.6	5.1	73.9	63.7	277.8	24.4	183.5	9.4	90.0	20.0	297.3	67.7	62	54
							170.0	55.0	350.0	35.0	80.0	0.0	170.0	10.0	350.0	80.0	62	54
143	70 2 4	191746	36.44	140.77	55.4	4.8	290.0	35.0	110.0	55.0	20.0	0.0	110.0	10.0	290.0	80.0	32	29
							32.0	54.0	191.5	34.3	288.3	9.9	20.0	10.0	154.6	75.9	32	29
144	70 210	194039	36.18	140.12	60.2	4.8	330.0	25.0	150.0	65.0	60.0	0.0	150.0	20.0	330.0	70.0	29	24
145	70 211	202510	36.00	139.91	52.7	4.1	177.0	41.0	290.1	24.3	41.7	39.3	140.0	10.0	241.7	49.0	13	12
146	70 215	13 135	37.38	141.41	55.4	5.1	133.4	37.8	6.6	37.8	250.0	30.0	160.0	0.0	70.0	60.0	26	21
							115.0	0.0	25.0	0.0	340.0	90.0	160.0	0.0	70.0	0.0	26	21
147	70 3 8	35222	37.10	141.55	48.2	4.9	290.0	35.0	110.0	55.0	20.0	0.0	110.0	10.0	290.0	80.0	34	28
							50.0	55.0	230.0	35.0	320.0	0.0	50.0	10.0	230.0	80.0	34	28
148	70 315	171832	36.01	140.28	46.5	4.6	142.3	54.8	318.6	35.1	49.9	1.7	310.0	80.0	140.2	9.9	17	12
149	70 416	105553	34.47	141.92	51.4	5.3	237.9	54.8	358.0	19.5	98.8	28.0	200.0	20.0	320.6	54.5	60	60
150	70 417	019 2	38.23	141.65	56.1	4.7	102.7	32.8	217.3	32.8	340.0	40.0	70.0	0.0	160.0	50.0	15	13

Eq	Date y m d	Time h m s	Latit deg	Long deg	Dep km	Mag	Pole-X dd	Pole-X d	Pole-Y dd	Pole-Y d	B-axis dd	B-axis d	P-axis dd	P-axis d	T-axis dd	T-axis d	Number read	Number used
151	70 526	11534	37.08	141.20	46.2	4.7	60.0	65.0	240.0	25.0	330.0	0.0	60.0	20.0	240.0	70.0	22 /	20
							290.0	45.0	110.0	45.0	200.0	0.0	290.0	0.0	110.0	90.0	22 /	20
152	70 610	225422	36.09	139.82	54.3	4.2	205.6	52.1	77.1	25.8	333.7	25.7	120.0	60.0	236.6	14.5	11 /	11
							203.2	14.0	296.8	14.0	70.0	70.0	160.0	0.0	250.0	20.0	11 /	11
153	70 711	232815	36.50	140.60	51.0	5.1	32.0	54.0	191.5	34.3	288.3	9.9	20.0	10.0	154.6	75.9	52 /	49
							129.9	44.1	290.2	44.1	30.0	10.0	120.0	0.0	210.0	80.0	52 /	49
154	70 714	31128	36.16	139.85	53.8	4.0	95.4	7.1	4.6	7.1	230.0	80.0	140.0	0.0	50.0	10.0	11 /	11
155	70 727	20 447	36.44	141.34	60.5	4.3	135.0	0.0	45.0	0.0	270.0	90.0	90.0	0.0	180.0	0.0	12 /	12
							80.2	44.1	279.9	44.1	180.0	10.0	90.0	0.0	0.0	80.0	12 /	12
156	70 728	541 3	35.59	140.23	70.9	4.2	29.1	46.5	263.8	28.7	155.7	29.5	60.0	10.0	313.3	58.5	13 /	12
							125.1	73.1	337.3	14.5	245.0	8.7	150.0	30.0	349.4	58.5	13 /	12
157	70 8 2	43318	35.55	140.13	63.9	4.2	119.9	44.1	280.2	44.1	20.0	10.0	110.0	0.0	200.0	80.0	11 /	10
							69.1	20.7	330.9	20.7	200.0	60.0	110.0	0.0	20.0	30.0	11 /	10
158	70 824	11 018	35.57	141.02	53.8	4.4	15.4	41.3	107.8	2.7	200.9	48.6	70.0	30.0	323.9	25.7	12 /	12
159	70 827	55436	34.61	141.14	51.0	5.1	37.3	32.8	282.7	32.8	160.0	40.0	70.0	0.0	340.0	50.0	30 /	29
160	70 930	42624	35.49	139.69	46.1	4.8	310.0	15.0	130.0	75.0	40.0	0.0	130.0	30.0	310.0	60.0	34 /	24
							248.4	35.0	342.1	5.2	79.4	54.5	200.0	20.0	301.2	28.0	34 /	24
161	701013	1048 4	35.93	140.10	76.8	4.3	359.2	68.3	234.4	12.8	140.3	17.2	40.0	30.0	256.1	54.5	14 /	13
							156.6	37.8	283.4	37.8	40.0	30.0	130.0	0.0	220.0	60.0	14 /	13
162	701020	31022	31.54	140.45	78.9	5.0	141.6	35.0	47.9	5.2	310.6	54.5	190.0	20.0	88.8	28.0	23 /	20
							103.4	66.7	241.8	17.8	336.6	14.5	220.0	60.0	73.7	25.7	23 /	20
							28.9	56.5	276.0	14.5	177.6	29.5	310.0	50.0	72.7	24.4	23 /	20
163	701030	81442	35.96	139.99	63.3	4.9	245.4	7.1	154.6	7.1	20.0	80.0	200.0	10.0	290.0	0.0	37 /	28
164	71 1 1	225717	36.08	139.90	57.0	4.1	192.4	69.3	79.1	8.5	346.1	18.8	100.0	50.0	243.0	33.8	11 /	11
							188.4	35.0	282.1	5.2	19.4	54.5	140.0	20.0	241.2	28.0	11 /	11
165	71 1 3	191140	33.64	138.67	55.3	5.5	233.5	48.7	341.9	15.5	84.0	37.2	190.0	20.0	302.2	46.0	60 /	59
166	71 1 5	6 853	34.49	137.17	44.0	6.1	259.9	45.9	99.3	42.5	0.2	9.9	170.0	80.0	269.9	1.7	103 /	87
167	71 1 5	143137	36.43	141.17	43.6	4.8	310.0	35.0	130.0	55.0	40.0	0.0	130.0	10.0	310.0	80.0	14 /	13
168	71 1 6	15 421	36.39	141.19	49.0	5.5	130.0	45.0	310.0	45.0	40.0	0.0	130.0	0.0	310.0	90.0	102 /	99
169	71 1 7	24040	35.74	140.24	58.8	4.6	43.2	14.0	136.8	14.0	270.0	70.0	0.0	0.0	90.0	20.0	12 /	12
170	71 118	181758	35.58	140.08	64.3	4.0	130.2	49.3	327.6	39.4	230.4	8.7	20.0	80.0	139.6	5.0	11 /	10
							95.9	14.1	5.9	0.1	275.4	75.9	50.0	10.0	141.8	9.9	11 /	10
171	71 121	6 245	36.41	141.16	45.1	4.5	146.1	63.7	302.3	24.4	36.6	9.4	130.0	20.0	282.7	67.7	11 /	10
							81.6	35.0	347.9	5.2	250.6	54.5	130.0	20.0	28.8	28.0	11 /	10
172	71 227	175635	38.34	141.82	53.7	5.1	40.0	55.0	220.0	35.0	310.0	0.0	40.0	10.0	220.0	80.0	52 /	49
							100.0	65.0	280.0	25.0	10.0	0.0	100.0	20.0	280.0	70.0	52 /	49
							182.0	54.0	341.5	34.3	78.3	9.9	170.0	10.0	304.6	75.9	52 /	49

Eq	Date y m d	Time h m s	Latit deg	Long deg	Dep km	Mag	Pole-X dd	Pole-X d	Pole-Y dd	Pole-Y d	B-axis dd	B-axis d	P-axis dd	P-axis d	T-axis dd	T-axis d	Number read	Number used
173	71 311	0 830	35.48	140.05	76.1	4.2	30.0	25.0	210.0	65.0	120.0	0.0	210.0	20.0	30.0	70.0	13	11
							103.4	37.8	336.6	37.8	220.0	30.0	130.0	0.0	40.0	60.0	13	11
							333.5	48.7	81.9	15.5	184.0	37.2	290.0	20.0	42.2	46.0	13	11
174	71 326	11950	38.44	142.21	41.9	5.5	99.9	44.1	260.2	44.1	0.0	10.0	90.0	0.0	180.0	80.0	88	83
							121.1	41.6	338.9	41.6	230.0	20.0	140.0	0.0	50.0	70.0	88	83
175	71 6 3	20 414	37.10	141.16	53.9	4.5	21.1	41.6	238.9	41.6	130.0	20.0	40.0	0.0	310.0	70.0	12	12
							122.0	54.0	281.5	34.3	18.3	9.9	110.0	10.0	244.6	75.9	12	12
176	71 612	115345	35.29	140.71	43.9	4.7	75.0	62.9	187.6	11.2	282.7	24.4	160.0	50.0	27.6	29.5	14	12
177	71 621	75711	36.18	139.79	57.4	4.9	191.3	34.8	295.1	19.0	48.3	49.0	150.0	10.0	248.3	39.3	50	38
178	71 7 4	32846	36.19	140.99	41.6	4.2	25.1	73.1	237.3	14.5	145.0	8.7	50.0	30.0	249.4	58.5	10	10
							214.9	73.1	2.7	14.5	95.0	8.7	190.0	30.0	350.6	58.5	10	10
179	71 7 8	24124	36.84	141.27	54.9	4.7	332.7	32.8	87.3	32.8	210.0	40.0	300.0	0.0	30.0	50.0	14	14
180	71 727	8 841	35.98	140.10	68.0	5.1	78.0	54.0	278.5	34.3	181.8	9.9	90.0	10.0	315.4	75.9	37	33
181	71 8 4	03243	36.29	140.11	77.0	4.4	41.2	28.0	131.7	0.8	223.2	62.0	90.0	20.0	352.9	18.8	11	11
							222.5	70.8	75.4	16.3	342.5	9.9	90.0	60.0	247.2	28.0	11	11
182	71 812	4 2 7	35.76	140.06	57.4	4.8	37.2	46.5	138.5	10.6	238.1	41.6	100.0	40.0	349.6	22.5	34	28
183	71 9 8	162513	37.15	141.50	50.3	5.5	30.0	45.0	210.0	45.0	300.0	0.0	30.0	0.0	210.0	90.0	79	76
							119.9	44.1	280.2	44.1	20.0	10.0	110.0	0.0	200.0	80.0	79	76
184	711012	142454	36.75	141.85	57.0	4.8	280.0	35.0	100.0	55.0	10.0	0.0	100.0	10.0	280.0	80.0	11	10
							40.0	65.0	220.0	25.0	310.0	0.0	40.0	20.0	220.0	70.0	11	10
							330.0	45.0	150.0	45.0	60.0	0.0	150.0	0.0	330.0	90.0	11	10
							214.9	73.1	2.7	14.5	95.0	8.7	190.0	30.0	350.6	58.5	11	10
185	711023	143836	36.21	141.81	49.1	5.0	27.5	81.1	267.1	4.5	176.5	7.6	80.0	40.0	275.3	49.0	20	20
186	711030	85411	35.80	139.46	49.3	4.0	305.4	41.3	37.8	2.7	130.9	48.6	0.0	30.0	253.9	25.7	12	12
187	711116	34722	36.07	139.93	46.0	4.4	183.5	48.7	291.9	15.5	34.0	37.2	140.0	20.0	252.2	46.0	16	16
188	711116	639 5	36.44	141.14	44.1	4.6	108.0	54.0	308.5	34.3	211.8	9.9	120.0	10.0	345.4	75.9	21	17
189	72 1 4	91959	35.90	140.52	43.4	5.0	150.2	44.1	349.9	44.1	250.0	10.0	160.0	0.0	70.0	80.0	36	33
190	72 1 7	122912	35.86	140.16	66.3	4.4	69.1	46.5	303.8	28.7	195.7	29.5	100.0	10.0	353.3	58.5	14	13
191	72 127	234058	35.69	139.12	48.4	4.8	3.5	34.3	267.8	8.3	166.1	54.5	310.0	30.0	50.3	17.2	22	21
192	72 131	191218	36.01	140.39	55.3	4.2	158.9	41.6	301.1	41.6	50.0	20.0	140.0	0.0	230.0	70.0	11	10
193	72 225	05311	36.07	139.85	47.2	4.4	192.7	32.8	307.3	32.8	70.0	40.0	160.0	0.0	250.0	50.0	19	18
194	72 229	182257	33.32	141.15	70.2	7.1	139.9	44.1	300.2	44.1	40.0	10.0	130.0	0.0	220.0	80.0	178	177
195	72 229	184237	33.28	141.32	64.2	5.6	135.0	45.0	315.0	45.0	45.0	0.0	135.0	0.0	315.0	90.0	60	60
196	72 229	21 123	33.47	141.23	68.9	5.1	156.5	34.3	252.2	8.3	354.0	54.5	210.0	30.0	109.7	17.2	11	11
							127.5	70.8	274.6	16.3	7.5	9.9	260.0	60.0	102.8	28.0	11	11

Eq	Date y m d	Time h m s	Latit deg	Long deg	Dep km	Mag	Pole-X dd	Pole-X d	Pole-Y dd	Pole-Y d	B-axis dd	B-axis d	P-axis dd	P-axis d	T-axis dd	T-axis d	Number read	Number used
197	72 3 3	510 7	33.48	141.07	78.1	5.5	109.9	44.1	270.2	44.1	10.0	10.0	100.0	0.0	190.0	80.0	121	121
							140.0	45.0	320.0	45.0	50.0	0.0	140.0	0.0	320.0	90.0	121	121
198	72 311	181557	33.62	139.98	41.9	4.5	207.5	81.1	87.1	4.5	356.5	7.6	260.0	40.0	95.3	49.0	15	13
							351.7	27.4	254.1	14.3	139.4	58.5	300.0	30.0	35.0	8.7	15	13
							39.1	62.1	149.0	10.2	243.9	25.7	350.0	30.0	120.9	48.6	15	13
199	72 314	947 9	33.06	141.37	72.3	5.4	320.0	55.0	140.0	35.0	230.0	0.0	320.0	10.0	140.0	80.0	41	31
200	72 314	20 731	38.57	141.70	52.6	4.7	113.9	63.7	317.8	24.4	223.5	9.4	130.0	20.0	337.3	67.7	15	13
							243.5	48.7	351.9	15.5	94.0	37.2	200.0	20.0	312.2	46.0	15	13
201	72 319	81733	33.56	141.92	44.1	5.7	162.5	70.8	15.4	16.3	282.5	9.9	30.0	60.0	187.2	28.0	100	97
							278.4	27.4	15.9	14.3	130.6	58.5	330.0	30.0	235.0	8.7	100	97
202	72 4 3	183650	33.97	140.39	40.6	5.0	236.5	48.7	128.1	15.5	26.0	37.2	280.0	20.0	167.8	46.0	27	24
							233.2	14.0	326.8	14.0	100.0	70.0	280.0	20.0	190.0	0.0	27	24
203	72 5 4	125024	33.28	141.45	67.5	5.5	347.3	81.6	117.1	5.4	207.7	6.4	110.0	50.0	303.0	39.3	69	69
204	72 523	205144	33.34	141.33	64.8	4.9	239.0	60.0	14.8	22.5	112.9	18.8	210.0	20.0	343.2	62.0	13	12
205	72 6 3	0 246	33.39	141.24	70.7	5.1	275.3	79.4	10.6	1.0	100.7	10.6	0.0	45.0	200.8	43.1	13	11
							105.0	45.0	285.0	45.0	15.0	0.0	105.0	0.0	285.0	90.0	13	11
206	72 615	32722	36.35	141.47	43.2	4.8	150.5	42.4	23.4	33.4	271.5	29.5	80.0	60.0	178.7	5.0	15	13
							322.6	27.0	217.5	27.0	90.0	50.0	270.0	40.0	0.0	0.0	15	13
							180.2	45.9	340.7	42.5	79.9	9.9	270.0	80.0	170.2	1.7	15	13
207	72 628	105043	37.48	141.47	53.5	5.3	0.0	45.0	180.0	45.0	90.0	0.0	180.0	0.0	0.0	90.0	74	67
208	72 811	141212	35.89	140.30	55.8	4.3	346.8	14.0	253.2	14.0	120.0	70.0	30.0	0.0	300.0	20.0	11	10
							325.0	62.9	77.6	11.2	172.7	24.4	50.0	50.0	277.6	29.5	11	10
209	72 922	23 920	34.27	140.45	49.2	4.9	115.0	62.9	2.4	11.2	267.3	24.4	30.0	50.0	162.4	29.5	27	24
							295.4	7.1	204.6	7.1	70.0	80.0	250.0	10.0	340.0	0.0	27	24
210	72 925	182732	38.40	142.10	52.9	5.5	133.0	41.0	19.9	24.3	268.3	39.3	170.0	10.0	68.3	49.0	63	50
211	7210 9	2 242	35.84	140.62	41.3	4.4	282.6	27.0	177.5	27.0	50.0	50.0	320.0	0.0	230.0	40.0	15	15
							317.4	51.0	176.6	32.1	73.6	19.7	340.0	10.0	224.5	67.7	15	15
212	721018	104819	35.73	140.11	71.8	5.1	73.9	63.7	277.8	24.4	183.5	9.4	90.0	20.0	297.3	67.7	52	50
213	7211 1	232249	38.26	141.95	46.6	4.9	9.1	46.5	243.8	28.7	135.7	29.5	40.0	10.0	293.3	58.5	42	36
							90.0	55.0	270.0	35.0	0.0	0.0	90.0	10.0	270.0	80.0	42	36
							130.2	44.1	329.9	44.1	230.0	10.0	140.0	0.0	50.0	80.0	42	36
214	7211 5	64022	35.59	140.07	57.5	4.3	5.7	62.0	138.9	20.0	236.1	18.8	110.0	60.0	334.1	22.5	12	12
							337.3	75.7	94.1	6.6	185.6	12.7	80.0	50.0	285.4	37.2	12	12
215	7211 6	43058	36.44	140.74	55.9	4.1	64.9	73.1	212.7	14.5	305.0	8.7	40.0	30.0	200.6	58.5	11	10
							147.5	27.0	252.6	27.0	20.0	50.0	110.0	0.0	200.0	40.0	11	10
216	7211 6	203949	36.07	139.86	53.0	5.1	197.5	27.0	302.6	27.0	70.0	50.0	160.0	0.0	250.0	40.0	51	47

Eq	Date y m d	Time h m s	Latit deg	Long deg	Dep km	Mag	Pole-X dd	Pole-X d	Pole-Y dd	Pole-Y d	B-axis dd	B-axis d	P-axis dd	P-axis d	T-axis dd	T-axis d	Number read	Number used
217	7212 1	12 210	35.70	140.66	46.8	4.6	40.0	35.0	220.0	55.0	130.0	0.0	220.0	10.0	40.0	80.0	18	15
							90.0	55.0	270.0	35.0	0.0	0.0	90.0	10.0	270.0	80.0	18	15
							330.0	45.0	150.0	45.0	60.0	0.0	150.0	0.0	330.0	90.0	18	15
218	7212 4	13226	36.16	140.06	52.4	4.0	330.0	35.0	150.0	55.0	60.0	0.0	150.0	10.0	330.0	80.0	10	10
							195.4	21.2	288.0	6.6	34.5	67.7	150.0	10.0	243.6	19.7	10	10
219	7212 4	1916 8	33.24	141.12	61.2	7.2	120.0	45.0	300.0	45.0	30.0	0.0	120.0	0.0	300.0	90.0	221	220
220	7212 4	205035	33.10	141.10	63.4	5.3	338.8	28.0	248.4	0.8	156.8	62.0	290.0	20.0	27.1	18.8	37	32
221	7212 5	1311 5	33.24	141.16	59.3	4.9	107.5	27.0	212.6	27.0	340.0	50.0	70.0	0.0	160.0	40.0	17	14
222	7212 6	13 336	33.21	140.43	69.1	5.2	351.1	60.0	215.2	22.5	117.1	18.8	20.0	20.0	246.8	62.0	16	16
223	7212 7	512 2	32.97	141.31	65.2	5.3	135.0	0.0	45.0	0.0	270.0	90.0	90.0	0.0	180.0	0.0	39	39
							179.5	46.9	27.8	39.5	285.5	14.5	90.0	75.0	194.5	3.8	39	39
224	7212 7	91446	32.97	141.29	50.9	4.7	49.9	44.1	210.2	44.1	310.0	10.0	40.0	0.0	130.0	80.0	22	17
							310.0	45.0	130.0	45.0	40.0	0.0	130.0	0.0	310.0	90.0	22	17
225	7212 8	04556	32.91	141.98	57.4	4.5	93.4	37.8	326.6	37.8	210.0	30.0	30.0	60.0	120.0	0.0	12	12
226	7212 8	83756	35.63	139.99	68.9	4.8	33.4	37.8	266.6	37.8	150.0	30.0	60.0	0.0	330.0	60.0	40	37
227	721212	195029	33.58	140.61	45.6	4.8	115.4	48.4	22.8	2.3	290.8	41.6	170.0	30.0	57.2	33.8	39	29
							288.8	28.0	198.4	0.8	106.8	62.0	240.0	20.0	337.1	18.8	39	29
228	721215	105154	33.07	141.24	61.0	5.2	312.7	75.7	195.9	6.6	104.4	12.7	210.0	50.0	4.6	37.2	17	16
							314.0	28.1	51.1	13.0	163.3	58.5	270.0	10.0	5.7	29.5	17	16
229	721215	151542	34.47	140.01	76.0	4.9	68.2	20.9	335.4	7.3	227.3	67.7	20.0	20.0	113.5	9.4	43	34
230	721218	12431	37.15	141.53	42.5	4.6	50.0	55.0	230.0	35.0	320.0	0.0	50.0	10.0	230.0	80.0	15	13
							126.6	37.8	253.4	37.8	10.0	30.0	100.0	0.0	190.0	60.0	15	13
231	73 120	15 450	34.99	140.93	40.0	4.6	310.0	75.0	130.0	15.0	40.0	0.0	130.0	60.0	310.0	30.0	22	19
232	73 121	15517	34.81	141.16	40.8	4.8	85.4	7.1	354.6	7.1	220.0	80.0	40.0	10.0	130.0	0.0	19	16
							307.3	81.6	77.1	5.4	167.7	6.4	70.0	50.0	263.0	39.3	19	16
233	73 121	171619	36.07	139.86	52.8	4.8	172.6	51.0	313.4	32.1	56.4	19.7	150.0	10.0	265.5	67.7	38	31
234	73 124	192413	37.32	142.23	40.9	4.6	145.9	14.1	55.9	0.1	325.4	75.9	100.0	10.0	191.8	9.9	12	12
							222.1	44.2	336.1	22.7	84.6	37.2	290.0	50.0	184.4	12.7	12	12
235	73 2 4	22 112	34.60	141.75	60.0	4.7	49.1	20.7	310.9	20.7	180.0	60.0	0.0	30.0	90.0	0.0	10	10
							153.4	66.7	291.8	17.8	26.6	14.5	270.0	60.0	123.7	25.7	10	10
236	73 210	141211	32.87	141.27	79.4	5.1	273.5	48.7	21.9	15.5	124.0	37.2	230.0	20.0	342.2	46.0	40	40
237	73 320	2 3 8	36.56	141.11	51.5	4.7	55.4	41.3	147.8	2.7	240.9	48.6	110.0	30.0	3.9	25.7	22	15
							297.9	44.2	183.9	22.7	75.4	37.2	230.0	50.0	335.6	12.7	22	15
238	73 327	23515	36.65	142.19	40.0	5.0	74.5	43.1	225.5	43.1	330.0	15.0	150.0	75.0	60.0	0.0	37	29
239	73 327	11 831	35.55	139.96	58.8	4.9	17.2	46.5	118.5	10.6	218.1	41.6	80.0	40.0	329.6	22.5	51	43
240	73 417	52339	35.60	140.78	42.7	4.5	280.0	35.0	100.0	55.0	10.0	0.0	100.0	10.0	280.0	80.0	21	17
							50.0	45.0	230.0	45.0	320.0	0.0	50.0	0.0	230.0	90.0	21	17

Eq	Date y m d	Time h m s	Latit deg	Long deg	Dep km	Mag	Pole-X dd	Pole-X d	Pole-Y dd	Pole-Y d	B-axis dd	B-axis d	P-axis dd	P-axis d	T-axis dd	T-axis d	Number read	Number used
241	73 425	232110	33.41	141.16	73.7	5.5	69.1	20.7	330.9	20.7	200.0	60.0	110.0	0.0	20.0	30.0	78	72
242	73 428	113337	35.99	140.28	49.0	4.5	238.8	28.0	148.4	0.8	56.8	62.0	190.0	20.0	287.1	18.8	14	13
243	73 5 5	125226	37.11	141.51	49.5	5.3	20.0	55.0	200.0	35.0	290.0	0.0	20.0	10.0	200.0	80.0	75	70
							110.0	45.0	290.0	45.0	20.0	0.0	110.0	0.0	290.0	90.0	75	70
244	73 5 5	141224	36.13	140.09	72.3	4.5	19.2	68.3	254.4	12.8	160.3	17.2	60.0	30.0	276.1	54.5	22	21
245	73 518	04415	33.00	141.14	59.9	5.2	120.0	45.0	300.0	45.0	30.0	0.0	120.0	0.0	300.0	90.0	46	46
246	73 526	111535	37.16	141.49	47.9	5.1	79.2	68.3	314.4	12.8	220.3	17.2	120.0	30.0	336.1	54.5	43	39
247	73 6 6	75226	38.35	142.28	40.7	4.6	310.0	35.0	130.0	55.0	40.0	0.0	130.0	10.0	310.0	80.0	19	19
							88.7	34.8	344.9	19.0	231.7	49.0	130.0	10.0	31.7	39.3	19	19
248	73 6 8	192449	36.12	140.07	68.8	4.7	132.0	54.0	291.5	34.3	28.3	9.9	120.0	10.0	254.6	75.9	45	36
249	73 6 9	173719	35.77	140.04	65.9	4.5	172.5	70.8	25.4	16.3	292.5	9.9	40.0	60.0	197.2	28.0	11	10
250	73 617	52721	35.94	140.16	63.4	4.6	84.9	73.1	232.7	14.5	325.0	8.7	60.0	30.0	220.6	58.5	34	27
251	73 620	73120	36.51	140.46	42.2	5.0	122.0	54.0	281.5	34.3	18.3	9.9	110.0	10.0	244.6	75.9	66	63
252	73 7 5	22625	36.21	139.80	57.8	4.6	212.6	51.0	353.4	32.1	96.4	19.7	190.0	10.0	305.5	67.7	10	10
253	73 720	171253	36.42	141.07	42.5	5.9	48.9	41.6	191.1	41.6	300.0	20.0	30.0	0.0	120.0	70.0	148	142
							120.0	45.0	300.0	45.0	30.0	0.0	120.0	0.0	300.0	90.0	148	142
254	73 722	103734	36.49	140.60	52.7	4.2	290.0	45.0	110.0	45.0	20.0	0.0	110.0	0.0	290.0	90.0	10	10
255	73 727	235222	36.16	140.08	74.8	4.6	337.5	81.1	217.1	4.5	126.5	7.6	30.0	40.0	225.3	49.0	31	25
256	73 8 1	15118	36.46	140.59	48.6	4.5	0.0	55.0	180.0	35.0	270.0	0.0	0.0	10.0	180.0	80.0	11	10
							50.0	45.0	230.0	45.0	320.0	0.0	50.0	0.0	230.0	90.0	11	10
							90.0	45.0	270.0	45.0	0.0	0.0	90.0	0.0	270.0	90.0	11	10
							320.0	45.0	140.0	45.0	50.0	0.0	140.0	0.0	320.0	90.0	11	10
257	73 821	01520	36.07	139.89	52.9	4.4	0.0	45.0	180.0	45.0	270.0	0.0	0.0	0.0	180.0	90.0	14	11
258	73 919	20 043	33.15	141.05	69.6	4.5	86.8	14.0	353.2	14.0	220.0	70.0	130.0	0.0	40.0	20.0	13	11
259	73 930	151752	35.66	140.68	55.1	5.9	129.9	44.1	290.2	44.1	30.0	10.0	120.0	0.0	210.0	80.0	172	164
260	7310 1	231622	35.74	140.71	44.2	5.8	129.9	44.1	290.2	44.1	30.0	10.0	120.0	0.0	210.0	80.0	103	88
261	731022	44018	35.61	140.73	47.5	4.8	9.1	46.5	243.8	28.7	135.7	29.5	40.0	10.0	293.3	58.5	31	25
262	731029	72212	35.54	140.87	49.4	4.7	20.0	65.0	200.0	25.0	290.0	0.0	20.0	20.0	200.0	70.0	26	21
263	731113	1012 9	38.55	142.48	75.9	5.5	205.0	62.9	92.4	11.2	357.3	24.4	120.0	50.0	252.4	29.5	83	82
264	731119	22 155	38.90	142.16	50.2	6.4	20.0	45.0	200.0	45.0	290.0	0.0	20.0	0.0	200.0	90.0	167	159
							90.0	55.0	270.0	35.0	0.0	0.0	90.0	10.0	270.0	80.0	167	159
265	731120	61116	38.88	142.11	46.0	5.5	20.0	45.0	200.0	45.0	290.0	0.0	20.0	0.0	200.0	90.0	50	49
							100.0	65.0	280.0	25.0	10.0	0.0	100.0	20.0	280.0	70.0	50	49
266	731222	101959	35.22	140.29	65.6	5.0	168.4	35.0	262.1	5.2	359.4	54.5	120.0	20.0	221.2	28.0	29	26
							149.0	60.0	284.8	22.5	22.9	18.8	120.0	20.0	253.2	62.0	29	26

Eq	Date y m d	Time h m s	Latit deg	Long deg	Dep km	Mag	Pole-X dd	Pole-X d	Pole-Y dd	Pole-Y d	B-axis dd	B-axis d	P-axis dd	P-axis d	T-axis dd	T-axis d	Number read	Number used
267	731227	530 3	33.47	141.15	52.9	5.5	135.0	45.0	315.0	45.0	45.0	0.0	135.0	0.0	315.0	90.0	79	74
268	74 110	214444	36.29	141.77	46.6	5.1	33.2	42.0	293.5	10.7	192.2	46.0	80.0	20.0	334.0	37.2	41	38
269	74 129	5 233	38.45	141.57	48.8	4.7	356.0	28.1	258.9	13.0	146.7	58.5	40.0	10.0	304.3	29.5	15	12
							72.2	54.8	312.0	19.5	211.2	28.0	110.0	20.0	349.4	54.5	15	12
							194.9	73.1	342.7	14.5	75.0	8.7	170.0	30.0	330.6	58.5	15	12
270	74 3 3	135049	35.58	140.74	49.0	6.1	138.9	41.6	281.1	41.6	30.0	20.0	120.0	0.0	210.0	70.0	99	99
271	74 319	21 052	35.25	141.00	47.8	4.8	45.4	7.1	314.6	7.1	180.0	80.0	0.0	10.0	90.0	0.0	33	30
272	74 4 5	433 7	35.98	140.14	67.9	4.3	80.0	5.0	260.0	85.0	350.0	0.0	80.0	50.0	260.0	40.0	17	16
273	74 423	54816	35.57	142.37	53.9	4.6	269.9	44.1	70.2	44.1	170.0	10.0	350.0	80.0	260.0	0.0	15	12
274	74 423	2052 1	37.09	141.21	51.1	4.7	75.1	73.1	287.3	14.5	195.0	8.7	100.0	30.0	299.4	58.5	15	14
275	74 6 2	221219	35.68	139.91	52.7	4.1	337.3	75.7	94.1	6.6	185.6	12.7	80.0	50.0	285.4	37.2	14	12
276	74 627	1049 9	33.69	139.29	49.8	6.1	46.4	33.3	301.7	21.1	185.3	49.0	350.0	40.0	86.5	7.6	60	57
277	74 8 4	31635	36.07	139.87	42.8	5.8	200.0	55.0	20.0	35.0	110.0	0.0	200.0	10.0	20.0	80.0	117	104
278	74 819	211730	33.13	139.57	65.1	5.2	233.5	34.3	137.8	8.3	36.1	54.5	180.0	30.0	280.3	17.2	27	26
279	74 825	101836	32.08	142.79	44.0	5.8	239.5	46.9	87.8	39.5	345.5	14.5	150.0	75.0	254.5	3.8	135	135
							149.5	43.1	300.5	43.1	45.0	15.0	225.0	75.0	135.0	0.0	135	135
280	74 828	950 4	36.45	141.12	43.6	4.8	300.0	25.0	120.0	65.0	30.0	0.0	120.0	20.0	300.0	70.0	46	39
281	74 915	234338	35.66	141.22	40.3	4.5	40.0	75.0	220.0	15.0	130.0	0.0	220.0	60.0	40.0	30.0	14	14
282	74 927	1210 6	33.68	141.43	77.5	6.4	234.1	14.1	324.1	0.1	54.6	75.9	280.0	10.0	188.3	9.9	151	147
							237.2	46.5	338.5	10.6	78.1	41.6	300.0	40.0	189.6	22.5	151	147
283	74 929	1 1 8	36.48	140.61	56.1	4.3	73.9	63.7	277.8	24.4	183.5	9.4	90.0	20.0	297.3	67.7	17	14
284	74 930	914 8	38.63	141.77	45.7	4.7	328.7	34.8	224.9	19.0	111.7	49.0	10.0	10.0	271.7	39.3	21	16
							325.7	62.0	98.9	20.0	196.1	18.8	70.0	60.0	294.1	22.5	21	16
285	7410 9	4 916	36.02	139.94	48.1	4.6	170.9	46.5	296.2	28.7	44.3	29.5	140.0	10.0	246.7	58.5	25	20
286	7410 9	442 9	36.03	139.90	50.9	4.8	76.1	63.7	232.3	24.4	326.6	9.4	60.0	20.0	212.7	67.7	36	35
287	741024	142645	33.44	141.10	55.3	5.0	120.0	45.0	300.0	45.0	30.0	0.0	120.0	0.0	300.0	90.0	68	68
288	741029	20 0 1	35.58	140.30	45.4	4.9	156.4	53.4	326.0	36.2	59.6	5.0	300.0	80.0	150.4	8.7	15	14
289	741031	93244	36.04	139.92	55.4	4.6	196.8	42.0	296.6	10.7	37.8	46.0	150.0	20.0	256.0	37.2	19	19
290	7411 3	65519	36.34	141.81	43.1	5.4	122.6	81.1	242.9	4.5	333.5	7.6	70.0	40.0	234.7	49.0	43	38
							169.0	60.0	304.8	22.5	42.9	18.8	140.0	20.0	273.2	62.0	43	38
291	7411 3	74511	36.43	141.73	44.2	4.9	107.7	54.8	291.4	35.1	200.2	1.7	300.0	80.0	109.9	9.9	13	11
292	741116	83242	35.82	141.13	43.2	6.1	103.9	63.7	307.8	24.4	213.5	9.4	120.0	20.0	327.3	67.7	160	141
293	741121	205928	35.57	140.40	65.7	4.7	74.6	7.1	165.4	7.1	300.0	80.0	30.0	0.0	120.0	10.0	13	11
							327.4	38.4	81.8	27.6	197.0	39.3	30.0	50.0	292.3	6.4	13	11
294	75 2 8	14115	35.78	140.11	54.2	5.4	7.7	63.1	204.4	25.9	111.1	6.7	220.0	70.0	18.8	18.8	51	42

Eq	Date y m d	Time h m s	Latit deg	Long deg	Dep km	Mag	Pole-X dd	Pole-X d	Pole-Y dd	Pole-Y d	B-axis dd	B-axis d	P-axis dd	P-axis d	T-axis dd	T-axis d	Number read	Number used
295	75 221	44538	34.42	141.24	61.2	4.7	330.0	25.0	150.0	65.0	60.0	0.0	150.0	20.0	330.0	70.0	18 /	15
							20.0	25.0	200.0	65.0	110.0	0.0	200.0	20.0	20.0	70.0	18 /	15
							58.7	34.8	314.9	19.0	201.7	49.0	100.0	10.0	1.7	39.3	18 /	15
							198.8	28.0	108.4	0.8	16.8	62.0	150.0	20.0	247.1	18.8	18 /	15
296	75 224	1123 0	37.64	141.70	51.6	4.6	94.6	7.1	185.4	7.1	320.0	80.0	50.0	0.0	140.0	10.0	10 /	10
							120.5	42.4	353.4	33.4	241.5	29.5	50.0	60.0	148.7	5.0	10 /	10
297	75 327	13214	36.98	141.87	43.4	4.6	280.0	45.0	100.0	45.0	190.0	0.0	280.0	0.0	100.0	90.0	15 /	14
298	75 330	457 1	36.16	140.09	76.6	5.4	112.0	54.0	271.5	34.3	8.3	9.9	100.0	10.0	234.6	75.9	126 /	120
299	75 330	13 818	36.13	140.13	66.3	4.2	80.0	65.0	260.0	25.0	350.0	0.0	80.0	20.0	260.0	70.0	11 /	11
							128.2	20.9	35.4	7.3	287.3	67.7	80.0	20.0	173.5	9.4	11 /	11
300	75 4 2	174358	33.63	140.78	75.7	5.8	46.8	14.0	313.2	14.0	180.0	70.0	90.0	0.0	0.0	20.0	97 /	90
301	75 412	71548	36.10	140.02	53.1	5.0	142.6	51.0	283.4	32.1	26.4	19.7	120.0	10.0	235.5	67.7	51 /	47
302	75 418	341 8	36.14	139.84	51.9	5.0	203.5	48.7	311.9	15.5	54.0	37.2	160.0	20.0	272.2	46.0	52 /	50
303	75 421	124515	36.46	140.69	49.0	4.8	70.0	45.0	250.0	45.0	340.0	0.0	70.0	0.0	250.0	90.0	54 /	42
304	75 427	16 711	33.44	141.18	71.0	4.9	90.0	45.0	270.0	45.0	0.0	0.0	90.0	0.0	270.0	90.0	73 /	64
305	75 524	63914	35.63	140.25	54.3	4.2	5.0	0.0	275.0	0.0	230.0	90.0	50.0	0.0	320.0	0.0	13 /	12
							139.9	45.9	339.3	42.5	240.2	9.9	50.0	80.0	149.9	1.7	13 /	12
306	75 6 4	175656	35.65	140.17	59.6	4.1	95.1	73.1	307.3	14.5	215.0	8.7	120.0	30.0	319.4	58.5	15 /	15
307	75 6 4	181130	35.62	140.18	58.5	4.2	159.1	62.1	269.0	10.2	3.9	25.7	110.0	30.0	240.9	48.6	15 /	14
							60.9	62.1	311.1	10.2	216.1	25.7	110.0	30.0	339.1	48.6	15 /	14
308	75 615	83627	36.28	143.58	48.4	5.9	105.5	50.8	259.4	36.3	359.1	13.0	210.0	75.0	90.9	7.4	157 /	157
309	75 618	05448	38.25	141.91	52.1	4.8	71.1	41.6	288.9	41.6	180.0	20.0	90.0	0.0	0.0	70.0	23 /	21
							192.0	54.0	351.5	34.3	88.3	9.9	180.0	10.0	314.6	75.9	23 /	21
310	75 625	124214	35.84	140.15	57.1	4.1	44.6	7.1	135.4	7.1	270.0	80.0	90.0	10.0	0.0	0.0	11 /	11
311	75 716	184219	37.06	141.51	47.1	4.4	142.6	27.0	37.5	27.0	270.0	50.0	90.0	40.0	180.0	0.0	18 /	18
312	75 720	10 244	32.90	141.01	78.1	4.9	340.8	68.3	105.6	12.8	199.7	17.2	300.0	30.0	84.0	54.5	35 /	29
313	75 8 9	3 634	36.01	140.27	44.1	4.6	320.0	15.0	140.0	75.0	50.0	0.0	140.0	30.0	320.0	60.0	16 /	16
314	75 815	3 928	37.08	141.14	52.3	5.5	90.0	45.0	270.0	45.0	0.0	0.0	90.0	0.0	270.0	90.0	104 /	103
315	75 9 3	438 8	33.71	142.36	47.7	4.8	51.0	50.8	246.5	38.1	150.4	7.6	290.0	80.0	59.6	6.4	18 /	15
316	7510 5	51455	33.80	142.17	40.0	4.6	183.4	64.5	12.2	25.2	280.6	3.4	20.0	70.0	189.4	19.7	22 /	18
							236.5	34.3	332.2	8.3	74.0	54.5	290.0	30.0	189.7	17.2	22 /	18
317	751025	8 652	33.51	141.20	48.6	4.5	30.0	65.0	210.0	25.0	300.0	0.0	30.0	20.0	210.0	70.0	12 /	12
							169.1	62.1	279.0	10.2	13.9	25.7	120.0	30.0	250.9	48.6	12 /	12
318	751215	954 1	35.54	140.09	65.3	4.6	126.1	63.7	282.3	24.4	16.6	9.4	110.0	20.0	262.7	67.7	30 /	29
319	751229	12938	37.49	141.60	47.2	4.7	280.0	35.0	100.0	55.0	10.0	0.0	100.0	10.0	280.0	80.0	15 /	15
							209.9	44.1	10.2	44.1	110.0	10.0	200.0	0.0	290.0	80.0	15 /	15

Eq	Date y m d	Time h m s	Latit deg	Long deg	Dep km	Mag	Pole-X dd	Pole-X d	Pole-Y dd	Pole-Y d	B-axis dd	B-axis d	P-axis dd	P-axis d	T-axis dd	T-axis d	Number read	Number used
320	76 117	05021	36.10	139.90	59.3	4.3	203.8	73.9	42.7	15.3	311.3	5.0	50.0	60.0	218.5	29.5	14 /	13
							288.7	34.8	184.9	19.0	71.7	49.0	330.0	10.0	231.7	39.3	14 /	13
321	76 229	182715	36.67	140.89	48.0	5.0	140.9	46.5	266.2	28.7	14.3	29.5	110.0	10.0	216.7	58.5	33 /	30
322	76 330	202322	35.59	140.14	70.2	4.0	188.2	20.9	95.4	7.3	347.3	67.7	140.0	20.0	233.5	9.4	18 /	17
							69.6	42.4	196.6	33.4	308.5	29.5	140.0	60.0	41.3	5.0	18 /	17
323	76 5 1	73846	36.61	140.68	42.4	4.2	116.8	42.0	216.6	10.7	317.8	46.0	70.0	20.0	176.1	37.2	15 /	13
324	76 514	52854	36.43	140.68	57.1	4.1	116.1	63.7	272.3	24.4	6.6	9.4	100.0	20.0	252.7	67.7	15 /	14
325	76 6 6	62040	35.52	140.19	70.7	4.0	217.7	63.1	54.4	25.9	321.1	6.7	70.0	70.0	228.8	18.8	12 /	12
326	76 6 6	23 121	36.05	139.62	65.5	4.8	34.7	74.5	136.0	3.1	226.8	15.2	330.0	40.0	120.5	46.0	50 /	42
327	76 7 9	25934	33.54	140.84	52.6	4.6	311.1	41.6	168.9	41.6	60.0	20.0	330.0	0.0	240.0	70.0	17 /	15
328	76 714	1238 0	36.02	139.91	60.6	4.8	176.6	37.8	303.4	37.8	60.0	30.0	150.0	0.0	240.0	60.0	38 /	30
329	76 721	22724	35.55	140.12	71.4	4.0	41.1	60.0	265.2	22.5	167.1	18.8	70.0	20.0	296.8	62.0	12 /	12
330	76 8 4	83745	36.17	139.83	60.3	4.7	162.7	81.6	32.9	5.4	302.3	6.4	40.0	50.0	207.0	39.3	38 /	30
331	76 8 7	44235	37.33	141.70	41.5	5.2	10.2	44.1	209.9	44.1	110.0	10.0	20.0	0.0	290.0	80.0	88 /	83
							99.9	44.1	260.2	44.1	0.0	10.0	90.0	0.0	180.0	80.0	88 /	83
332	7610 6	202737	36.60	141.19	40.8	4.7	73.4	37.8	306.6	37.8	190.0	30.0	100.0	0.0	10.0	60.0	17 /	15
							55.0	0.0	325.0	0.0	280.0	90.0	100.0	0.0	10.0	0.0	17 /	15
333	761029	10 020	33.61	140.47	76.8	4.6	201.3	34.8	305.1	19.0	58.3	49.0	160.0	10.0	258.3	39.3	25 /	19
							137.4	51.0	356.6	32.1	253.6	19.7	160.0	10.0	44.5	67.7	25 /	19
334	7611 9	124641	35.71	140.40	66.3	4.2	35.0	62.9	147.6	11.2	242.7	24.4	120.0	50.0	347.6	29.5	11 /	11
335	761115	21059	37.11	141.52	44.7	4.7	66.5	48.7	318.1	15.5	216.0	37.2	110.0	20.0	357.8	46.0	31 /	25
336	761120	014 3	35.98	141.48	46.1	4.3	134.0	28.1	231.1	13.0	343.3	58.5	90.0	10.0	185.7	29.5	11 /	10
							59.1	46.5	293.8	28.7	185.7	29.5	90.0	10.0	343.3	58.5	11 /	10
337	761218	12 557	38.26	141.86	46.6	4.5	162.7	32.8	277.3	32.8	40.0	40.0	130.0	0.0	220.0	50.0	15 /	15
338	761222	0 654	37.06	141.20	53.4	4.6	88.0	54.0	288.5	34.3	191.8	9.9	100.0	10.0	325.4	75.9	23 /	18
339	77 121	1125 6	36.72	141.03	51.9	4.5	34.6	21.2	302.0	6.6	195.5	67.7	80.0	10.0	346.4	19.7	18 /	18
340	77 214	18 826	35.74	140.12	70.3	4.7	45.1	73.1	257.3	14.4	165.0	8.7	70.0	30.0	269.4	58.5	32 /	32
341	77 219	55126	32.97	141.41	72.5	5.7	337.0	41.0	90.1	24.3	201.7	39.3	300.0	10.0	41.7	49.0	207 /	175
342	77 219	13 222	33.16	141.29	59.2	5.2	42.2	47.2	169.7	29.4	277.2	28.0	120.0	60.0	12.5	9.9	55 /	46
343	77 320	9 746	35.55	140.15	69.1	4.4	197.3	67.5	289.3	0.8	19.6	22.5	130.0	40.0	268.1	41.6	20 /	20
344	77 324	101435	36.31	141.13	43.7	4.1	0.0	15.0	180.0	75.0	90.0	0.0	180.0	30.0	0.0	60.0	12 /	12
345	77 328	1415 1	35.89	140.96	42.5	4.4	96.1	63.7	252.3	24.4	346.6	9.4	80.0	20.0	232.7	67.7	22 /	19
346	77 330	84538	36.15	140.07	66.7	4.4	139.1	62.1	249.0	10.2	343.9	25.7	90.0	30.0	220.9	48.6	25 /	22
347	77 331	9 730	37.80	142.72	57.5	4.5	50.0	45.0	230.0	45.0	320.0	0.0	50.0	0.0	230.0	90.0	17 /	13
							80.0	45.0	260.0	45.0	350.0	0.0	80.0	0.0	260.0	90.0	17 /	13
							359.9	44.1	160.2	44.1	260.0	10.0	350.0	0.0	80.0	80.0	17 /	13
348	77 4 4	16 817	35.85	140.72	58.0	4.4	184.6	48.4	277.2	2.3	9.2	41.6	130.0	30.0	242.8	33.8	20 /	20

Eq	Date y m d	Time h m s	Latit deg	Long deg	Dep km	Mag	Pole-X dd	Pole-X d	Pole-Y dd	Pole-Y d	B-axis dd	B-axis d	P-axis dd	P-axis d	T-axis dd	T-axis d	Number read	Number used
349	77 4 6	22 747	37.00	141.19	54.3	4.1	30.2	44.1	229.9	44.1	130.0	10.0	40.0	0.0	310.0	80.0	11	11
							80.0	45.0	260.0	45.0	350.0	0.0	80.0	0.0	260.0	90.0	11	11
							132.0	54.0	291.5	34.3	28.3	9.9	120.0	10.0	254.6	75.9	11	11
350	77 419	1515 0	36.49	140.59	53.5	5.1	110.0	45.0	290.0	45.0	20.0	0.0	110.0	0.0	290.0	90.0	102	93
351	77 5 3	2154 5	35.75	140.10	67.1	4.3	280.0	15.0	100.0	75.0	10.0	0.0	100.0	30.0	280.0	60.0	18	17
							149.1	20.7	50.9	20.7	280.0	60.0	100.0	30.0	190.0	0.0	18	17
352	77 513	102644	38.30	141.85	48.3	5.0	90.0	15.0	270.0	75.0	180.0	0.0	270.0	30.0	90.0	60.0	25	19
353	77 513	192739	35.57	140.24	71.6	4.4	50.0	5.0	230.0	85.0	320.0	0.0	50.0	50.0	230.0	40.0	26	21
							137.5	27.0	242.6	27.0	10.0	50.0	100.0	0.0	190.0	40.0	26	21
354	77 516	65130	33.57	140.99	75.1	4.3	182.7	75.7	65.9	6.6	334.4	12.7	80.0	50.0	234.6	37.2	11	11
							290.0	45.0	110.0	45.0	20.0	0.0	110.0	0.0	290.0	90.0	11	11
							72.6	27.0	327.5	27.0	200.0	50.0	110.0	0.0	20.0	40.0	11	11
355	77 520	42030	35.55	140.70	45.2	4.3	20.0	75.0	200.0	15.0	290.0	0.0	20.0	30.0	200.0	60.0	19	15
							114.9	73.1	262.7	14.5	355.0	8.7	90.0	30.0	250.6	58.5	19	15
							152.6	51.0	293.4	32.1	36.4	19.7	130.0	10.0	245.5	67.7	19	15
356	77 6 4	82730	35.53	140.00	59.6	4.6	45.4	48.4	312.8	2.3	220.8	41.6	100.0	30.0	347.2	33.8	35	29
357	77 616	235056	36.08	139.87	54.0	4.4	54.1	14.1	324.1	0.1	234.6	75.9	100.0	10.0	8.3	9.9	21	18
							147.0	41.1	260.1	24.3	11.7	39.3	110.0	10.0	211.7	49.0	21	18
358	77 623	32813	35.06	140.36	42.6	4.4	139.6	58.2	291.2	28.6	28.3	12.7	260.0	70.0	121.8	15.2	19	17
359	77 623	433 7	35.12	140.34	40.2	4.3	97.7	54.8	281.4	35.1	190.2	1.7	290.0	80.0	99.9	9.9	13	12
360	77 8 7	84337	35.43	141.10	46.8	4.7	202.7	81.6	72.9	5.4	342.3	6.4	80.0	50.0	247.0	39.3	40	38
361	77 821	026 0	35.95	140.07	68.9	4.1	172.7	75.7	55.9	6.6	324.4	12.7	70.0	50.0	224.6	37.2	23	20
							147.9	54.8	268.0	19.5	8.8	28.0	110.0	20.0	230.6	54.5	23	20
362	77 9 5	13946	33.17	141.08	51.9	5.3	99.9	44.1	260.2	44.1	0.0	10.0	90.0	0.0	180.0	80.0	51	46
							150.0	45.0	330.0	45.0	60.0	0.0	150.0	0.0	330.0	90.0	51	46
363	77 914	011 9	33.29	141.36	68.8	4.2	71.1	41.6	288.9	41.6	180.0	20.0	90.0	0.0	0.0	70.0	15	12
							175.0	62.9	62.4	11.2	327.3	24.4	90.0	50.0	222.4	29.5	15	12
364	7710 5	0 1 3	35.73	140.12	72.4	4.6	149.1	62.1	259.0	10.2	353.9	25.7	100.0	30.0	230.9	48.6	37	33
365	7710 5	03857	36.13	139.86	56.6	5.4	179.8	39.8	76.4	15.6	329.5	46.0	120.0	40.0	223.2	15.2	114	100
366	7710 5	04652	36.12	139.85	55.4	4.3	230.5	58.2	78.8	28.6	341.7	12.7	110.0	70.0	248.2	15.2	21	18
367	7710 5	61454	36.13	139.87	58.4	4.3	43.3	60.9	246.6	27.1	151.5	9.9	270.0	70.0	58.4	17.2	18	17
368	7710 8	63244	36.47	140.68	59.4	4.1	151.3	34.8	255.1	19.0	8.3	49.0	110.0	10.0	208.3	39.3	13	12
369	771022	205845	36.71	141.40	42.7	4.9	2.1	44.2	116.1	22.7	224.6	37.2	70.0	50.0	324.4	12.7	39	30
370	771024	1045 8	33.40	141.12	69.6	4.4	290.2	44.1	129.9	44.1	30.0	10.0	300.0	0.0	210.0	80.0	19	17
371	771026	655 7	36.26	141.45	41.3	4.7	40.0	45.0	220.0	45.0	310.0	0.0	40.0	0.0	220.0	90.0	46	41
							270.0	25.0	90.0	65.0	0.0	0.0	90.0	20.0	270.0	70.0	46	41

Eq	Date y m d	Time h m s	Latit deg	Long deg	Dep km	Mag	Pole-X dd	Pole-X d	Pole-Y dd	Pole-Y d	B-axis dd	B-axis d	P-axis dd	P-axis d	T-axis dd	T-axis d	Number read	Number used
372	771027	24752	36.12	139.86	59.5	4.1	232.1	52.2	65.3	37.0	330.4	6.4	100.0	80.0	239.6	7.6	14	12
							6.7	50.3	120.2	18.3	223.0	33.8	80.0	50.0	326.1	18.8	14	12
373	7711 4	201750	36.14	139.82	52.7	4.2	196.6	66.7	58.2	17.8	323.4	14.5	80.0	60.0	226.3	25.7	21	19
374	771217	01028	36.60	141.16	44.9	5.6	99.9	44.1	260.2	44.1	0.0	10.0	90.0	0.0	180.0	80.0	157	147
375	78 125	82322	35.90	140.58	46.2	4.1	173.5	34.3	77.8	8.3	336.1	54.5	120.0	30.0	220.3	17.2	17	13
							160.8	68.3	285.6	12.8	19.7	17.2	120.0	30.0	264.0	54.5	17	13
376	78 217	215147	36.08	139.88	56.7	4.3	310.0	35.0	130.0	55.0	40.0	0.0	130.0	10.0	310.0	80.0	19	18
							53.9	63.7	257.8	24.4	163.5	9.4	70.0	20.0	277.3	67.7	19	18
377	78 220	133657	38.78	142.22	58.0	6.7	215.4	48.4	122.8	2.3	30.8	41.6	270.0	30.0	157.2	33.8	167	145
378	78 220	135329	38.66	142.10	71.9	4.9	212.5	70.8	65.4	16.3	332.5	9.9	80.0	60.0	237.2	28.0	19	16
							183.2	14.0	276.8	14.0	50.0	70.0	140.0	0.0	230.0	20.0	19	16
							166.6	37.8	293.4	37.8	50.0	30.0	140.0	0.0	230.0	60.0	19	16
379	78 220	14 031	38.78	142.02	62.9	4.7	286.1	63.7	82.3	24.4	176.6	9.4	270.0	20.0	62.7	67.7	15	12
							340.0	45.0	160.0	45.0	250.0	0.0	340.0	0.0	160.0	90.0	15	12
380	78 221	23843	38.74	142.07	60.3	4.6	129.1	62.1	239.0	10.2	333.9	25.7	80.0	30.0	210.9	48.6	14	13
381	78 228	31013	38.08	142.72	54.3	4.5	217.9	54.8	338.0	19.5	78.8	28.0	180.0	20.0	300.6	54.5	21	19
382	78 313	25948	38.77	142.13	69.7	5.0	90.0	45.0	270.0	45.0	0.0	0.0	90.0	0.0	270.0	90.0	53	44
							0.2	44.1	199.9	44.1	100.0	10.0	10.0	0.0	280.0	80.0	53	44
383	78 320	192413	36.09	139.87	57.4	5.5	10.0	45.0	190.0	45.0	280.0	0.0	10.0	0.0	190.0	90.0	158	139
384	78 331	223658	32.86	141.20	63.3	4.5	356.0	28.1	258.9	13.0	146.7	58.5	40.0	10.0	304.3	29.5	18	15
385	78 4 7	122947	36.68	140.74	58.7	4.1	160.5	42.4	33.4	33.4	281.5	29.5	90.0	60.0	188.7	5.0	11	10
							154.6	48.4	247.2	2.3	339.2	41.6	100.0	30.0	212.8	33.8	11	10
386	78 4 8	12120	35.70	140.73	49.7	4.8	39.6	42.4	166.6	33.4	278.5	29.5	110.0	60.0	11.3	5.0	24	24
387	78 419	194752	36.46	140.74	51.4	4.3	27.4	38.4	141.8	27.6	257.0	39.3	90.0	50.0	352.3	6.4	15	13
							324.2	57.1	194.1	22.7	94.1	22.5	230.0	60.0	356.0	18.8	15	13
388	78 517	175221	34.17	141.82	48.3	4.9	205.4	7.1	114.6	7.1	340.0	80.0	160.0	10.0	250.0	0.0	41	31
389	78 526	31813	35.58	139.99	48.1	4.2	293.1	60.4	27.1	2.3	118.3	29.5	0.0	40.0	232.6	35.9	15	13
							182.4	69.3	69.1	8.5	336.1	18.8	90.0	50.0	233.0	33.8	15	13
390	78 6 5	340 7	36.39	141.05	43.7	4.8	57.3	75.7	174.1	6.6	265.6	12.7	160.0	50.0	5.4	37.2	39	30
391	78 6 5	211722	36.04	139.92	47.9	4.2	195.9	14.1	285.9	0.1	15.4	75.9	150.0	10.0	241.8	9.9	14	13
							162.0	54.0	321.5	34.3	58.3	9.9	150.0	10.0	284.6	75.9	14	13
392	78 612	201418	38.17	142.17	44.6	4.7	344.0	28.1	81.1	13.0	193.3	58.5	300.0	10.0	35.7	29.5	15	13
393	78 614	54520	38.08	141.95	47.0	4.7	333.5	34.3	237.8	8.3	136.1	54.5	280.0	30.0	20.3	17.2	18	14
394	78 616	0 339	37.94	141.94	48.8	5.4	110.2	44.1	309.9	44.1	210.0	10.0	120.0	0.0	30.0	80.0	92	91
395	78 616	205835	38.58	143.12	51.5	4.9	297.7	63.1	134.4	25.9	41.1	6.7	150.0	70.0	308.8	18.8	23	19
396	78 617	82421	38.18	143.44	76.9	4.9	255.0	62.9	142.4	11.2	47.3	24.4	170.0	50.0	302.4	29.5	31	25
							226.8	14.0	133.2	14.0	0.0	70.0	180.0	20.0	270.0	0.0	31	25

Eq	Date y m d	Time h m s	Latit deg	Long deg	Dep km	Mag	Pole-X dd	Pole-X d	Pole-Y dd	Pole-Y d	B-axis dd	B-axis d	P-axis dd	P-axis d	T-axis dd	T-axis d	Number read	Number used
397	78 619	115850	37.96	143.12	52.8	4.9	246.9	60.4	152.9	2.3	61.7	29.5	180.0	40.0	307.5	35.9	19 /	15
398	78 619	163011	38.38	142.27	40.9	4.7	73.4	37.8	306.6	37.8	190.0	30.0	100.0	0.0	10.0	60.0	15 /	15
							119.2	68.3	354.4	12.8	260.3	17.2	160.0	30.0	16.1	54.5	15 /	15
399	78 621	195423	38.34	141.85	45.8	5.8	90.2	44.1	289.9	44.1	190.0	10.0	100.0	0.0	10.0	80.0	141 /	135
							10.0	45.0	190.0	45.0	280.0	0.0	10.0	0.0	190.0	90.0	141 /	135
400	78 7 5	047 3	38.32	142.85	61.7	4.7	289.6	58.2	81.2	28.6	178.3	12.7	50.0	70.0	271.8	15.2	15 /	13
401	78 7 5	14 825	36.46	140.64	56.6	4.1	280.0	25.0	100.0	65.0	10.0	0.0	100.0	20.0	280.0	70.0	17 /	14
402	78 7 5	232857	38.07	143.81	60.0	4.5	58.2	20.9	325.4	7.3	217.3	67.7	10.0	20.0	103.5	9.4	14 /	11
							280.0	65.0	100.0	25.0	10.0	0.0	100.0	70.0	280.0	20.0	14 /	11
403	78 712	211145	38.19	142.43	51.0	4.6	280.0	45.0	100.0	45.0	10.0	0.0	100.0	0.0	280.0	90.0	14 /	11
							138.0	54.0	338.5	34.3	241.8	9.9	150.0	10.0	15.4	75.9	14 /	11
404	78 714	23 456	37.50	141.55	52.0	4.8	10.0	35.0	190.0	55.0	100.0	0.0	190.0	10.0	10.0	80.0	53 /	51
							58.0	54.0	258.5	34.3	161.8	9.9	70.0	10.0	295.4	75.9	53 /	51
405	78 727	1624 9	37.94	141.73	48.0	5.1	90.2	44.1	289.9	44.1	190.0	10.0	100.0	0.0	10.0	80.0	48 /	47
							10.0	45.0	190.0	45.0	280.0	0.0	10.0	0.0	190.0	90.0	48 /	47
406	78 727	222913	36.15	141.95	41.6	5.1	292.4	69.3	179.1	8.5	86.1	18.8	200.0	50.0	343.0	33.8	21 /	21
407	78 813	54824	36.07	139.88	57.4	4.1	320.0	25.0	140.0	65.0	50.0	0.0	140.0	20.0	320.0	70.0	17 /	15
408	78 813	222249	35.60	140.03	78.2	4.7	124.9	73.1	272.7	14.5	5.0	8.7	100.0	30.0	260.6	58.5	45 /	40
409	78 821	63114	38.14	141.95	48.3	4.3	92.2	54.8	332.0	19.5	231.2	28.0	130.0	20.0	9.4	54.5	12 /	12
410	78 924	743 8	38.38	143.43	52.2	5.4	339.1	46.5	213.8	28.7	105.7	29.5	10.0	10.0	263.3	58.5	89 /	85
							179.1	62.1	289.0	10.2	23.9	25.7	130.0	30.0	260.9	48.6	89 /	85
411	781019	19 711	35.78	140.31	54.2	4.2	13.4	37.8	246.6	37.8	130.0	30.0	40.0	0.0	310.0	60.0	13 /	13
412	781028	1558 1	37.78	141.87	54.5	4.3	129.9	44.1	290.2	44.1	30.0	10.0	120.0	0.0	210.0	80.0	11 /	11
							82.6	27.0	337.5	27.0	210.0	50.0	120.0	0.0	30.0	40.0	11 /	11
413	7811 6	11726	36.64	141.13	48.6	4.8	132.6	51.0	273.4	32.1	16.4	19.7	110.0	10.0	225.5	67.7	49 /	46
414	781113	12 141	38.72	142.20	42.6	5.2	77.4	51.0	296.6	32.1	193.6	19.7	100.0	10.0	344.5	67.7	50 /	44
415	7812 2	8 341	38.49	143.21	59.4	4.8	55.0	0.0	325.0	0.0	190.0	90.0	10.0	0.0	100.0	0.0	21 /	19
							296.2	73.9	97.3	15.3	188.7	5.0	90.0	60.0	281.5	29.5	21 /	19
416	7812 7	1447 3	38.31	141.91	53.3	4.2	157.0	41.0	270.1	24.3	21.7	39.3	120.0	10.0	221.7	49.0	10 /	10
							76.0	28.1	338.9	13.0	226.7	58.5	120.0	10.0	24.3	29.5	10 /	10
417	7812 7	175214	34.57	140.71	55.6	4.4	320.0	35.0	140.0	55.0	50.0	0.0	140.0	10.0	320.0	80.0	22 /	21
418	7812 8	33724	37.11	141.57	51.7	4.8	112.0	54.0	271.5	34.3	8.3	9.9	100.0	10.0	234.6	75.9	43 /	37
419	7812 8	143244	35.99	140.41	55.0	4.1	330.0	25.0	150.0	65.0	60.0	0.0	150.0	20.0	330.0	70.0	13 /	11
							101.6	35.0	7.9	5.2	270.6	54.5	150.0	20.0	48.8	28.0	13 /	11

Eq	Date y m d	Time h m s	Latit deg	Long deg	Dep km	Mag	Pole-X dd	Pole-X d	Pole-Y dd	Pole-Y d	B-axis dd	B-axis d	P-axis dd	P-axis d	T-axis dd	T-axis d	Number read	Number used
420	781220	13221	33.23	140.78	58.2	4.5	52.0	54.0	211.5	34.3	308.3	9.9	40.0	10.0	174.6	75.9	47	36
							80.0	45.0	260.0	45.0	350.0	0.0	80.0	0.0	260.0	90.0	47	36
							169.9	44.1	330.2	44.1	70.0	10.0	160.0	0.0	250.0	80.0	47	36
421	781231	114735	35.73	140.01	69.0	4.0	146.6	64.5	317.8	25.2	49.4	3.4	310.0	70.0	140.6	19.7	14	12
422	781231	195140	36.34	144.65	46.5	5.1	119.5	46.9	327.8	39.5	225.5	14.5	30.0	75.0	134.5	3.8	59	58
423	79 1 2	233451	37.15	141.42	51.3	4.2	76.1	63.7	232.3	24.4	326.6	9.4	60.0	20.0	212.7	67.7	11	10
							105.1	73.1	317.3	14.5	225.0	8.7	130.0	30.0	329.4	58.5	11	10
424	79 1 3	03155	35.95	140.09	68.1	4.7	330.0	35.0	150.0	55.0	60.0	0.0	150.0	10.0	330.0	80.0	31	27
425	79 120	18 149	36.53	141.09	54.7	4.6	69.1	46.5	303.8	28.7	195.7	29.5	100.0	10.0	353.3	58.5	43	36
426	79 3 6	225649	35.97	140.10	72.7	4.2	166.6	37.8	293.4	37.8	50.0	30.0	140.0	0.0	230.0	60.0	25	22
427	79 3 8	72719	36.39	140.69	51.0	4.5	290.0	45.0	110.0	45.0	20.0	0.0	110.0	0.0	290.0	90.0	21	20
428	79 311	52153	37.29	141.72	41.4	5.5	20.0	45.0	200.0	45.0	290.0	0.0	20.0	0.0	200.0	90.0	108	103
							100.0	45.0	280.0	45.0	10.0	0.0	100.0	0.0	280.0	90.0	108	103
429	79 4 3	22629	38.49	142.29	54.3	5.3	103.5	48.7	211.9	15.5	314.0	37.2	60.0	20.0	172.2	46.0	68	64
							16.5	48.7	268.1	15.5	166.0	37.2	60.0	20.0	307.8	46.0	68	64
430	79 519	9 841	36.07	139.88	52.6	4.0	183.5	48.7	291.9	15.5	34.0	37.2	140.0	20.0	252.2	46.0	18	15
431	79 521	233727	35.90	140.47	59.7	5.2	130.0	65.0	310.0	25.0	40.0	0.0	130.0	20.0	310.0	70.0	116	103
432	79 530	134014	37.16	141.45	50.0	4.3	150.2	44.1	349.9	44.1	250.0	10.0	160.0	0.0	70.0	80.0	11	10
							112.0	54.0	271.5	34.3	8.3	9.9	100.0	10.0	234.6	75.9	11	10
433	79 6 1	7 954	38.31	141.87	56.5	4.3	300.0	35.0	120.0	55.0	30.0	0.0	120.0	10.0	300.0	80.0	11	11
434	79 626	1750 2	37.09	141.16	57.2	4.4	40.0	45.0	220.0	45.0	310.0	0.0	40.0	0.0	220.0	90.0	13	10
							109.9	44.1	270.2	44.1	10.0	10.0	100.0	0.0	190.0	80.0	13	10
							10.0	45.0	190.0	45.0	100.0	0.0	190.0	0.0	10.0	90.0	13	10
435	79 7 2	112832	36.03	139.92	54.4	4.1	36.7	50.3	150.2	18.3	253.0	33.8	110.0	50.0	356.1	18.8	14	12
							346.6	66.7	208.2	17.8	113.4	14.5	230.0	60.0	16.3	25.7	14	12
436	79 711	184143	36.64	141.28	44.6	4.0	318.4	35.0	52.1	5.2	149.4	54.5	270.0	20.0	11.2	28.0	11	10
437	79 720	0 713	35.43	140.10	64.8	4.0	166.5	34.3	262.2	8.3	4.0	54.5	220.0	30.0	119.7	17.2	21	18
							80.5	58.2	288.8	28.6	191.7	12.7	320.0	70.0	98.2	15.2	21	18
438	79 730	51216	38.45	142.40	45.5	4.6	289.1	50.8	93.5	38.1	189.6	7.6	50.0	80.0	280.4	6.4	15	13
439	79 812	161319	34.59	140.44	53.0	5.7	82.5	70.8	295.4	16.3	202.5	9.9	310.0	60.0	107.2	28.0	154	119
440	79 817	52321	34.69	140.55	57.5	4.1	320.0	35.0	140.0	55.0	50.0	0.0	140.0	10.0	320.0	80.0	11	10
							96.0	28.1	358.9	13.0	246.7	58.5	140.0	10.0	44.3	29.5	11	10
441	79 917	2010 4	35.73	140.09	66.2	4.5	124.9	73.1	272.7	14.5	5.0	8.7	100.0	30.0	260.6	58.5	29	25
442	7910 9	141849	36.16	139.83	56.1	4.1	330.0	35.0	150.0	55.0	60.0	0.0	150.0	10.0	330.0	80.0	14	13
443	791015	65832	31.43	142.46	46.4	5.2	262.6	81.1	22.9	4.5	113.5	7.6	210.0	40.0	14.7	49.0	24	24
							295.4	21.2	28.0	6.6	134.5	67.7	250.0	10.0	343.6	19.7	24	24
444	791119	31119	37.53	141.40	55.7	4.5	290.0	45.0	110.0	45.0	20.0	0.0	110.0	0.0	290.0	90.0	22	20

Eq	Date y m d	Time h m s	Latit deg	Long deg	Dep km	Mag	Pole-X dd	Pole-X d	Pole-Y dd	Pole-Y d	B-axis dd	B-axis d	P-axis dd	P-axis d	T-axis dd	T-axis d	Number read	Number used
445	791215	122721	35.57	140.30	76.0	4.2	184.0	28.1	281.1	13.0	33.3	58.5	140.0	10.0	235.7	29.5	13	11
446	791217	82349	36.46	140.61	59.4	4.3	157.5	27.0	262.6	27.0	30.0	50.0	120.0	0.0	210.0	40.0	17	15
							129.9	44.1	290.2	44.1	30.0	10.0	120.0	0.0	210.0	80.0	17	15
447	791217	162035	38.78	141.90	60.7	4.2	359.9	44.1	160.2	44.1	260.0	10.0	350.0	0.0	80.0	80.0	10	10
448	791219	204143	36.46	141.19	46.6	4.9	300.0	35.0	120.0	55.0	30.0	0.0	120.0	10.0	300.0	80.0	38	34
449	791225	32422	33.37	141.68	60.0	5.0	11.1	41.6	228.9	41.6	120.0	20.0	30.0	0.0	300.0	70.0	98	95
450	80 2 2	185715	36.11	139.84	55.7	4.2	320.0	25.0	140.0	65.0	50.0	0.0	140.0	20.0	320.0	70.0	13	13
451	80 2 4	195419	37.33	141.63	46.6	4.6	119.9	44.1	280.2	44.1	20.0	10.0	110.0	0.0	200.0	80.0	21	18
452	80 2 4	221012	35.56	140.12	64.4	4.2	212.7	75.7	95.9	6.6	4.4	12.7	110.0	50.0	264.6	37.2	11	11
453	80 312	64755	35.97	140.08	76.4	4.2	280.0	35.0	100.0	55.0	10.0	0.0	100.0	10.0	280.0	80.0	23	21
454	80 4 4	13659	35.66	140.84	61.7	4.1	280.0	25.0	100.0	65.0	10.0	0.0	100.0	20.0	280.0	70.0	15	14
							53.2	42.0	313.5	10.7	212.2	46.0	100.0	20.0	354.0	37.2	15	14
455	80 5 7	3 735	36.07	139.96	58.5	4.0	310.0	25.0	130.0	65.0	40.0	0.0	130.0	20.0	310.0	70.0	15	14
							39.2	68.3	274.4	12.8	180.3	17.2	80.0	30.0	296.1	54.5	15	14
456	80 5 7	213153	32.92	141.32	77.9	4.6	228.4	35.0	322.1	5.2	59.4	54.5	180.0	20.0	281.2	28.0	27	22
457	80 5 8	17 332	34.54	140.48	67.4	5.7	310.0	35.0	130.0	55.0	40.0	0.0	130.0	10.0	310.0	80.0	226	197
458	80 512	1 1 3	36.19	140.05	59.3	4.4	40.2	44.1	239.9	44.1	140.0	10.0	50.0	0.0	320.0	80.0	22	18
							152.0	54.0	311.5	34.3	48.3	9.9	140.0	10.0	274.6	75.9	22	18
459	80 520	35615	36.02	142.04	49.9	5.1	340.2	39.8	83.6	15.6	190.5	46.0	40.0	40.0	296.8	15.2	59	47
							290.0	75.0	110.0	15.0	20.0	0.0	110.0	60.0	290.0	30.0	59	47
							233.1	55.4	332.8	6.6	67.2	33.8	180.0	30.0	300.8	41.6	59	47
460	80 526	233618	38.11	143.84	49.0	4.7	326.8	14.0	233.2	14.0	100.0	70.0	10.0	0.0	280.0	20.0	22	17
							280.0	75.0	100.0	15.0	10.0	0.0	100.0	60.0	280.0	30.0	22	17
461	80 6 7	33833	33.55	141.10	57.0	4.6	237.4	38.4	351.8	27.6	107.0	39.3	300.0	50.0	202.3	6.4	31	27
462	80 610	11 031	35.90	139.56	55.7	4.3	26.6	37.8	153.4	37.8	270.0	30.0	0.0	0.0	90.0	60.0	14	14
463	80 614	1157 3	35.86	140.60	43.6	4.0	131.1	41.6	348.9	41.6	240.0	20.0	150.0	0.0	60.0	70.0	12	12
464	80 618	1625 8	35.60	140.05	73.1	4.6	116.1	63.7	272.3	24.4	6.6	9.4	100.0	20.0	252.7	67.7	54	48
465	80 629	153543	33.00	139.72	51.8	4.8	330.0	5.0	150.0	85.0	240.0	0.0	330.0	50.0	150.0	40.0	39	33
466	80 630	119 2	37.80	141.84	49.3	5.1	80.0	45.0	260.0	45.0	350.0	0.0	80.0	0.0	260.0	90.0	73	57
467	80 713	513 3	37.35	141.87	48.0	4.6	111.8	20.9	204.6	7.3	312.7	67.7	160.0	20.0	66.6	9.4	14	14
468	80 814	9 936	35.68	141.29	42.3	4.6	69.1	46.5	303.8	28.7	195.7	29.5	100.0	10.0	353.3	58.5	31	26
							56.0	28.1	318.9	13.0	206.7	58.5	100.0	10.0	4.3	29.5	31	26
469	80 9 3	102714	36.14	139.84	56.2	4.2	176.8	42.0	276.6	10.7	17.8	46.0	130.0	20.0	236.0	37.2	15	13
470	80 921	121846	35.83	139.48	58.3	4.5	13.5	48.7	121.9	15.5	224.0	37.2	330.0	20.0	82.2	46.0	30	23
471	80 924	41023	35.98	139.77	77.7	5.4	122.5	70.8	335.4	16.3	242.5	9.9	350.0	60.0	147.2	28.0	96	87
472	80 925	25423	35.55	140.19	77.0	6.1	142.0	54.0	301.5	34.3	38.3	9.9	130.0	10.0	264.6	75.9	230	200

Eq	Date y m d	Time h m s	Latit deg	Long deg	Dep km	Mag	Pole-X dd	Pole-X d	Pole-Y dd	Pole-Y d	B-axis dd	B-axis d	P-axis dd	P-axis d	T-axis dd	T-axis d	Number read	Number used
473	80 925	25948	35.57	140.21	68.0	5.3	334.5	54.3	147.3	35.5	239.7	3.4	130.0	80.0	330.0	9.4	22 /	18
474	80 925	32636	35.56	140.13	64.6	4.8	123.6	33.3	228.3	21.1	344.7	49.0	180.0	40.0	83.5	7.6	21 /	18
							269.9	45.9	109.3	42.5	10.2	9.9	180.0	80.0	279.9	1.7	21 /	18
475	80 925	45250	35.57	140.13	65.3	4.4	222.4	69.3	109.1	8.5	16.1	18.8	130.0	50.0	273.0	33.8	18 /	16
476	80 925	5 418	35.57	140.11	68.1	4.7	227.8	47.2	100.3	29.4	352.8	28.0	150.0	60.0	257.5	9.9	33 /	28
477	80 929	63658	38.75	141.81	70.1	5.0	348.2	20.9	255.4	7.3	147.3	67.7	300.0	20.0	33.5	9.4	58 /	48
							337.9	54.8	98.0	19.5	198.8	28.0	300.0	20.0	60.6	54.5	58 /	48
478	8010 3	24741	37.04	141.27	52.9	4.7	308.0	54.0	148.5	34.3	51.8	9.9	320.0	10.0	185.4	75.9	33 /	26
479	8010 6	142233	36.14	140.07	67.3	4.6	270.0	25.0	90.0	65.0	0.0	0.0	90.0	20.0	270.0	70.0	44 /	40
480	8010 9	11 732	36.34	140.98	43.6	5.1	139.0	60.0	274.8	22.5	12.9	18.8	110.0	20.0	243.2	62.0	67 /	52
481	801013	195536	35.53	140.07	65.6	4.2	140.8	68.3	265.6	12.8	359.7	17.2	100.0	30.0	244.0	54.5	14 /	11
482	801020	19 925	36.11	139.85	54.3	4.1	25.1	73.1	237.3	14.5	145.0	8.7	50.0	30.0	249.4	58.5	13 /	11
							187.0	41.0	300.1	24.3	51.7	39.3	150.0	10.0	251.7	49.0	13 /	11
483	801030	24913	36.43	140.69	58.7	4.2	116.1	63.7	272.3	24.4	6.6	9.4	100.0	20.0	252.7	67.7	18 /	16
484	8011 9	114144	35.79	140.12	41.8	4.1	151.1	41.6	8.9	41.6	260.0	20.0	170.0	0.0	80.0	70.0	14 /	14
485	801116	93550	36.01	140.10	70.6	4.1	11.1	60.0	235.2	22.5	137.1	18.8	40.0	20.0	266.8	62.0	16 /	15
							182.7	75.7	65.9	6.6	334.4	12.7	80.0	50.0	234.6	37.2	16 /	15
							138.9	41.6	281.1	41.6	30.0	20.0	120.0	0.0	210.0	70.0	16 /	15
486	8012 1	154046	36.42	141.02	48.5	4.2	149.0	60.0	284.8	22.5	22.9	18.8	120.0	20.0	253.2	62.0	13 /	12
487	801227	1232 3	33.09	141.09	71.3	4.2	202.7	81.6	72.9	5.4	342.3	6.4	80.0	50.0	247.0	39.3	11 /	10
							294.6	21.2	202.0	6.6	95.5	67.7	340.0	10.0	246.4	19.7	11 /	10

(20 / 20)